Direct Force Measurements on the Colloidal Scale: From Modified Electrodes to Particle Manipulation

DISSERTATION

zur Erlangung des akademischen Grades
eines Doktors der Naturwissenschaften (Dr. rer. nat.)
im Fach Chemie der Fakultät für
Biologie, Chemie und Geowissenschaften
der Universität Bayreuth

vorgelegt von
Volodymyr Kuznetsov
Geboren in Stachanov

Bayreuth, 2013

II

Die vorliegende Arbeit wurde an der Universität Bayreuth und der Universität Genf (Schweiz) angefertigt. Von Dezember 2008 bis April 2010 arbeitete ich am Abteilung für anorganische, analytische, und angewandte Chemie in der Universität Genf unter der Betreuung von Prof. Dr. Michal Borkovec und co-Betreuung von Prof. Dr. Georg Papastavrou; und von April 2010 bis Dezember 2012 am Lehrstuhl für Physikalische Chemie II in der Universität Bayreuth unter Betreuung von Prof. Dr. Georg Papastavrou.

Vollständiger Abdruck der von der Fakultät für Biologie, Chemie und Geowissenschaften der Universität Bayreuth genehmigten Dissertation zur Erlangung des akademischen Grades Doktor der Naturwissenschaften (Dr. rer. Nat.).

Amtierender Dekan: Prof. Dr. Beate Lohnert

Tag des Einreichens der Dissertation:

Tag des wissenschaftlichen Kolloquiums:

Prüfungsausschuss:

Prof. Dr. Georg Papastavrou   (Erstgutachter)

IV

The larger the island of knowledge,
the longer the shoreline of wonder.

Ralph W. Sockman

VI

To my family

VIII

Table of Contents

X

Summary

In this thesis the interfacial surface forces and mechanical properties of thin films have been studied by the colloidal probe technique. One central point is the combination of direct force measurements with an electrochemical setup in order to tune interfacial properties of an electrode modified with an organic layer. In particular the adhesion and ion adsorption have been studied, which are ubiquitous phenomena in the colloid science, electrochemistry, and biology. Moreover, a novel technique has been developed to fabricate chemically and mechanically stable colloidal probes for atomic force microscopy (AFM). Additionally, the elastic properties of polyelectrolyte multilayer films were locally resolved under controlled humidity.

The adhesive behaviour of colloidal particles on modified electrodes has been studied by direct force measurements with a micrometre-sized silica probe attached to an AFM-cantilever. By controlling the external potential applied to the modified electrode by means of a potentiostat, separate adhesion contributions at the modification layers in electrolyte solution were quantified. In particular, to determine the influence of the terminating functional groups, gold electrodes modified with self-assembled monolayers (SAMs) terminated in non-ionizable groups were used. It has been demonstrated that electrostatic double-layer forces dominate the adhesion of colloidal particles on hydrophobic and hydrophilic interfaces. In contrast to hydrophilic interface, for hydrophobic one forces due to the solvent exclusion play a significant role and leads to an offset in the adhesive force, which otherwise can be compensated by the external potential. However, the electrocapillarity is of minor importance and can be neglected.

To quantify the ion adsorption at organic interfaces a novel approach was followed, which is based on direct force measurements with silica colloidal probes on SAM-modified electrodes in electrolyte solutions. By variation of applied potential and concentration of specifically adsorbed ions, given by the solution's pH, the charging behaviour of hydrophilic SAM-OH and hydrophobic SAM-CH$_3$ has been determined. In difference to electrokinetic techniques, direct force measurements allow to probe the full range of the diffuse layer. The analysis of the diffuse layer potential as a function of externally applied potential provides important information. In particular, the shift of the potential of zero charge (pzc) indicates on the specific ion adsorption in the Stern layer as it alters the charging behaviour of the electrode's interface. It has been demonstrated that hydronium and hydroxide ions adsorb on both the hydrophobic and hydrophilic

interfaces. However, the presence of the background electrolyte (KCl) does not shift pzc and thus its ions have no specific affinity towards the interfacial adsorption. The adsorption of hydronium and hydroxide ions is stronger on hydrophobic, than on hydrophilic interface. This is in agreement with theoretical studies. The simple three-capacitor model based on a Langmuir-type adsorption isotherm provides semi-quantitative description of observed dependence of the diffuse double layer potential on applied potential.

A new technique for colloidal probe preparation was developed. A great challenge for the force measurements with the AFM is to ensure the cleanliness, chemical and mechanical stability of the used probes. The approach is based on high-temperature sintering of micrometer-sized silica particles to AFM cantilever with enhanced contact area. Due to a "neck" formed by nanometer-sized particles the increased mechanical stability of colloidal probes was achieved, which has been quantitatively determined by lateral force spectroscopy. The implementation of sintering procedure for silica colloids allowed the development of the highly stable colloidal probes, whose surface properties could be renewed by heating.

Finally, the mechanical properties of polyelectrolyte multilayer films have been determined by nanoindentation as a function of relative humidity. For these series of measurements again a colloidal probe has been used. It has been demonstrated that films containing polyglutamic acid have Young's modulus, which depends on humidity. The change of stiffness with ambient humidity has reversible character.

Zusammenfassung

Diese Arbeit beschäftigt sich mit der Charakterisierung von Grenzflächenphänomenen auf modifizierten Elektroden und anorganischen Verbundmaterialien sowie den mechanischen Eigenschaften von ultradünnen Schichten. Fundamentale neue Aspekte zur Adhäsion auf der Mikro- und Nanoskala wurden entdeckt. Desweiteren wurde eine Methode zur Quantifizierung von elektrochemischen Doppelschicht-Effekten entwickelt, die erfolgreich auf Modellsysteme angewendet werden konnte. Die Adhäsion an Elektroden mit hydrophilen selbstorganisierten Monoschichten (SAMs) wurde erfolgreich für die Manipulation von mikroskopischen Objekten ohne Scherkräfte implementiert. Eine neuartige Technik zur Herstellung von chemisch und mechanisch stabilen kolloidalen Sonden für die Rasterkraftmikroskopie (AFM) wurde entwickelt. Diese Sonden wurden später verwendet, um die Oberflächenladung und die Eigenschaften der diffusen Schicht von natürlichen und synthetischen Tonmineralien zu quantifizieren. Desweiteren wurden die elastischen Eigenschaften dünner Filme mittels Rasterkraftmikroskopie mit kolloidalen Sonden untersucht. Dabei wurde der Einfluss der relativen Luftfeuchtigkeit auf die mechanischen Eigenschaften von Polyelektrolyt Multilagen-Filmen betrachtet.

In dieser Arbeit werden Oberflächenkräfte und mechanische Eigenschaften verschiedener grenzflächenbasierter Systeme, wie modifizierte Elektroden oder Polymerfilme, mit Hilfe von kolloidalen Sonden untersucht. Ein zentraler Punkt der Arbeit liegt hierbei auf der Implementierung von direkten Kraftmessungen an Elektroden, die mit einer organischen Schicht modifiziert sind. Insbesondere wurden die Adhäsion und Ionenadsorption auf solchen Elektroden untersucht, beides sind allgegenwärtige Phänomene in der Kolloidwissenschaft, der Elektrochemie oder der Biologie dar. Weiterhin wurde im Rahmen dieser Arbeit auch ein neue Technik zur Präparation kolloidaler Sonden für die Rasterkraftmikroskopie (engl. atomic force microscopy, AFM) entwickelt. Diese kolloidalen Sonden zeichnen sich durch eine besonders große chemische und mechanische Stabilität aus. Mit den Sonden wurden daher beispielsweise die Elastizitätseigenschaften von Polyelektrolytmultischichten in Abhängigkeit von Luftfeuchtigkeit bestimmt.

Die adhäsiven Eigenschaften von kolloidalen Partikeln auf modifizierten Elektroden wurden anhand von direkten Kraftmessungen untersucht. Hierfür wurden kolloidale

Silica-Partikel mit Abmessungen im Mikrometerbereich als Sonden verwendet. Anhand der Kontrolle des externen an der Elektrode anliegenden Potentials über einen Potentiostaten wurden die verschiedenen Beiträge zu den Adhäsionskräften auf den modifizierten Elektroden identifiziert. Um den Einfluss der funktionellen Gruppen auf die Adhäsionskräfte zu bestimmen wurden Goldelektroden mit selbstorganisierenden Monoschichten (*engl.* self-assembled monolayers, SAMs) aus Thiolverbindungen mit nicht-dissoziierenden Endgruppen modifiziert. Es konnte demonstriert werden, dass der Überlapp der Doppelschichten und damit Kräfte elektrostatischen Ursprungs die Änderung des Adhäsionsverhalten auf hydrophilen sowie hydrophoben Oberflächen dominieren. Im Gegensatz zu hydrophilen Grenzflächen, spielt bei hydrophoben Grenzflächen die Kraft durch Lösungsmittelausschluss (*engl.* forces due to solvent exclusion) eine signifikante Rolle und führt zu einem „Offset" bei den Adhäsionskräften, welcher jedoch durch das externe Potential kompensiert werden kann. Bei diesen Adhäsionsprozessen ist Elektrokapillarität von untergeordneter Bedeutung und kann vernachlässigt werden.

Um Ionenadsorption an organischen Grenzflächen quantifizieren zu können wurde ein neuer Ansatz eingeführt, der auf direkten Kraftmessungen mit kolloidalen Sonden auf SAM-modifizierten Elektroden basiert. Durch Variation des angelegten Potentials und der Ionenkonzentration, im speziellen des pH, kann das Ladungsverhalten auf hydrophilen (OH-terminierten) oder hydrophoben (CH$_3$-terminierten) SAMs bestimmt werden. Im Unterschied zu elektrophoretischen Methoden kann über direkte Kraftmessungen die gesamte Ausdehnung der elektrischen Doppelschicht untersucht werden. Die Analyse des Doppelschichtpotentials als Funktion des angelegten Potentials erlaubt wichtige Rückschlüsse auf die Ionenadsorptionsprozesse. Insbesondere die Veränderung des „potential of zero charge" (pzc) zeigt das Vorliegen von spezifischer Ionenadsorption in der Sternschicht, die das Ladungsverhalt an der Elektroden/Elektrolyte-Grenzfläche beeinflusst. Es konnte hier gezeigt werden, dass sowohl Hydronium- (OH$_3^+$) als auch Hydroxyl-(OH$^-$) Ionen an den hydrophoben oder hydrophilen Grenzflächen adsorbieren. Hingegen beeinflusst ein „Hintergrund"-Elektrolyt wie Kaliumchlorid die Lage des pzc nicht und zeigt damit dass die entsprechenden Ionen nicht oder wesentlich schwächer an den entsprechenden Grenzflächen adsorbieren. Die Adsorption von OH$_3^+$ - und OH$^-$ - Ionen ist wesentlich ausgeprägter auf den hydrophoben SAMs als auf den hydrophilen SAMs. Dieses Verhalten ist in Einklang mit theoretischen Voraussagen. Anhand eines einfachen

Models, in dem drei Kapazitäten (SAM, Stern-Schicht und Doppelschicht) an der Elektrode in Serie vorliegen und die Beschreibung der Ionenadsorption durch eine Langmuir-Adsorptionsisotherme, können die experimentellen Ergebnisse für die Abhängigkeit des Doppelschichtpotentials vom angelegten Potential sehr gut semi-quantitativ beschrieben werden.

Im Rahmen dieser Arbeit wurde insbesondere eine neue Technik zur Präparation von kolloidalen Sonden entwickelt. Eine große Herausforderung bei direkten Kraftmessungen mit dem AFM ist es die Sauberkeit sowie chemische und mechanische Stabilität der Sonden zu garantieren. Der hier vorgestellte neue Präparationsansatz basiert auf einem Hochtemperatur-Sinterverfahren zur Verbindung von kolloidalen Silica-Partikeln mit einem AFM-Hebelarm (engl. cantilever). Durch die Ausbildung eines „Kragens" aus nanometergroßen Partikeln kann eine erhöhte mechanische Stabilität erzielt werden, die auch quantitativ durch Messung der Lateralkräfte nachgewiesen werden konnte. Die Implementierung dieser Sinterprozedur für Silica-Kolloide erlaubt es zum ersten Mal hochstabile kolloidale Sonden aus diesem Material herzustellen. Weiterhin können die chemischen Eigenschaften dieser kolloidalen Sonden durch Hochtemperaturbehandlung wieder in den Ausgangszustand versetzt werden.

Die mechanischen Eigenschaften von Polyelektrolyt-Multischichten wurden über Nano-Eindringtests (engl. nanoindentation) als Funktion der Luftfeuchtigkeit bestimmt. Für diese Messserien wurden die oben beschriebenen kolloidalen Sonden verwendet. Es konnte gezeigt werden, dass das Elastizitätsmodul nach Young von Multischichtfilme, die Polyglutaminsäure enthalten von der Luftfeuchtigkeit abhängt, wobei die entsprechende Änderung jedoch reversibel ist.

List of abbreviations and symbols

A	Hamaker constant
AFM	Atomic force microscopy
C	Capacitance
CV	Cyclic voltammetry or cyclic voltammogram
D	Distance
DL	Diffuse layer
DLVO	Derjaguin, Landau, Verwey, Overbeek (theory, forces)
DMT	Derjaguin, Müller, Toporov (theory, equation)
F	Force
FIB	Focused ion beam
I	ionic strength
iHP	Inner Helmholz plane
JKR	Johnson, Kendall, Roberts (theory, equation)
k	Normal cantilever constant
kT	Thermal energy
LbL	Layer-by-layer
MASIF	Measurement and analysis of surface interaction forces
MEMS	Microelectromechanical system(s)
oHP	Outer Helmholz plane
PAH	Poly(allylamine hydrochloride)
PB	Poisson-Boltzmann (distribution, equation)
PEM	Polyelectrolyte multilayer
PGA	Poly(glutamic acid)
PSS	Poly(styrenesulfonate)
pzc, ϕ_{PZC}	Potential of zero charge
pzf	Potential of zero force
R	Radius
R_{eff}	Effective radius of interaction given by Derjaguin approximation
SAM	Self-assembled monolayer
SCE	Saturated calomel electrode
SECM	Scanning electrochemical microscopy

|	
SEM	Scanning electron microscopy
SFA	Suface force apparatus
SFM	Scanning force microscopy
STM	Scanning tunneling microscopy
TEM	Transmission electron microscopy
TIRM	Total internal reflection microscopy
vdW	van der Waals (forces)
W	Interaction energy
γ	Interfacial tension or surface free energy
ζ	Zeta potential
κ^{-1}	Debye screening length
σ^{a}	Surface charge density on an SAM surface
σ^{D}	Diffuse layer charge density
σ^{e}	Surface charge density on an electrode
ϕ	Externally applied potential, electronic potential
ψ^{a}	Surface potential on an SAM surface
ψ^{D}	Diffuse layer potential

1. Introduction

Direct force measurements have been essential in recent years for our understanding of interfacial phenomena.[1-3] They contributed in the fields of polymer research, biology, physical chemistry, physics to name just a few. Quantification of such phenomena as adhesion, friction, or interfacial charge accumulation became only possible by probing the processes on the nanometer-scale. The quantitative description of complex biological, polymer, and inorganic systems advanced profoundly due to revealing interactions at the nanoscale.[4,5]

Historically, the first device allowing the interaction profiles determination with sub-nanometer resolution was the surface force apparatus (SFA).[6] Although in the recent 35 years other techniques have emerged, the SFA is still being used in many laboratories.[7] The two other important techniques are the MASIF technique (i.e. measurement and analysis of surface interaction forces) and the colloidal probe technique based on atomic force microscopy (AFM). All three techniques have defined interaction geometry. While the SFA and the MASIF use rather large probes in the order of a few millimeters, and employ force-determining sensors with relatively high spring constant, their force resolution is limited to some hundreds of piconewtons.[8] By contrast, the colloidal probe technique, utilizing micrometer-sized probes, allows determining forces down to a few piconewtons. Additionally, the range of sensed forces is controlled by the stiffness of an AFM cantilever. Thus, for probing interactions within the wide force range of the colloid domain the colloidal probe technique has the highest force resolution.[9]

Currently, the colloidal probe technique is the most widely used method to determine the interactions between colloidal objects and surfaces.[8] The great advantage of such a probe is its versatility in terms of geometry, surface chemistry, and possibility to attach practically all types of objects on the colloidal scale to the AFM cantilever. For instance, sphere-sphere, sphere-plane, and crossed cylinders geometries are readily accessible.[10] Among the materials for probe reported so far are silica, glass, latex, and cellulose[11], and even gas- or air-bubbles.[12]

Because of the large number of different applications the colloidal probe force spectroscopy contributed in the past to various branches of colloid science.[8] A selection of typical applications is presented in **Figure 1**. They include measurements of adhesion force (A, cf. section 5 of this thesis)[13] and forces due to diffuse layer overlap (B, cf. sections 5, 7 of this thesis).[14] Using this approach the particle-particle interaction as a

function of separation can be obtained (C, cf. sections 5, 7 of this thesis)[15], while performing the nanoindentation experiment with defined geometry of the indenter (D, cf. section 8 of this thesis) allows mechanical properties determination of nanoobjects of different nature such as films, capsules, or cells.[16] Therefore, force spectroscopy with a colloidal probe represents a complimentary approach to universal surface tester in the cases (A) and (D), to electrochemical techniques for studying diffuse layer properties (B), and, finally, complements the spectroscopic and electrokinetic measurements to determine properties of colloidal suspensions (C).[7,17] Thus, the colloidal probe technique allows addressing a number of phenomena on the nanoscale.
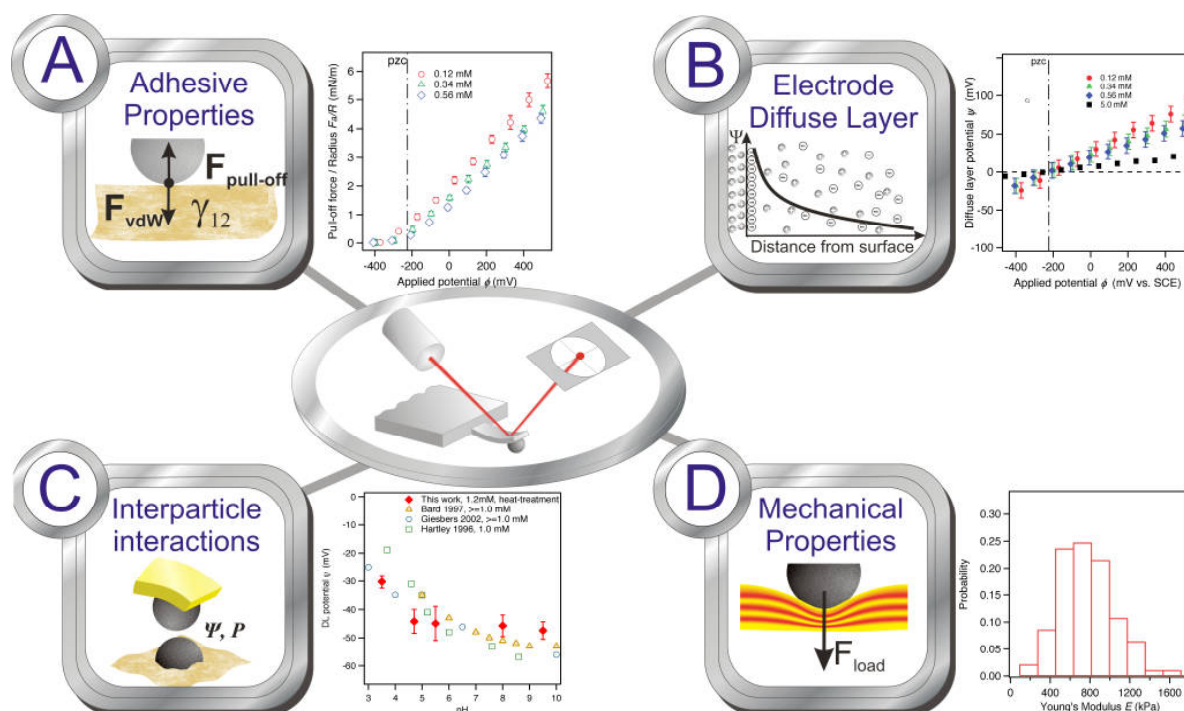
Figure 1: Applications of direct force measurements with colloidal probe: (A) measurement of adhesion; (B) quantification of diffuse layer properties; (C) probing interparticle interaction; (D) characterization of laterally resolved mechanical properties.

By employing colloidal probe technique it is possible to measure the interacting forces and mechanical properties in various media, such as air and electrolyte solutions. Together with adhesion and elasticity measurements the technique is widely used for measuring DLVO (Derjaguin, Landau, Verwey and Overbeek) and chemical forces, friction and steric forces, etc. Therefore, interfacial phenomena and forces causing them could be quantified. For example, by varying the ionic strength of solution the electrostatic diffuse double layer forces could be separated from the Van der Waals forces.[18]

In this thesis new approaches to apply the colloidal probe technique have been pursued. One important application is the combination of the direct force measurements with potentiostatic control of modified electrodes in electrolyte solution to identify different contributions in adhesion force between colloidal particles and modification layer. By utilizing cantilevers with high spring constant it became possible to correlate forces upon approach and adhesion. In particular the separation of electrostatic diffuse double layer, van der Waals, and solvent exclusion forces in total adhesive force has been addressed. Additionally the role of electrocapillarity effects for organic layers on electrodes could be assessed. Thus, in difference to previous studies[19,20], the influence of long- and short-ranged interaction forces on the adhesion could be identified in unambiguous manner.

The control of adhesion force provides means to pursue micro- and nanomanipulation of colloidal particles. The same micrometer-sized silica particles used as colloidal probes for studying adhesion could be employed for micromanipulation to provide a proof of principle. Therefore, studying adhesive properties of modified electrodes became a prerequisite for micromanipulation application.

Ion adsorption on non-ionizable organic interfaces has been also studied by colloidal probe technique. While the electrochemical control of modified electrodes allows variation of their diffuse layer properties, using direct force measurements those properties could be determined. In particular the variation of diffuse layer potential as a function of applied potential has been of major interest, since such data could be compared to the theoretical predictions.

A novel approach to prepare colloidal probes by a sintering technique has been developed. For surface force measurements and nanoindentation experiments probes with mechanical stability are important to ensure the defined interaction geometry at high pressure.[21,22] Due to their smoothness and predictable surface chemistry silica particles are potentially well-suited as nanoindenter.[23] However, the fixation of such particles on an AFM cantilever without polymeric glue has not been possible so far. Here, a preparation by sintering with fixation "neck" made of Ludox particles allowed to prepare probes suitable for any solvent. The high-temperature treatment during the preparation could solve also the problem of organic contaminants and reproducible surface chemistry[17].

The preparation of the thin polyelectrolyte multilayer (PEM) films by layer-by-layer technique has numerous applications in medical, cosmetic, and sensor industries to name

just a few.[24-26] Probes prepared by this sintering technique were applied to characterize mechanical properties of ultrathin organic films. Namely the elastic modulus of polyelectrolyte multilayer films susceptible to surrounding humidity was addressed by nanoindentation measurements. Primarily the change of the stiffness upon alteration of humidity conditions and the reversibility of this process were studied.

References:

1.   Senden, T. J. Force Microscopy and Surface Interactions. *Current Opinion in Colloid & Interface Science* **6**, 95-101 (2001).

2.   Butt, H. J. Analyzing Electric Double Layers with the Atomic Force Microscope. *Encyclopedia of electrochemistry* 225-252 (2003).

3.   Leckband, D. & Israelachvili, J. Intermolecular Forces in Biology. *Q. Rev. Biophys.* **34**, 105-267 (2001).

4.   Stuart, M. A. C. et al. Emerging Applications of Stimuli-Responsive Polymer Materials. *Nature materials* **9**, 101-113 (2010).

5.   Butt, H.-J., Berger, R., Bonaccurso, E., Chen, Y. & Wang, J. Impact of Atomic Force Microscopy on Interface and Colloid Science. *Adv. Colloid Interface Sci.* **133**, 91-104 (2007).

6.   Israelachvili, J. N. & Adams, G. E. Direct Measurement of Long Range Forces between Two Mica Surfaces in Aqueous KNO_3 Solutions. *Nature* **262**, 774-776 (1976).

7.   Claesson, P. M., Ederth, T., Bergeron, V. & Rutland, M. W. Techniques for Measuring Surface Forces. *Adv. Colloid Interface Sci.* **67**, 119-183 (1996).

8.   Butt, H.-J., Cappella, B. & Kappl, M. Force Measurements with the Atomic Force Microscope: Technique, Interpretation and Applications. *Surface Science Reports* **59**, 1-152 (2005).

9.   Holmberg, K., Shah, D. O. & Schwuger, M. J. *Handbook of Applied Surface and Colloid Chemistry* (John Wiley & Sons Inc, 2002), p. 388.

10.   Israelachvili, J. N. *Intermolecular and Surface Forces* (Academic Press, 2011).

11.   Giesbers, M., Kleijn, J. M. & Cohen Stuart, M. A. Interactions between Acid- and Base-Functionalized Surfaces. *J. Colloid Interface Sci.* **252**, 138-148 (2002).

12.   Chan, D. Y. C., Klaseboer, E. & Manica, R. Theory of Non-equilibrium Force Measurements Involving Deformable Drops and Bubbles. *Adv. Colloid Interface Sci.* **165**, 70-90 (2011).

13. Pericet-Camara, R., Papastavrou, G., Behrens, S. H., Helm, C. A. & Borkovec, M. Interaction Forces and Molecular Adhesion between Pre-adsorbed Poly(ethylene imine) Layers. *J. Colloid Interface Sci.* **296**, 496-506 (2006).

14. Toikka, G. & Hayes, R. A. Direct Measurement of Colloidal Forces between Mica and Silica in Aqueous Electrolyte. *J. Colloid Interface Sci.* **191**, 102-109 (1997).

15. Popa, I., Trulsson, M., Papastavrou, G., Borkovec, M. & Jönsson, B. Long-Ranged Attractive Forces Induced by Adsorbed Dendrimers: Direct Force Measurements and Computer Simulations. *Langmuir* **25**, 12435-12438 (2009).

16. Richert, L., Engler, A. J., Discher, D. E. & Picart, C. Elasticity of Native and Cross-Linked Polyelectrolyte Multilayer Films. *Biomacromolecules* **5**, 1908-1916 (2004).

17. Kobayashi, M., Skarba, M., Galletto, P., Cakara, D. & Borkovec, M. Effects of Heat Treatment on the Aggregation and Charging of Stöber-type Silica. *J. Colloid Interface Sci.* **292**, 139-147 (2005).

18. Dishon, M., Zohar, O. & Sivan, U. From Repulsion to Attraction and Back to Repulsion: The Effect of NaCl, KCl, and CsCl on the Force between Silica Surfaces in Aqueous Solution. *Langmuir* **25**, 2831-2836 (2009).

19. Rentsch, S., Siegenthaler, H. & Papastavrou, G. Diffuse Layer Properties of Thiol-Modified Gold Electrodes Probed by Direct Force Measurements. *Langmuir* **23**, 9083-9091 (2007).

20. Rentsch, S. Direct Force Measurements Between Surfaces Under Potentiostatic Control. *PhD thesis,* University of Geneva, Geneva, Switzerland (2008).

21. Dimitriadis, E. K., Horkay, F., Maresca, J., Kachar, B. & Chadwick, R. S. Determination of Elastic Moduli of Thin Layers of Soft Material Using the Atomic Force Microscope. *Biophys Journal* **82**, 2798-2810 (2002).

22. Gouldstone, A. et al. Indentation Across Size Scales and Disciplines: Recent Developments in Experimentation and Modeling. *Acta Materialia* **55**, 4015-4039 (2007).

23. Matijevic, E. Preparation and Properties of Uniform Size Colloids. *Chem. Mater.* **5**, 412-426 (1993).

24. Ariga, K., Hill, J. P. & Ji, Q. Layer-by-Layer Assembly as a Versatile Bottom-up Nanofabrication Technique for Exploratory Research and Realistic Application. *Physical Chemistry Chemical Physics* **9**, 2319-2340 (2007).

25.   Tang, Z., Wang, Y., Podsiadlo, P. & Kotov, N. A. Biomedical Applications of Layer-by-Layer Assembly: From Biomimetics to Tissue Engineering. *Advanced Materials* **18**, 3203-3224 (2006).

26.   Bertrand, P., Jonas, A. & Laschewsky, A. Ultrathin Polymer Coatings by Complexation of Polyelectrolytes at Interfaces: Suitable Materials, Structure and Properties. *Macromolecular Rapid Communications* **21**, 319-348 (2000).

2. Theory / Status of the field

A milestone in surface science was the development of scanning tunneling microscopy (STM) by Rohrer and Binnig in 1982.[1] It was followed by the atomic force microscopy (AFM) in 1986.[2] The latter has allowed imaging topography and measuring surface forces on the nanoscale with sub-nanometer resolution. Both methods use the micrometer-sized cantilever or a wire with a nanometer-sharp tip to scan over the sample surface with simultaneous detection of tip-sample current (STM) or interaction (AFM). In contrast to STM the AFM does not require conductive samples, nor it requires semi-transparent samples like the surface force apparatus (SFA)[3], where the distance between two surfaces is controlled interferometrically. Therefore probing interaction forces on the nanoscale as a function of the tip-sample distance became possible.

2.1. AFM and direct force measurements

Figure 2 schematically illustrates the working principle of atomic force microscope for imaging in so-called contact mode. The cantilever with a sharp tip presses on the sample surface, while the deflection of the cantilever is acquired by a laser reflected from it to a position-sensitive photodetector, connected to the controller. The latter receives a signal from the photodetector and is connected to a translational stage, which consists of X-, Y-, Z- piezos. When the tip scans a sample surface laterally (X- and Y- piezos are used), the deflection of the cantilever is kept constant by movement of the translational stage in Z-direction. Hence, the topography of the surface can be reconstructed. The controller is operated from a computer, where the resulting topographical data are displayed.

Besides the deflection of cantilever other signals can be monitored during scanning.[4] For example, if the cantilever is set to oscillate during scanning then the change of the amplitude or frequency shift can be monitored. That gives the origin to different working modes of AFM. In various working modes not only topographical data can be obtained, but also one can determine the adhesive properties of the surface or laterally resolve the mechanical properties. Measurements of surface properties by AFM are based on determination of interaction forces between the tip or a probe and a sample.[5] Such forces are determined as a function of tip-sample separation. An overview on the different imaging modes is given elsewhere.[6]
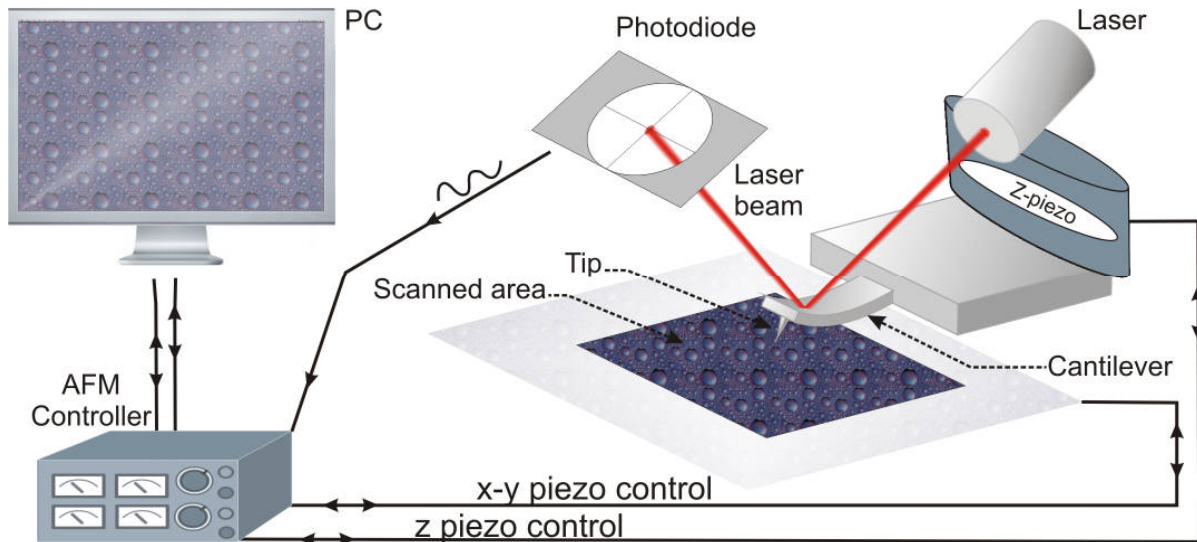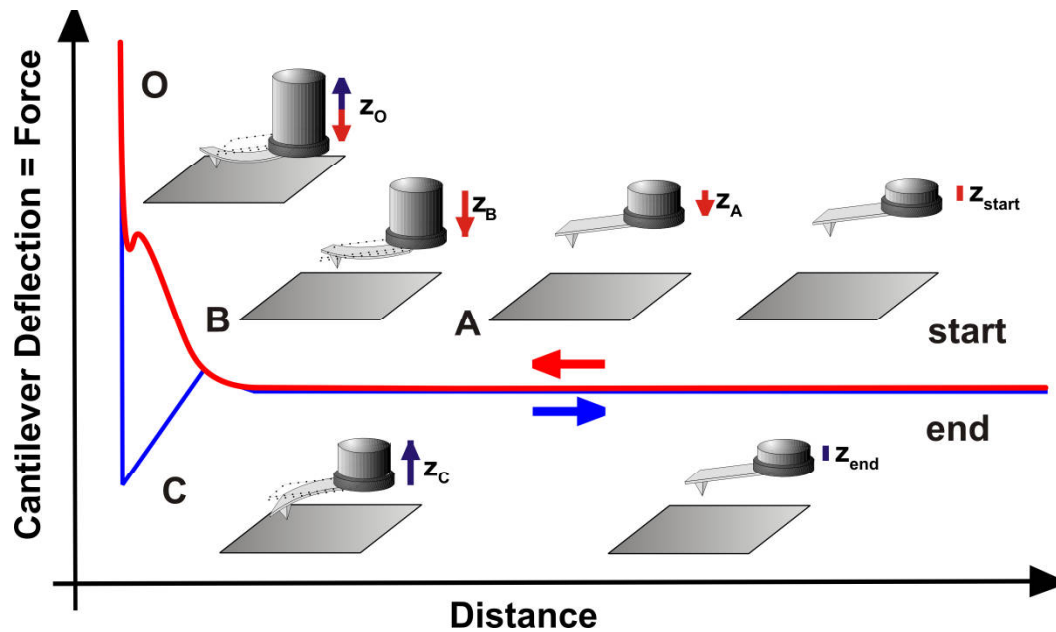
Figure 2: Schematic representation of an atomic force microscope. The movement of the cantilever is controlled via the PC software using a feedback loop. Data acquisition is based on z-piezo movement and the signal on position-sensitive photodiode.

Methods, which involve determination of probe-sample interaction from contact to some hundreds of nanometers are referred in the literature as direct force measurement methods. Both contact and non-contact forces measured in quasi-static regime can be addressed thereby. If the AFM is used for direct force measurements, then the cantilever is moved towards the surface and back by Z-piezo, while the deflection is recorded as a function of its position. The movement is carried at sufficiently slow speed to ensure that deflection happens only due to interaction forces, while hydrodynamic drag is eliminated.

2.2. Data acquisition and interpretation in direct force measurements

The principle of direct force measurements by AFM is presented in more detail in **Figure 3**. As example, the interaction between two likewise-charged, non-compressible surfaces in electrolyte solution is considered. Since both surfaces are charged, they possess so-called diffuse layers, where the distribution of ions differs from the bulk solution. At the initial position (upper right position) the cantilever is situated far away from the surface and the interaction force is negligible (pos. A). Upon approaching the sample repulsive, long-ranged forces start to act on the probe, so the cantilever starts to bend from the surface (pos. B). The further approach of the cantilever towards the surface leads to the tip-sample contact (pos. O), passing through an instability. In this interval the attractive force, i.e. van der Waals force, overcomes repulsion due to overlap of diffuse layers. The instability on a force-versus-distance curve looks like a short bend before contact, and therefore it is called "jump-in". Since in contact the deflection of the

cantilever is equal to the z-piezo movement, e.i. the former complies with the latter, the data acquired at contact are called *constant compliance region*. As soon as a given load force is reached, the piezo movement is reversed. Upon reversal of piezo movement the AFM-tip rests in contact with the surface until the restoring forces due to cantilever bending are sufficient to overcome the adhesion between tip and surface (pos. C). Since the separation occurs rapidly, the cantilever "jumps" out of contact. Thus on the force curve the so-called "jump-out" is observed. Further increase of the separation leads to a long-range interactions identical to those obtained upon approach.[7]

Figure 3: Schematic representation of direct force measurements by AFM (adapted from the review of G. Papastavrou[8]). In this example, the AFM tip and sample are charged likewise. Hence, long-range interactions are repulsive due to the overlap of diffuse double layers. At the same time short-range attraction is present due to van der Waals (vdW) forces. While approaching the surface the cantilever bends depending on tip-sample interaction. At long separation distance no deflection of the cantilever takes place (A), then due to overlap of diffuse layers cantilever bends (B), afterwards it contacts the surface allowing the small "jump-in" due to vdW force. Upon contact when the loading force is reached the piezo reverses its movement (O). The separation occurs when the force exerted by bended cantilever is equal to the adhesion between surfaces (C). This produces characteristic "jump-out" on the force curve. Afterwards the profile due to long-range forces follows the same trend as recorded upon approach.

2.3. Data analysis in direct force measurements

To analyze quantitatively the data obtained by direct force measurements the deflection of cantilever versus the Z-piezo displacement have to be converted into force versus tip-sample separation distance. An example of the initial force curve is shown in

Figure 4a. There the long-range interaction force is generally attractive, though it becomes repulsive upon contact. The reason for repulsive force between two quasi-non-deformable surfaces is the interaction of their two electron clouds (Born repulsion). The following conversion calculations are valid only if no detectable deformation of either tip or sample occurs during contact.[9]

Initially the deflection of cantilever Z_C' is measured by the photodiode signal in volts and plotted against the piezo-displacement Z_P at the abscissa axis (**Figure 4**a). From the linear fit of constant compliance region marked by the dashed line in (a) the inverse optical lever sensitivity *InvOLS* (m/V) is determined. Hence the real deflection of the cantilever in meters Z_C can be determined:

$$Z_C(i) = Z_C'(i) \cdot InvOLS \tag{1}$$

where the *i*-index represents the ordinal number of the data points (b). The *InvOLS* value depends on experimental conditions, such as the laser alignment, the surrounding media, and the reflectance of the cantilever. Therefore, this parameter has to be determined for each set of measurements individually.[10]

At the same time with the determination of *InvOLS* the data deviation from linear constant compliance region indicates on the zero separation distance $D(i) = 0$ between the AFM probe and a sample, which is related to the piezo-displacement by

$$D(i) = Z_C(i) + Z_P(i). \tag{2}$$

While for two quasi-non-deformable surfaces the determination of *InvOLS* and zero separation distance is rather straightforward, for experiments, where deformation of sample takes place, those parameters should be additionally determined. Namely, the *InvOLS* is determined separately against hard wall, and the zero contact point is found by analysis of the base line or others details. These questions concerning nanoindentation experiments are further addressed in the Section 7 of this thesis.
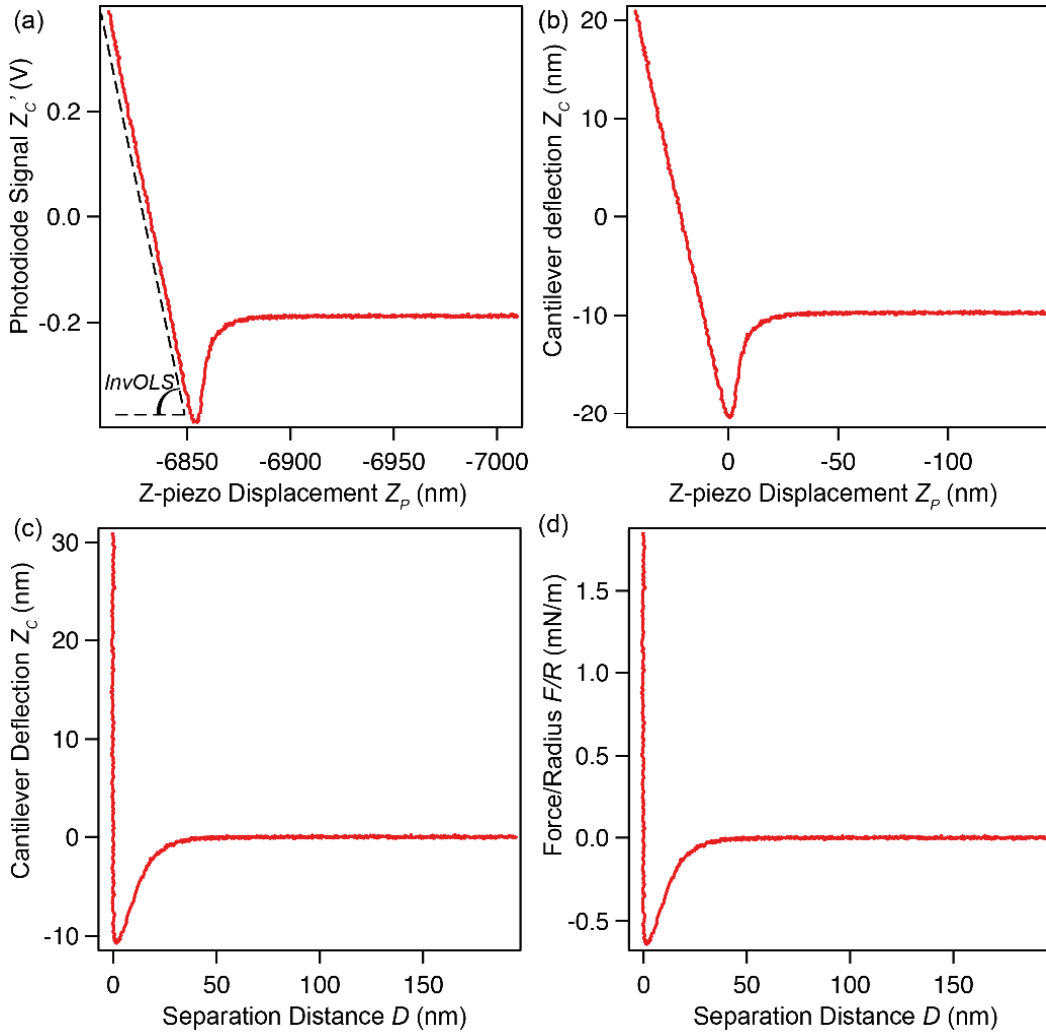
Figure 4: Data processing for direct force measurements. Only the approach curve is shown. (a) Initial data: photodiode signal vs. Z-piezo displacement. (b) After the determination of inverse optical lever sensitivity from the constant compliance region the photodiode signal converted into cantilever deflection; the zero-separation distance is found. (c) The Z-piezo displacement converted into probe-sample separation distance; baseline in deflection data is found due to absent interaction at high separation. (d) Deflection of cantilever is converted to interaction force, which is further normalized by the effective radius of the probe-sample system.

Next, taking into account that at large separation distances (normally above 100 nm) no interaction is detectable, the base-line is fitted and subtracted from the force profile (c). Finally the deflection of the cantilever is converted into force

$$F(i) = k_C \cdot Z_C(i). \qquad (3)$$

where k_C is the normal cantilever constant. The latter usually determined by one of three standard methods: Hutter-Bechhoefer or thermal noise method [11], Sader method [12,13], or alternatively by Cleveland or added mass method[14]. Nevertheless, many more elaborate methods exist.[15] Typical error in cantilever constant determination ranges from 10 to

30%. The force is further normalized (d)[16] to facilitate the comparison with the theoretical calculations by the effective radius of interaction R_{eff}, which is

$$R_{eff} = (R_1 \cdot R_2) / (R_1 + R_2). \qquad (4)$$

where R_2 and R_1 are the radii of two interacting spheres in the case of sphere-sphere interaction. However, the equation (4) further simplifies in the case of sphere-plane interaction to $R_{eff} = R_{sphere}$. In the case of the AFM tip the spherical radius of the apex can be estimated from SEM images and from deconvolution data obtained from the cross-section of the AFM image.[17] Thus the normalized forces are prone to high inaccuracy as a result of poorly defined geometry and imprecise radius determination of the tip apex.

2.4. Application of direct force measurements

Force profiles determined in the described way are classically used for the determination of local adhesion, short- and long-range forces.[18-20] For example, using silicon nitride tip, H.-J. Butt probed the surfaces of mica and glass in aqueous solutions.[18] As was theoretically expected, he found an evidence for electrostatic diffuse double layer, vdW and hydration forces. In another study the aspects of bacterial adhesion was studied extensively.[21] There the dominating role of long-range electrostatic and steric interactions due to presence of polysaccharides at bacteria's interphase was revealed. Warszynski et al.[22] have shown that the interpretation of adhesion force as well as work of adhesion determined by an AFM tip can be done using the theory of condensed phases. The theory, which considers vdW and acid-base force components, is applicable for interaction between similarly solvated surfaces. Thus, by direct force measurements the evaluation of forces is possible in systems, which are related to Nanoscience, Material Science, or Biology to name a few.

Furthermore, by direct force measurements the mechanical properties of a sample can be determined.[23] From the experimental point of view this is achieved by nanoindentation of films or other colloidal systems, like microcapsules.[24,25] For instance, Horkay and Lin[26] were studying mechanical properties of PVA gels by employing AFM tip for indenation. In similar fashion the thickness of thin soft films can be determined as was demonstrated by Üzüm et al.[27]

The force curves obtained in different systems contain valuable information on the superposition of acting forces. In air such forces as electrostatic, van der Waals, capillary, and hydrophobic often dominate the observed interaction. In contrast to air, in liquid environment like electrolyte solution many more force contributions may manifest

themselves. They include solvation, structural, depletion, and other forces.[16] Moreover, the large part of publications on direct force measurements in liquid often addresses the description of forces resulting from the overlap of electrostatic diffuse double layers. Together with vdW force the latter is known as DLVO forces, described by Derjaguin-Landau-Verwey-Overbeek theory.[16,28] If a polymer layer is present between interacting bodies, then also steric interactions play significant role at low separation distances. Therefore analysis of interactions on a colloidal scale can deepen the understanding on the superposition of forces.

2.5. Colloidal probe technique and data interpretation

In order to relate measured forces to the interaction energy more precisely the AFM tip (cf. **Figure 5**a) could be replaced with a probe of defined interaction geometry. Colloidal particles of spherical shape are commonly used for this purpose (cf. **Figure 5**b). The cantilever with such a particle is called colloidal probe (CP) and the corresponding technique to measure forces at the nanoscale is known as colloidal probe technique or colloidal probe force spectroscopy (CPFS).
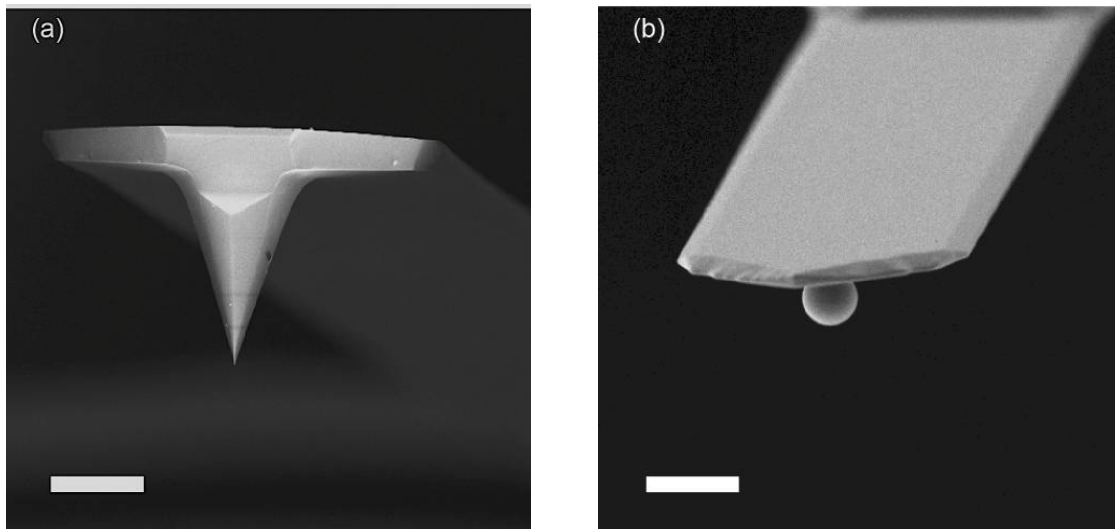
Figure 5: Scanning electron microscopy images[1] of (a) AFM Silicon-tip and (b) silica colloidal probe. Scale bar is 10 μm

Colloidal probes can be chosen from a wide range of materials.[29-33] The choice depends on the application and includes natural and synthetic materials. Furthermore, the size of the probe is limited from ca. 1 μm up to dozens of micrometers. Because the former is usually restricted with the optical microscope resolution, and the latter is in the

---

[1] Courtesy of Carmen Kunert

order of AFM cantilever width. Among colloidal probes made of natural materials cellulose beads, hair and skin pieces, even bacteria cells should be mentioned.[29-31,34] The natural material probes are object specific and may have large variation in their properties. By contrast, synthetic probes often possess stable chemical and physical properties. Examples of those include latex, glass, silica, alumina and zirconia colloidal beads.[32] Special place in this row belongs to silica particles, which have very high Young's modulus and their surface chemistry can be controlled by preparation method.[33]

Various methods have been described to prepare colloidal probes. To attach probes to the cantilevers a polymer-based glue is commonly used.[9] Therefore independently from the glue-curation method the possibility of contamination is present. Moreover, another aspect concerning cleanliness is the removal of suspension stabilizing surfactants, which are usually employed to protect colloid suspensions from coagulation. One way to overcome the problems associated with polymer- and surfactant-contamination is to use a sintering preparation method. For the first time it was demonstrated by Vinogradova et al.[35] for polystyrene spheres and soon afterwards by Bonaccurso et al.[36] for glass beads. In the latter experiment the sintering temperature was close to 800 ^{0}C at ambient atmosphere, that insured the burning out of any organic contaminations. However, in this method the contact area between a colloidal particle and a cantilever remains small, hence questions about mechanical stability could be raised.

The CPFS can be applied towards a number of practical and fundamental problems. For instance, the interparticle interaction potential can be accessed directly by sphere-sphere measurement (cf. **Figure 6**a) instead of indirect light scattering or rheological measurements.[37] In **Figure 6**b the interaction force between two silica particles as a function of separation distance in electrolyte solution is presented. Since particles from the same material have been used, they acquire same charge in electrolyte solution. Therefore due to the overlap of diffuse layers upon approach, the long-range forces are repulsive. The interaction force can be further converted into interaction energy per unit area of infinite planes W by the approximation initially published by Derjaguin in 1937:

$$W = F / (2\pi \cdot \mathrm{R}_{eff}),\qquad\qquad(5)$$

where the value of W is equal to normalized force (cf. **Figure 4**d) divided by 2π.[38] Thereby the interparticle interaction energy versus separation distance is deduced as shown in the insert of **Figure 6**b. In semi-logarithmic representation this curve appears linear, because the interaction between weekly charged colloids could be described by the

Gouy-Chapman-Stern theory, and thus the ionic distribution in diffuse layers obeys the Poisson-Boltzmann distribution. This allows for the fitting of the data by full Poisson-Boltzmann equation.[39]
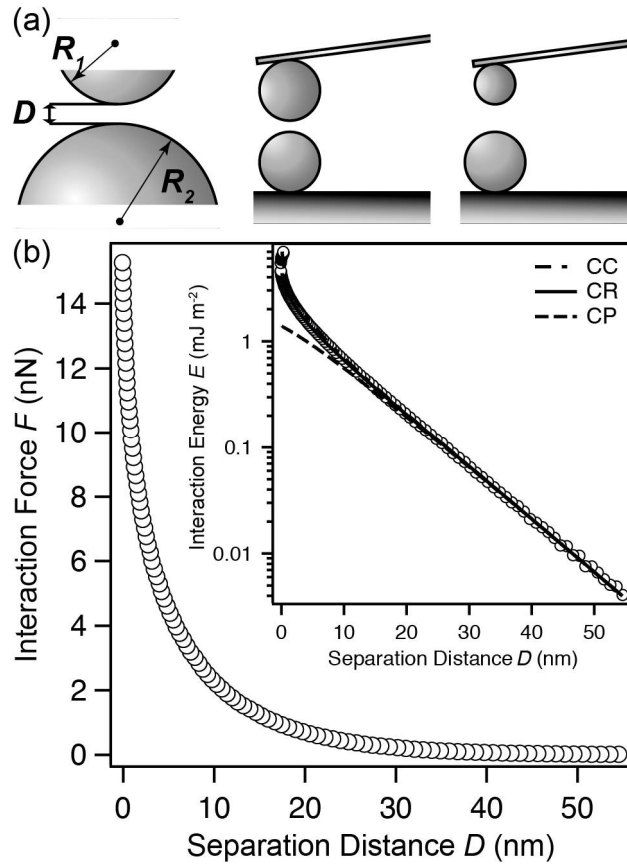
Figure 6: (a) Scheme for the interaction measurement between bodies of different geometries. (b) Interaction profile between two silica beads of 6.8 μm in diameter in electrolyte solution (I = 10^{-4}M, pH 4.7). Derjaguin approximation allows converting interaction forces into interaction energy by normalization on the effective interaction radius (b: insert). The interaction energy profile in the insert is fitted according to full Poisson-Boltzmann equation including constant charge (CC), constant potential (CP), and constant regulation approximation (CR) (reproduced from Rentsch et al.[40]).

The Gouy-Chapman-Stern theory originates from Gouy-Chapman model, which was developed in the beginning of XX century to describe ion distribution over charged surface in electrolyte solution.[41] It involves the Boltzmann's law, describing the distribution of charged species over the charged wall; and the Poisson equation, that relates a charge distribution with an apparent surface potential. Therefore its analytical expression is called Poisson-Boltzmann (PB) distribution. It is commonly expressed as[42]

$$\frac{d^2\psi(x)}{dx^2} = \frac{e}{\varepsilon\varepsilon_0}\sum_i n_i^0 z_i \exp\left(\frac{z_i e\psi}{kT}\right) \tag{6}$$

where $\varepsilon\varepsilon_0$ is the total permittivity of solvent, kT is the thermal energy at given absolute temperature, e is the elementary charge, n_i and z_i – volume concentration and charge of ionic species of type i. For a one-dimentional diffuse layer the surface diffuse layer potential (ψ^0) decay could be described by integration of eq. (6) with boundary conditions. Then in the direction perpendicular to a flat charged surface in $z{:}z$ electrolyte the potential (ψ) is given by eq. (7)[43]

$$\left(\frac{\tanh(ze\psi/4kT)}{\tanh(ze\psi^0/4kT)}\right) = \exp(-\kappa x) \tag{7}$$

where κ is a pre-factor, which characterizes the decay of the surface potential ψ^0 with increasing distance x from the surface. The reciprocal value of the pre-factor is known as Debye length[39]

$$\kappa^{-1} = \sqrt{\varepsilon\varepsilon_0 kT \Big/ 2N_A e^2 I} \tag{8}$$

where N_A is Avogadro's number, and I is the solution's ionic strength.

The PB equation (6) can be used as a starting point for the determination of electrostatic potential distribution $\psi(x)$ between two charged surfaces, yielding

$$\frac{d^2\psi(x)}{dx^2} = \frac{\kappa^2 kT}{e}\sinh\left(\frac{e\psi}{kT}\right) \tag{9}$$

As soon as such potential profile is known for surfaces in 1:1 electrolyte solution the disjoining pressure $\prod(x)$ between them can be found from[44]

$$\Pi(x) = 2n_i^0 kT[\cosh(e\psi/kT)-1] - \frac{\varepsilon\varepsilon_0}{2}\left(\frac{d^2\psi(x)}{dx^2}\right)^2 \tag{10}$$

This analytical solution relates the disjoining pressure between surfaces with their diffuse layer potentials under the assumption that one surface is situated at zero-distance of x-axis and the other is at a distance x.[45] Integration of the pressure over a given separation distance D gives the interaction energy per unit area $W(D)$[39]

$$W(D) = \int_{x=0}^{D} \Pi(x)\,dx. \tag{11}$$

The interaction energy $W(D)$ can be directly inferred from the experimental interaction force and the Derjaguin approximation (cf. eq. (5)). Thus, the model could be directly fit to the experimental force data.

It should be noted that in Gouy-Chapman model the surface potential (ψ^0) is considered identical to diffuse layer potential (ψ^D). The relation between ψ^D and diffuse layer charge density σ^D is commonly given by eq. (12), which is also known as Grahame equation[44]

$$\sigma^D = \varepsilon\varepsilon_0 \left(\frac{\partial\psi}{\partial x}\right)_{x=0} = (8kT\varepsilon\varepsilon_0 IN_A)^{1/2} \sinh\left(\frac{ze\psi^D}{2kT}\right). \tag{12}$$

The diffuse layer capacitance, which is considered to be identical to the total capacitance within the model[42], is given by

$$C_{GC}^{total} = C^D = \left(\frac{\partial\sigma^D}{\partial\psi^D}\right) = \left(\frac{2z^2e^2\varepsilon\varepsilon_0 IN_A}{kT}\right)^{1/2} \cosh\left(\frac{ze\psi^D}{2kT}\right). \tag{13}$$

In the model of Louis Gouy and David Chapman the diffuse double layer starts directly at the solid-liquid interface and consists of infinitely small ions.[46] Otto Stern extended this model by adding an adsorbed layer of ions of finite size.[42] As a result a total capacitance has to be described by two capacitances in series. Namely by internal layer capacitance C^I representing the rigid compact layer of adsorbed ions and the diffuse layer capacitance C^D:

$$\frac{1}{C^{total}} = \frac{1}{C^I} + \frac{1}{C^D}. \tag{14}$$

As a consequence two different surface potentials have to be distinguished. The potential ψ^0 at the interface or inner Helmholz plane (iHP) and the diffuse layer potential ψ^D originating at the outer Helmholz plane (oHP). In order to solve the Poisson-Boltzmann equation for two approaching surfaces, boundary conditions are necessary. Classically constant charge (CC) and constant potential (CP) approximations are used. However, in real systems the charge regulation takes place and those approximations fail to describe the situation at relatively short separation distances.[47]

Behrens and Borkovec[45] developed a simple approach, where the charge regulation is taken into account. They summarized the charge regulation of an interface by a single charge regulation parameter p:

$$p = \lim_{D\to\infty} p(D) = \frac{C^D}{C^D + C^I} \tag{15}$$

where D is the separation distance between surfaces. Hence in the case of asymmetric system the charge regulation of each surface should be accounted by corresponding charge regulation parameter. Numerically, the condition of constant potential corresponds

to $p = 0$, and that of constant charge corresponds to $p = 1$. The applicability of this approach to describe experimental data for colloidal systems has been demonstrated experimentally.[48]
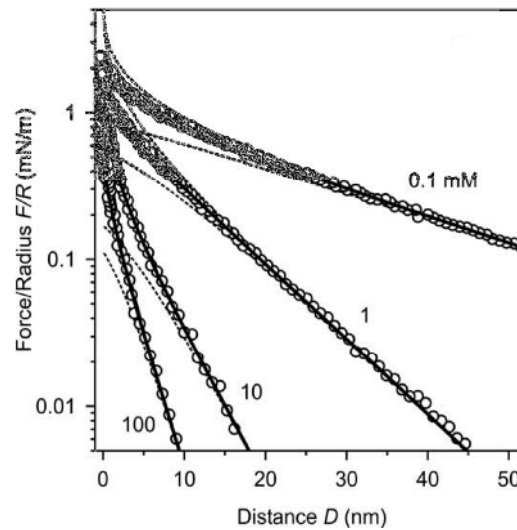
Figure 6b shows experimental data with fits according to full Poisson-Boltzmann equation including constant charge (CC), constant potential (CP), and constant regulation approximation (CR). As can be seen all three approximations describe the interaction profile well at large separation distances. Nevertheless, at close separation the CR approximation provides the most adequate description. In a symmetrical system there are only two fit parameters to be determined, namely the diffuse layer potential ψ^D and the charge regulation parameter p.[44]

The colloidal probes with known parameters can be further used for analytical purposes. After the "calibration" by determining the necessary parameters (ψ^D and p) of a colloidal probe in a symmetrical system, i.e. with sphere-sphere geometry one can determine those parameters for an unknown surface by fitting the corresponding interaction profiles determined in asymmetrical system. While fitting the latter the parameters for the colloidal probe are fixed. Then the fitted value of diffuse layer potential can be converted to apparent diffuse layer charge density, i.e. oHP charge density, using equation (12). If the sample surface has acquired the surface charge due to specific ion adsorption the latter equation is also called Grahame equation, because Grahame introduced for the first time the notion of specific and non-specific ion adsorption at an interface.[49] Hence an acquisition of force profiles on a sample locally allows resolving laterally the surface diffuse layer charge density. This is a noticeable advantage of colloidal probe technique in respect to electrokinetic and electrochemical methods.

As follows from eq. (8) the Debye length decreases with increasing ionic strength of solution. As shown in **Figure 7** the interaction profile between poly(ethylene imine) layers changes with changing ionic strength of the surrounding electrolyte solution. This alteration of the slope in semi-logarithmic representation corresponds to the change in charge screening effect characterized by Debye length. All profiles are repulsive because the surfaces are identical and hence have likewise charged electrostatic diffuse double layers.

Besides Debye length, also the effective diffuse layer potential decreases. The full Poisson-Boltzmann equation fits to the data presented in **Figure 7** shows that upon

increase of ionic strength from 10^{-4}M to 10^{-1}M the diffuse layer potential reduces from 58.2 mM to 7.4 mV. However, the charge regulation parameter demonstrates very weak dependence on the ionic strength if any.

Figure 7: Force-distance profiles obtained upon approach between poly(ethylene imine) (PEI) layers in aqueous solutions at pH 4 and different ionic strengths. Profiles are fitted according to the full Poisson-Boltzmann equation including constant charge (CC, dotted curve top), constant potential (CP, dotted curve bottom), and constant regulation (CR, solid line) approximations. The molecular mass of the PEI is ca. 2kDa. The fitted diffuse layer potential ψ^d and regulation parameter p for a single surface in the symmetrical system are as follows: (0.1mM) ψ^d = 58.2 mV and p = 0.69; (1mM) ψ^d = 31.6 mV and p = 0.69; (10mM) ψ^d = 15.2 mV and p = 0.76; (100mM) ψ^d = 7.4 mV and p = 0.78 (reproduced from Pericet-Camara et al.[50]).

The diffuse layer properties of surfaces depend not only on the presence of ionizable groups, but also on ion-adsorption in electrolyte solution. This effect can take place on inorganic interfaces, such as clays, as well as on organic interfaces of different surface energy. It is especially pronounced for hydrophobic surfaces in aqueous solutions, where the charging mechanism remains under discussion.[51-54] This question has been addressed by various experimental techniques. On the one hand, at the presence of a positively charged acidic interface indicated some results of molecular dynamic simulations and vibrational sum-frequency spectroscopy.[51,55,56] On the other hand, the existence of basic interface is supported by electrokinetic[57-62] and other spectroscopic experimental data[54,63] and is supported by some theoretical studies[64,65]. To provide further background for precise theoretical modeling alternative experimental approaches are in demand.

2.6. Adhesion and short-range forces

In addition to long-range forces the forces acting only during contact of two bodies are extensively studied (cf. **Figure 8**a). [66,67] The latter play essential role in composite manufacturing process, paper making, colloidal transport in soils, friction between solids. In solution a number of forces typically ascribed to short-range forces.[68,69] To this category may belong various combinations of solvation[70] and structural[71] forces as well as forces due to chemical bonds[72] to name just a few. They can be identified upon approach of two colloidal bodies shortly before their contact and by forces necessary to separate those bodies being in contact with each other. The short-range forces are acting primarily from the contact area (cf. **Figure 8**a).[16]

Although the short-range forces make significant contribution in adhesive properties of a material, the adhesion comprises both short- and long-range forces. Thus, all forces contribute to the total adhesive force. Generally, the work of adhesion is described as the work needed for separation between two colloids from contact to infinity in a given medium.[9,66] Often for two solids it is given by the so-called pull-off force F_a (cf. F_a/R **Figure 8**b). The latter represent the maximum applied force needed for the sample-probe separation, which can be readily measured upon retraction in a direct force measurement experiment. To describe the pull-off force obtained in this way various continuum models of contact mechanics can be applied. Two the most commonly used are the JKR model (Johnson-Kendal-Roberts) and DMT model (Derjaguin-Müller-Toporov).[9] Their limitation is based on the assumption that elastic deformation of bodies in contact agrees with the prediction of Hertz model.[16] Furthermore, both models presume the scalability of the force with the effective radius R_{eff} of interaction.[38] However, they consider different ranges of interaction forces to bring dominant contribution. In the JKR model it is assumed that only the short-range interactions acting in the contact area contribute to the pull-off force (**Figure 8**a):

$$F_a = -(3/2) \cdot \pi R_{eff} W_a, \qquad (16)$$

where W_a is the work of adhesion per unit contact area. For the DMT model the short-range forces are neglected, and only the long-range forces outside the contact area are assumed to contribute to the total interaction force (**Figure 8**a). In this case the pull-off force is given by

$$F_a = -2 \cdot \pi R_{eff} W_a. \qquad (17)$$
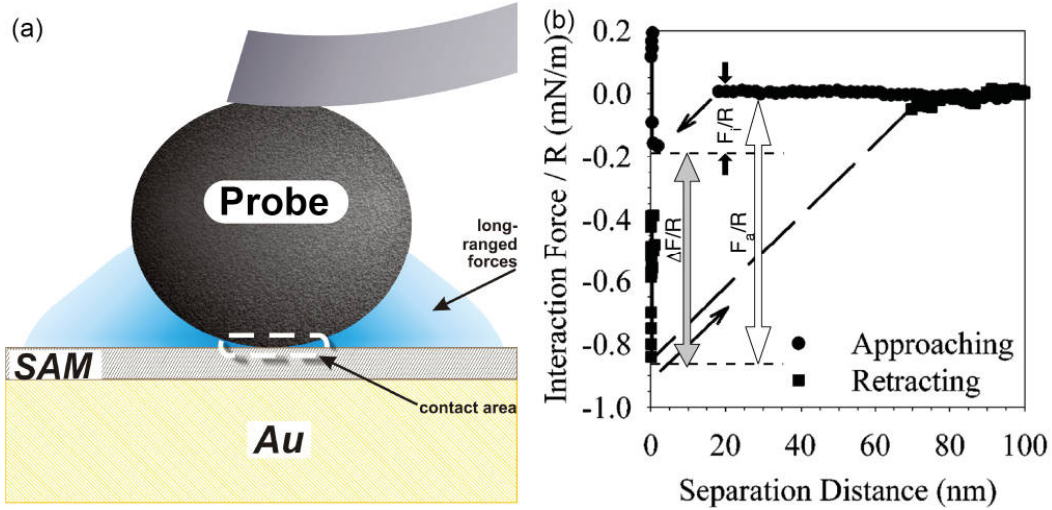
Figure 8: Adhesion force measurements with colloid probe force microscopy. (a) A scheme showing the adhesion contributions between colloidal probe and a crystalline self-assembled monolayer in liquid. (b) Example of force-distance profiles between glass surface and glass 40 mkm-sphere in electrolyte solution at pH 2, I=0.2M. Profiles obtained upon approach and upon retraction are presented. Black arrows indicate the direction of the cantilever movement during the instability jumps (adapted from Adler et al.[73]).

In order to decide, which model to apply for a particular system Daniel Maugis[67] has developed a simple indicator by means of the following dimensionless parameter λ:

$$\lambda = \frac{64}{3\pi D_0} \sqrt[3]{\frac{W_a^2 R_{eff}}{4\pi E_{tot}^2}} . \qquad (18)$$

where E_{tot} is the reduced elastic modulus of the system, D_0 is the equilibrium separation of the surfaces in contact, and W_a is the adhesion energy predicted by the Young-Dupré theory as

$$W_a = \gamma_{sample/H_2O} + \gamma_{probe/H_2O} - \gamma_{sample/probe}. \qquad (19)$$

where $\gamma_{i/j}$ are the interfacial energies of a probe and a sample in aqueous solutions. While at $\lambda \to 0$ the DMT model describes the observed forces more appropriately, at $\lambda \to \infty$ ($\lambda > 10$) the JKR would provide a better description. That means in the case of small R_{eff} and stiff samples, where the deformation of a sample can be neglected, the DMT model can be applied. For large R_{eff} and soft samples the JKR model is commonly used. Thus, most of the surfaces represent some intermediate situations between two limiting models and the more general Maugis theory has to be applied.

By colloidal probe technique the pull-off forces can be measured together with the interaction force profile upon approach.[7,72] For example, Giesbers et al.[32] studied interactions between acid- and base-functionalized surfaces on the system of two self-

assembled monolayers terminated in amino $-NH_2$ and carboxy $-COOH$ groups. They found a strong correlation between the long-range forces and the ionization state of groups on interacting surfaces, which can be explained on the basis of DLVO theory. However, also the adhesion between $-NH_2$ and $-COOH$ terminated surfaces appeared to be pH-dependent. Giesbers et al. attributed this adhesive behavior to the presence of both acid-base interactions and hydrogen bonds. The adhesion due to the former was comparable to work of adhesion calculated from DMT model.[32] Nalaskowski et al.[74] measured the interaction between polyethylene spheres and silicon wafers in electrolyte solutions. They found that the pull-off force increases either upon thermal treatment of the silicon wafer or upon silanization with a hydrophobic self-assembled monolayer of the wafer. By employing the Lifshitz/van der Waals-Lewis acid/base interaction theory a semi-quantitative explanation of the observed forces was given.[74] Those examples show that though the interpretation of pull-off forces can be successfully achieved, the separation of force contributions in adhesion remains obscure.

In addition to the pull-off force the maximum sample-probe force F_i determined from approach profile can reveal valuable information about different contributions in the total interaction (cf. F_i/R **Figure 8**b). Namely, the adhesive force contribution due to diffuse layer overlap, van der Waals and hydrophobic forces can be evaluated. However, well-known "jump-in" effect does blur such effort as shown by the black arrow on the approach curve in **Figure 8**b.[75] To overcome this limit a sufficiently stiff cantilever can be used for measurements, though some sensitivity is lost.[9] Alternatively, the active "feed-back" system[76] or dynamic force spectroscopy[77] has to be used. The latter two approaches appear to be most used to measure forces without instabilities.[9]

To separate different force contributions to the pull-off force, various approaches have been reported. For instance, by the variation of solution composition one can separate forces with electrostatic origin.[78] The influence of the substrate's surface chemistry can be addressed by the functionalization of surface with thin layers terminating in different groups.[79] Alternatively, the external forces may be employed to compensate for some intrinsic forces, like van der Waals or electrostatic diffuse layer forces.[8,80,81] As would be expected the superposition of those principles could further clarify the ascribing of various contributions to the pull-off force in a particular system.[48]

The surface roughness makes a quantification of the adhesive properties more difficult. There are many experimental and theoretical studies where the reduction of adhesion due to roughness effect has been reported.[71,82-85] Depending on the actual system

the typical reduction of experimentally determined work of adhesion reaches 20 – 200 times. In order to correct for the influence of roughness a number of models have been proposed.[75,82,86,87] Approaches developed by Rumpf[86], Rabinovich[82,87] and Cooper[75] are often used for this purpose. A recent review on the various models provides a comprehensive overview.[88] Thus, the reduction of forces acting in contact region due to surface roughness could be accounted for. However, if repulsive long-range forces dominate the sample-probe interaction, then no pull-off force or attractive force can be detected.[29]

Further it should be noted, that the surface roughness influences also long-range forces. For example Valtiner et al.[89] found that the strength of the electrostatic diffuse layer decreases if the roughness of substrate is increased. In their work the interaction between golden electrodes of different roughness and atomically smooth mica covered with self-assembled monolayer was studied. It was shown that the apparent diffuse layer potential decreases drastically with the increase of rms roughness from 3 to 12Å, though further increase until 17Å produced little effect.[89]

2.7. Adhesive properties of organic surfaces by AFM & Electrochemistry

Tuning the adhesive properties of organic interfaces is of high importance for a number of industrial and medical applications such as water purification or in artificial hearts, which pump the blood.[47,90] Therefore studying fundamental questions of their adhesive behavior promise to increase the effectiveness of purification processes and better predict biocompatibility of synthetic organic materials. As discussed earlier the defined variation of different force contributions would provide a possibility to better understand the adhesive properties of an interface and to tune the adhesion accordingly. In particular, one system that enables flexible change of short- and long-range interaction forces is an electrode covered with organic layer (cf. **Figure 9**a), which is impermeable for ions and solvent molecules. A suitable layer for this purpose is self-assembled monolayer (SAM) made by employing thiol chemistry on noble metal electrode.[91-96] Changing the groups terminating an SAM may additionally alter the interfacial properties of the organic surface designed in this manner. Indeed, as Vezenov et al.[97] have shown the adhesion over self-assembled monolayers depends on the nature of terminating group.

Interaction forces over a potentiostatically-controlled electrode have been studied previously either for bare gold electrodes or other electrode materials.[80,98,99] Studies with AFM on modified electrodes have been reported more rarely. [48,89,100,101] In attempt to

describe the diffuse layer of such electrodes models from electrochemistry can be applied.[48,93,101-103] Rentsch et al.[48] have successfully applied two-capacitor model shown at **Figure 9**b to describe the variation of diffuse layer potential with externally applied potential over non-ionizable SAMs. However, this approach would accommodate neither surface dissociable groups, nor interfacial ion adsorption. Moreover, the models describing metals modified with non-conductive oxide layer or semiconductive modification layer could be appropriate for interfacial charging behavior of SAMs as well.[104,105] Additionally electrocapillary effects may have to be taken into account for such systems.[8]
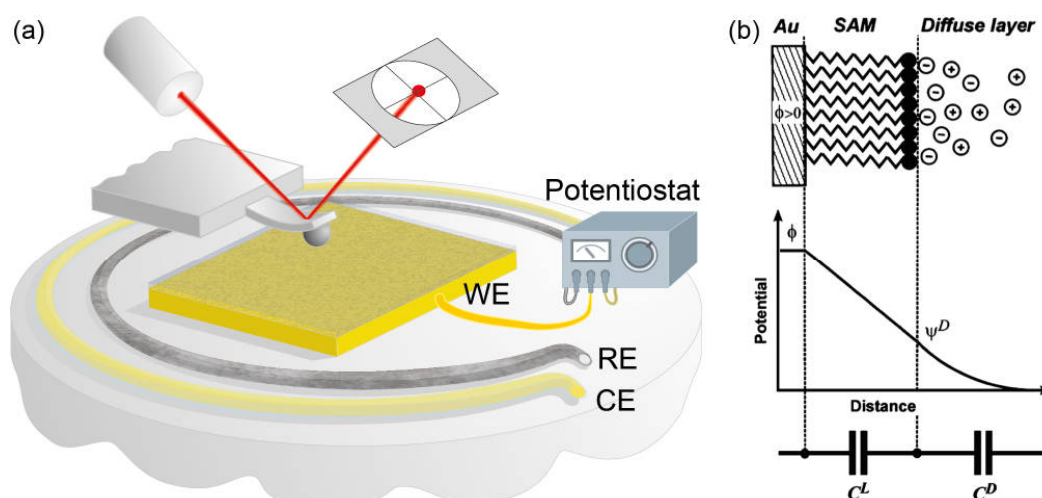
Figure 9: (a) Schematic representation of colloid probe force microscopy with electrochemical setup, which consists of working (WE), counter (CE) and reference (RE) electrodes. The WE is modified with covalently bound SAM. (b) Simple two-capacitor model can be employed to describe the electrode with SAM terminated in non-ionizable groups. (reproduced from Rentsch et al.[48]).

The electrostatic diffuse layer forces may be tuned externally by a potentiostat.[48] By designing the system, where those forces play substantial role in the total adhesive force, a possibility to alter the latter in a controllable manner emerges. For example, Campbell and Hillier[106] probed the adhesion on glassy carbon and sulfonate-derivatized poly(aniline)-coated electrodes by silica colloidal probe in electrolyte solution. As shown in **Figure 10** the pull-off force changes with applied potential for both electrodes in a narrow region of external potentials. Outside this region the force remains unchanged at characteristic plateau values. By fitting the data to titration-like curves they found the values corresponding to potentials of zero charge. The increase in adhesion against negatively charged probe with increasing potential (cf. **Figure 10**a) and b)) was attributed to domination of the electrostatic forces.[106]
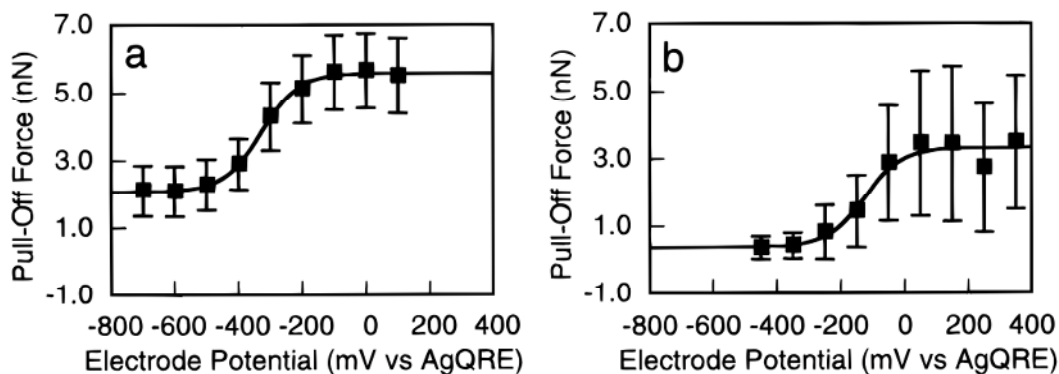
Figure 10: Dependence of pull-off force on the electrochemical potential determined between colloidal silica sphere and (a) bare glassy carbon and (b) sulfonate-derivatized poly(aniline)-coated electrodes in electrolyte solution (pH 5.2, I = 1mM). Each data point represents the average of 256 force curves, and the error bar is the standard deviation. The solid lines represent least squares fits to a titration curve. These curves give "half-wave" potential E_0 values of -341 and -100 mV for plots (a) and (b), respectively (reproduced from Campbell and Hillier[106]).

The dependence of adhesion force on applied potential theoretically can originate from various phenomena depending on the applied potential and the nature of the electrode:[100,107,108] 1) electrophoretic effect; 2) electrocapillarity effect, i.e. via change of interfacial tension of the electrode; 3) alteration of diffuse layer forces via interfacial polarization. However, the first effect is likely to be small at low applied potentials because the alteration of F_a/R is hardly possible within capacitive currents if the electrode interface is polarized chemically or due to adsorbed ionic species, where the adhesion plateaus are observed (cf. **Figure 10**).[98,107] The observations by Arai et al.[98] support this notion. They found that the interaction profiles between bare gold electrode and silicon nitride tip in basic solutions (pH > 10) depend on properties of diffuse layer given by electrolyte composition rather than on the magnitude of externally applied potential. Moreover, the electrocapillarity phenomenon for modified electrode is likely to be small in low potential regime, which is accessible by SAM-covered electrode.[109] By contrast, for bare electrode it may manifest itself. For example, the variation of interfacial tension for gold- and platinum-coated cantilevers in electrolyte solution has been demonstrated by Raiteri and Butt.[110]. Therefore, in the absence of electrophoresis and electrocapillarity the adhesion will depend on the alteration of potentiostatically-controlled diffuse layer properties.

Despite the large number of studies available, where the combination of electrochemistry and AFM have been used for imaging purposes, only a limited number of them are devoted to direct force measurements under potentiostatic control.[111] The first

studies of electrode systems by direct force spectroscopy were published almost simultaneously in 1996 by Arai et al.[98], Raiteri et al.[80], and Hillier et al.[99] While Arai and Raiteri used a silicone nitride tip to identify semi-quantitatively the interfacial forces on noble metal electrodes under potentiostatic control, in the work of Hillier the quantitative evaluation of forces over gold electrode by means of a colloidal probe was pursued. In all those studies the general agreement with DLVO theory of the observed interaction profiles has been confirmed. The variation of interaction force profiles has been observed mainly within a few hundreds of millivolts around the potential of zero force (pzf), i.e. the potential where long-range forces were negligible.(Raiteri, 1996, r11591; Arai, 1996, r02085; Hillier, 1996, r02750} The tuning of overall interaction from repulsive to attractive was demonstrated, unless the electrodes were polarized by specific adsorption of ions at high concentration.[98] Furthermore, the phenomenon of specific anion adsorption at the Stern layer on bare metal electrode was observed by force measurements, and qualitative results were additionally verified by differential capacity measurements.[99] However, at the time it remained unclear how the reduction of effective electrode potential down to ca. 10% of initial value happens.[80]

Later studies of modified and unmodified electrodes by direct force measurements were focused on theoretical aspects of electrostatic control of interface as well as practical application issues.[89,101,106,108,112-114] For example, Serafin and Gewirth[112] demonstrated a correlation between the redox state of the interfacial layer and the pull-off force. In this study the interaction between a silicon nitride tip and Au (111) has been measured in basic aqueous solution. According to authors this finding might be useful for monitoring the adsorption of electroactive species. Indeed, this principle was demonstrated later by adsorbing thiol molecules under potentiostatic control by Kwon and Gewirth.[113] They found that the coverage by electrochemically adsorbed ethanethiol and hexadecane thiol on the gold electrode could be characterized by measuring the pull-off force. Moreover, in the study of Campbell and Hillier[106] not only adhesive properties of electrodes were addressed, but also friction properties. It was the first work, where adhesive and friction properties of modified electrodes were studied. The variation of friction coefficients was found very dissimilar for bare and modified electrodes. The authors attributed the difference to significant variation in potential-dependent charging behavior of studied interfaces in electrolyte solutions and to variation in their elastic properties.[106]

2.8. Diffuse layer properties of modified electrodes by AFM

As mentioned before the various diffuse layer properties could be addressed by direct force measurements in combination with electrochemistry. Tuning of diffuse double layer charge potentiostatically and hence of the corresponding forces allows studying charging phenomena, which happen at electrode's interface.[81,100,101,103,106,111,115-126] On bare electrode interaction force profiles vary significantly within the 100 - 1500 mV around the pzf.[101,119-126] Beyond that region the saturation of force is observed.[115] In other words, the sigmoidal shape of properties as a function of applied potential is commonly observed (cf. **Figure 10**). Electrochemically this means that the capacitive limit of electrode's diffuse layer is reached at potentials corresponding to plateau values. By contrast to bare electrodes, the "active" range of potentials is noticeably smaller in systems with an electrode modified with a blocking dielectric layer. For instance, Hu et al.[100] found for an Au-electrode modified with ferrocene-terminated SAM that the "active" force-variation potential window is only around 300 mV wide at 1 mM of total ionic strength and pH $\approx$ 6. However, for bare gold electrode this range extends beyond 1200 mV as reported by Hillier et al.[99] for similar conditions (cf. **Figure 11**a). Thus, the range of tunable forces on bare electrodes is larger than on modified electrodes, though it depends on solution conditions. If the interface is polarized at high concentration of specifically adsorbed ions, the electrodes properties are purely determined by this layer of ions.[101,112]

In **Figure 11**a a set of force-distance profiles as a function of applied potential is presented. The profiles were determined upon approach between silica colloidal probe and Au-electrode in electrolyte solution.[99] As can be seen the electrostatic repulsion decreases with increasing applied potential towards the electrode. From every curve a diffuse layer properties can be obtained by applying Gouy-Chapman-Stern (GCS) theory for asymmetrical system if the diffuse layer parameters of the probe are known.[127] For example, Barten et al.[121] determined diffuse layer potentials of Au-electrode in electrolyte solutions by fitting full Poisson-Boltzmann equation to the experimental force profiles taking into account constant charge approximation. In **Figure 11**b the resulting diffuse layer potential dependences on external potential are presented for various pH of the solution.
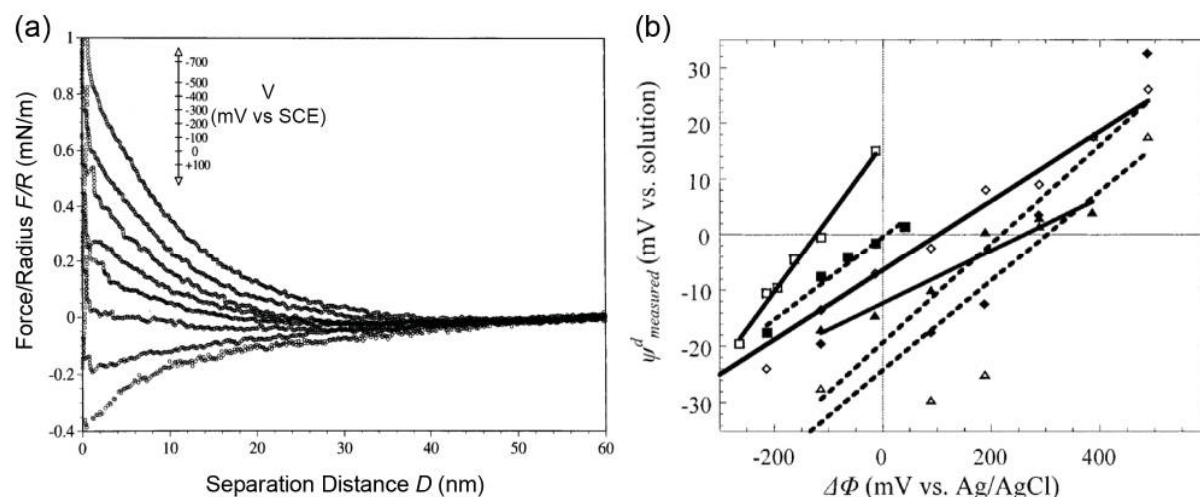
Figure 11: (a) Interaction force profiles determined upon approach between silica colloidal probe and Au-electrode as a function of externally applied potential in electrolyte solution ($I = 1$ mM, pH 5.5). Electrostatic repulsion decreases as the electrode potential increases from -700 to 100 mV vs SCE (reproduced from Hillier et al.[99]). (b) Dependence of diffuse layer potential of Au-electrode on externally applied potential in electrolyte solutions ($I = 1$ mM) with different pH values: ⊚, pH 3.5; ■, pH 3.9; ◇, pH 4.7; ◆, pH 5.1; △, pH 6.4; ▲, pH 6.8. The diffuse layer potentials were determined by fitting the full Poisson-Boltzmann equation with constant charge approximation to the force data. The lines are only meant to guide the eye (reproduced from Barten et al.[121]).

The validity of GCS theory can be evaluated by applying an external potential to an electrode in a much more unambiguous manner than for non-conductive inorganic or polymer surfaces. Recent studies by AFM have claimed some limitations of this theory.[119-121] One point is that the external electronic potential ϕ drops by around 90-97% to apparent diffuse layer potential ψ^D as demonstrated for gold[81,98,121] glassy carbon[106] copper[117] n-type TiO$_2$ single-crystal[115] electrodes. Another point was the increased apparent experimental decay length in attractive interactions induced by potentiostat between bare platinum and silicon nitride tip.[80] This apparent value appears to be bigger than the theoretical Debye length and also in comparison with decay length of repulsive force profiles. However to fit those attractive profiles only the classical boundary condition of constant potential was used, which might have limited use in this case. Possible solution to this problem lies in employing charge regulation approach. That is possible by considering charge regulation approximation while fitting of force curve[39] or by interpreting the apparent diffuse layer potentials using amphifunctional charging mechanism.[121]

Nevertheless, the comparability of diffuse layer properties, determined by electrochemical measurements and direct force measurements, suggests the applicability

of the GCS theory within the reasonable limits. Firstly, the pzf, which is close to isoelectric point, corresponds to the minimum of differential capacitance.[99] Secondly, the diffuse layer capacitance over modified electrodes determined by force measurements appears close to the one obtained from transient electrochemical techniques.[48]

Furthermore, the mechanisms, which lead to the reduction of electronic potential to apparent diffuse layer potential at metal-liquid interface, have been pointed out. Earlier the non-specific ion adsorption was mentioned to compensate the high electric charge on bare electrode.[99] Later a number of studies by Bard[119,120] indicated on more complex phenomena at the interface. For example, Wang et al.[119] assumed ion correlation and ion condensation effects to play a role in the charging of electrode interface and in building up of the diffuse layer. In order to decouple those effects on modified electrode, the modification layer must possess sufficiently high blocking qualities.[120]

SAMs of sufficient aliphatic chain length provide highly blocking electrochemical properties.[128-131] In the case of thiol-based SAMs on noble metals the dense packing of hydrocarbon tails can be achieved with aliphatic chain possessing more than 9 carbon atoms.[95] As can be seen from **Figure 12**(a-d), where the cyclic voltammograms of bare and HS-$(CH_2)_{17}$-CH_3-coated gold electrodes are presented, the oxidation of gold and the following oxide-stripping currents are suppressed to a large degree upon surface modification with the SAM. Longer adsorption times lead to maturity of the SAM, and hence the blocking properties are enhanced (b-d). Thus, no reduction of Cu^{2+}(e) and Fe^{3+}(f) occurs even at high overpotential.
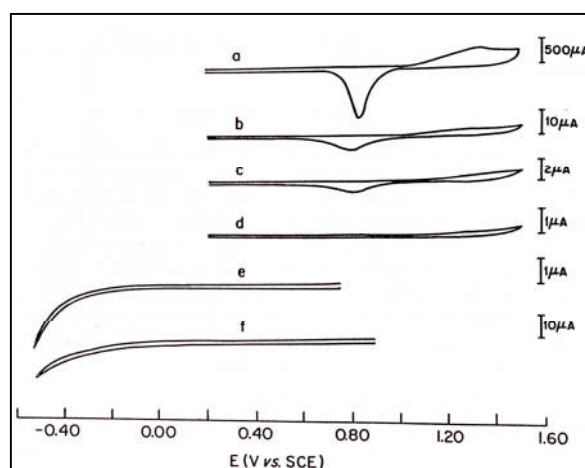
Figure 12: Cyclic voltammograms of bare and $HSC_{17}CH_3$-coated gold electrodes in 0.1 M H_2SO_4; scan rate 0.1 V/sec, electrode area 1 cm^2 (a-d) or 0.6 cm^2 (e,f). (a) Bare gold sputtered on glass and thermally annealed; (b) after 2 hr of modification in 10 mM ethanolic solution; (c) after an additional 1-hr modification; (d) after an additional 0.5-hr modification; (e) the electrode of (d) in 1.0 mM Cu^{2+};

(f) the same electrode in 3.0 mM Fe^{3+} (reproduced from Ref.[132]). Self-assembled films of thiols on gold reveal highly blocking electrochemical properties after sufficient deposition time as demonstrated by cyclic voltammetry.

By appropriate technique, such as template stripping methods, metal electrodes with low surface roughness can be obtained.[133] Alternative techniques include polishing and a self-cleavage. Moreover, highly homogeneous coverage of the noble metal surface can be achieved by means of self-assembled monolayers.[131]Electrodes modified in this manner have the desired functional groups and retain the roughness of the substrate, though some defects may be present.[134,135] Due to mentioned advantages SAMs are well-suited model systems for studying of various organic interfaces.[95,102]

To study surface forces and phenomena at organic interfaces SAM-covered electrodes represent a well-defined surfaces. Because the functional groups terminating the SAM can alter the interfacial properties, the system appears also to be very versatile. The approach to study such model systems with direct force measurement promises to extend the knowledge about adhesive behavior and specific ion adsorption at the interface. Due to tunability of diffuse layer properties by external potential the double layer forces may vanish or compensate other forces. Thus, different force contributions in adhesion may be studied separately.

2.9. Mechanical properties of ultrathin organic films

The increasing trend toward miniaturization of electro-mechanical devices leads to a decrease of functional coating thickness down to a few nanometers.[136,137] However, the simple assumption that mechanical properties remain similar to the bulk material often fails.[90] The reliability of properties such as elasticity can be crucial in applications ranging from corrosion protection to substrate-dependent adhesion of biological cultures. Therefore, the reliable estimation of ultrathin film properties is a prerequisite for designing advanced nanomaterials.

AFM-based setups for measuring mechanical properties by micro- and nanoindentation emerged soon after the invention of AFM in 1980s, though only in the end of 1990s they became popular in both biology and material science.[9,138] Up to now most of the experiments are performed with standard AFM tips. Nevertheless, those tips have poorly defined geometry and hence the resulting data are prone to high inaccuracies.[138] To improve the accuracy of the data one solution is to employ professional nanoindentation kits, which can be combined with existing AFMs. Another

solution is to use colloidal probes with micrometer-sized particles of known shape. In this case the range of materials, which can be indented, is determined by the stiffness of the cantilever.[9] Due to defined geometry and adjustable stiffness of the indenter the colloidal probe technique can be considered accurate and it is in particular very versatile for nanoindentation of soft films.[23,139]
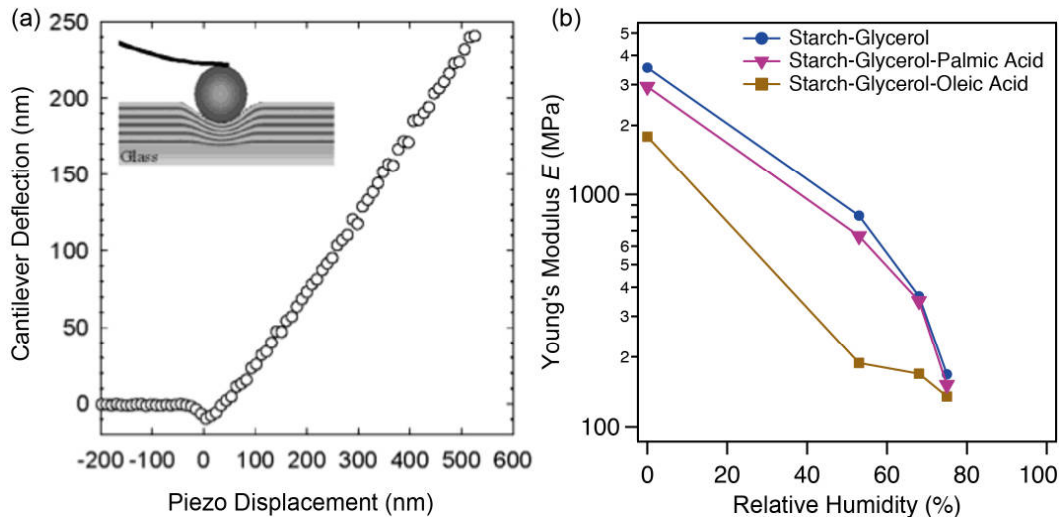
Figure 13: Elasticity measurements with colloidal probe force microscopy. (a) An exemplary force versus indentation curve with theoretical fit by modified Hertz model (reproduced from Richert et al.[140]). (b) Dependence Young's modulus on relative humidity of Starch films with different types of plasticizers (T = 298K). The mass ratios of Starch : Glycerol : Acid are 1 : 0.25 : 0.15. The lines represent eye-guide only (adapted from Jimenez et al.[141]).

The data acquisition for indentation experiment conducted with AFM is practically identical to direct force measurements. However, the force-displacement data are converted to loading force versus indentation depth. Various systems have been studied by this technique, though the most common are biological samples and polymeric coatings.[66] For example, Hassan et al.[24] studied semi-quantitatively the elasticity of living cells and obtained images of mechanical response with a good contrast for many species. As demonstrated by Lisunova et al.[142] the Young's modulus of polyelectrolyte multilayers varies from dozens-hundreds of kPa in the swollen state up to hundreds of MPa in dried one; while for hydrogels used as scaffolds for cell culturing the Young's modulus is typically within 1-100 kPa range.[27,66,143] In **Figure 13**a an example force-distance curve of a multilayer indented by a spherical probe is presented.[140] After taking into account bending of the cantilever, the resulting curve may be fitted by different models that assume linear or nonlinear elastic behavior of the sample.

To analyze indentation data obtained by the colloidal probe technique for synthetic quasi-homogeneous materials the Hertz model, based on the assumption of linear elasticity, is widely used.[138] However, this model has been criticized for its inaccuracy due to some limitations.[144] Nevertheless, Lin et al.[145] have recently shown, that this model can be used for description of the measured force versus indentation if two conditions are matched: low indentation strain (<20%) and indentation depth sufficiently higher than the surface roughness. In this case the indentation force profiles can be fitted by Hertz model with a small mean square error. Moreover, it was shown that models assuming non-linear elasticity (e.g. Mooney-Rivlin, Ogden, and Fung) provide similar description to constrained Hertz model if the number of fittable variables remains equal.[145]

The nanoindentation experiments are commonly performed under ambient conditions. While some polymers can adsorb moisture from the air, the condensed water may act as a plasticizer in a polymer film. Thus, the relative humidity may determine the apparent stiffness of multilayer film. As demonstrated by Jiménez et al.[141] the relative humidity has larger effect on the stiffness of the Starch-Glycerol film, than addition of plasticizers (cf. **Figure 13**b) Control of moisture-related change of mechanical characteristics promises also to improve the durability of packaging materials and stability of microelectromechanical devices.[146] Nevertheless, until now few studies have addressed the mechanical response of ultrathin film systems under controlled environmental conditions.

1.   Binnig, G., Rohrer, H., Gerber, C. & Weibel, E. Surface Studies by Scanning Tunneling Microscopy. *Phys. Rev. Lett.* **49**, 57-61 (1982).

2.   Binnig, G., Quate, C. F. & Gerber, C. Atomic Force Microscope. *Phys. Rev. Lett.* **56**, 930-933 (1986).

3.   Israelachvili, J. N. & Adams, G. E. Direct Measurement of Long Range Forces between Two Mica Surfaces in Aqueous KNO3 Solutions. *Nature* **262**, 774-776 (1976).

4.   Ralston, J., Larson, I., Rutland, M. W., Feiler, A. A. & Kleijn, M. Atomic Force Microscopy and Direct Surface Force Measurements (IUPAC Technical Report). *Pure Appl. Chem.* **77**, 2149-2170 (2005).

5.   Frederix, P. Atomic Force Bio-analytics. *Current Opinion in Chemical Biology* **7**, 641-647 (2003).

6.   Meyer, E., Hug, H. J. & Bennewitz, R. *Scanning Probe Microscopy* (Springer, 2003).

7.   Cappella, B. Force-Distance Curves by Atomic Force Microscopy. *Surface Science Reports* **34**, 1-104 (1999).

8.   Papastavrou, G. Combining Electrochemistry and Direct Force Measurements: From the Control of Surface Properties towards Applications. *Colloid Polym. Sci.* **288**, 1201-1214 (2010).

9.   Butt, H.-J., Cappella, B. & Kappl, M. Force Measurements with the Atomic Force Microscope: Technique, Interpretation and Applications. *Surface Science Reports* **59**, 1-152 (2005).

10. Senden, T. J. Force Microscopy and Surface Interactions. *Current Opinion in Colloid & Interface Science* **6**, 95-101 (2001).

11. Hutter, J. L. & Bechhoefer, J. Calibration of Atomic-Force Microscope Tips. *Rev. Sci. Instrum.* **64**, 1868-1873 (1993).

12. Sader, J. E., Larson, I., Mulvaney, P. & White, L. R. Method for the Calibration of Atomic Force Microscope Cantilevers. *Rev. Sci. Instrum.* **66**, 3789-3798 (1995).

13. Chon, J. W. M., Mulvaney, P. & Sader, J. E. Experimental Validation of Theoretical Models for the Frequency Response of Atomic Force Microscope Cantilever Beams Immersed in Fluids. *J. Appl. Phys.* **87**, 3978-3988 (2000).

14. Cleveland, J. P., Manne, S., Bocek, D. & Hansma, P. K. A Nondestructive Method for Determining the Spring Constant of Cantilevers for Scanning Force Microscopy. *Rev. Sci. Instrum.* **64**, 403-405 (1993).

15. Green, C. P. et al. Normal and Torsional Spring Constants of Atomic Force Microscope Cantilevers. *Rev. Sci. Instrum.* **75**, 1988 (2004).

16. Israelachvili, J. N. *Intermolecular and Surface Forces* (Academic Press, 2011).

17. Raşa, M., Kuipers, B. W. M. & Philipse, A. P. Atomic Force Microscopy and Magnetic Force Microscopy Study of Model Colloids. *J. Colloid Interface Sci.* **250**, 303-315 (2002).

18. Butt, H. J. Measuring Electrostatic, Van der Waals, and Hydration Forces in Electrolyte Solutions with an Atomic Force Microscope. *Biophys Journal* **60**, 1438-1444 (1991).

19. Butt, H. J., Jaschke, M. & Ducker, W. Measuring Surface Forces in Aqueous Electrolyte Solution with the Atomic Force Microscope. *Bioelectrochemistry and Bioenergetics* **38**, 191-201 (1995).

20. Abu-Lail, N. I. & Camesano, T. A. Polysaccharide Properties Probed with Atomic Force Microscopy. *Journal of Microscopy* **212**, 217-238 (2003).

21. Camesano, T. A. & Logan, B. E. Probing Bacterial Electrosteric Interactions Using Atomic Force Microscopy. *Environmental Science & Technology* **34**, 3354-3362 (2000).

22. Warszyński, P., Papastavrou, G., Wantke, K. D. & Möhwald, H. Interpretation of Adhesion Force between Self-Assembled Monolayers Measured by Chemical Force Microscopy. *Colloids and Surfaces A: Physicochemical and Engineering Aspects* **214**, 61-75 (2003).

23. Gouldstone, A. et al. Indentation Across Size Scales and Disciplines: Recent Developments in Experimentation and Modeling. *Acta Materialia* **55**, 4015-4039 (2007).

24. A-Hassan, E. et al. Relative Microelastic Mapping of Living Cells by Atomic Force Microscopy. *Biophys. J.* **74**, 1564-1578 (1998).

25. Fery, A., Dubreuil, F. & Möhwald, H. Mechanics of Artificial Microcapsules. *New Journal of Physics* **6**, 18-18 (2004).

26. Horkay, F. & Lin, D. C. Mapping the Local Osmotic Modulus of Polymer Gels. *Langmuir* **25**, 8735-8741 (2009).

27. Üzüm, C., Hellwig, J. & Madaboosi, N. Growth Behaviour and Mechanical Properties of PLL/HA Multilayer Films Studied by AFM. *Beilstein Journal of Nanotechnology* **3**, 778-788 (2012).

28. Leckband, D. & Israelachvili, J. Intermolecular Forces in Biology. *Q. Rev. Biophys.* **34**, 105-267 (2001).

29. Notley, S. M. & Norgren, M. Measurement of Interaction Forces between Lignin and Cellulose as a Function of Aqueous Electrolyte Solution Conditions. *Langmuir* **22**, 11199-11204 (2006).

30. Stiernstedt, J., Brumer, H., Zhou, Q., Teeri, T. T. & Rutland, M. W. Friction between Cellulose Surfaces and Effect of Xyloglucan Adsorption. *Biomacromolecules* **7**, 2147-2153 (2006).

31. Max, E. et al. A novel AFM Based Method for Force Measurements between Individual Hair Strands. *Ultramicroscopy* **110**, 320-324 (2010).

32. Giesbers, M., Kleijn, J. M. & Cohen Stuart, M. A. Interactions between Acid- and Base-Functionalized Surfaces. *J. Colloid Interface Sci.* **252**, 138-148 (2002).

33. Behrens, S. H. & Grier, D. G. The Charge of Glass and Silica Surfaces. *The Journal of Chemical Physics* **115**, 6716 (2001).

34. Ong, Y. L., Razatos, A., Georgiou, G. & Sharma, M. M. Adhesion Forces between E. c oli Bacteria and Biomaterial Surfaces. *Langmuir* **15**, 2719-2725 (1999).

35. Vinogradova, O. I., Yakubov, G. E. & Butt, H.-J. Forces between Polystyrene Surfaces in Water–Electrolyte Solutions: Long-Range Attraction of Two Types? *The Journal of Chemical Physics* **114**, 8124 (2001).

36. Bonaccurso, E., Kappl, M. & Butt, H.-J. Hydrodynamic Force Measurements: Boundary Slip of Water on Hydrophilic Surfaces and Electrokinetic Effects. *Phys. Rev. Lett.* **88**, 076103 (2002).

37. Behrens, S. H., Christl, D. I., Emmerzael, R., Schurtenberger, P. & Borkovec, M. Charging and Aggregation Properties of Carboxyl Latex Particles: Experiments versus DLVO Theory. *Langmuir* **16**, 2566-2575 (2000).

38. Derjaguin, B. A Theory of Interaction of Particles in Presence of Electric Double Layers and the Stability of Lyophobe Colloids and Disperse Systems. *Prog. Surf. Sci.* **43**, 1-14 (1993).

39. Behrens, S. H. & Borkovec, M. Exact Poisson-Boltzmann Solution for the Interaction of Dissimilar Charge-Regulating Surfaces. *Physical review. E,* **60**, 7040-7048 (1999).

40. Rentsch, S., Pericet-Camara, R., Papastavrou, G. & Borkovec, M. Probing the Validity of the Derjaguin Approximation for Heterogeneous Colloidal Particles. *Physical Chemistry Chemical Physics* **8**, 2531 (2006).

41. Holmberg, K., Shah, D. O. & Schwuger, M. J. *Handbook of Applied Surface and Colloid Chemistry* (John Wiley & Sons Inc, 2002).

42. Bard, A. J. & Faulkner, L. R. *Electrochemical Methods* (Wiley, 2000).

43. Biesheuvel, P. M. Simplifications of the Poisson–Boltzmann Equation for the Electrostatic Interaction of Close Hydrophilic Surfaces in Water. *J. Colloid Interface Sci.* **238**, 362-370 (2001).

44. Pericet-Camara, R., Papastavrou, G., Behrens, S. H. & Borkovec, M. Interaction between Charged Surfaces on the Poisson−Boltzmann Level: The Constant Regulation Approximation. *The Journal of Physical Chemistry B* **108**, 19467-19475 (2004).

45. Behrens, S. H. & Borkovec, M. Electrostatic Interaction of Colloidal Surfaces with Variable Charge. *The Journal of Physical Chemistry B* **103**, 2918-2928 (1999).

46. Brett, C. M. A. & Brett, A. M. O. *Electrochemistry: Principles, Methods, and Applications* (Oxford University Press, New York, 1993).

47. Adamczyk, Z. & Warszyński, P. Role of Electrostatic Interactions in Particle Adsorption. *Adv. Colloid Interface Sci.* **63**, 41-149 (1996).

48. Rentsch, S., Siegenthaler, H. & Papastavrou, G. Diffuse Layer Properties of Thiol-Modified Gold Electrodes Probed by Direct Force Measurements. *Langmuir* **23**, 9083-9091 (2007).

49. Grahame, D. C. The Electrical Double Layer and the Theory of Electrocapillarity. *Chemical Reviews* **41**, 441-501 (1947).

50. Pericet-Camara, R., Papastavrou, G., Behrens, S. H., Helm, C. A. & Borkovec, M. Interaction Forces and Molecular Adhesion between Pre-adsorbed Poly(ethylene imine) Layers. *J. Colloid Interface Sci.* **296**, 496-506 (2006).

51. Tarbuck, T. L., Ota, S. T. & Richmond, G. L. Spectroscopic Studies of Solvated Hydrogen and Hydroxide Ions at Aqueous Surfaces. *J. Am. Chem. Soc.* **128**, 14519-14527 (2006).

52. Roger, K. & Cabane, B. Why Are Hydrophobic/Water Interfaces Negatively Charged? *Angewandte Chemie International Edition* **51**, 5625-5628 (2012).

53. Leroy, P., Jougnot, D., Revil, A., Lassin, A. & Azaroual, M. A Double Layer Model of the Gas Bubble/Water Interface. *J. Colloid Interface Sci.* **388**, 243-256 (2012).

54. Vácha, R. et al. The Orientation and Charge of Water at the Hydrophobic Oil Droplet–Water Interface. *J. Am. Chem. Soc.* **133**, 10204-10210 (2011).

55. Vácha, R., Horinek, D., Buchner, R., Winter, B. & Jungwirth, P. Comment on "An Explanation for the Charge on Water's Surface" by A. Gray-Weale and J. K. Beattie, Phys. Chem. Chem. Phys., 2009, 11, 10994. *Physical Chemistry Chemical Physics* **12**, 14362 (2010).

56. Vácha, R., Horinek, D., Berkowitz, M. L. & Jungwirth, P. Hydronium and Hydroxide at the Interface between Water and Hydrophobic Media. *Physical Chemistry Chemical Physics* **10**, 4975 (2008).

57. Beattie, J. K., Djerdjev, A. M. & Warr, G. G. The Surface of Neat Water is Basic. *Faraday Discussions* **141**, 31 (2008).

58. Beattie, J. K. & Djerdjev, A. M. The Pristine Oil/Water Interface: Surfactant-Free Hydroxide-Charged Emulsions. *Angewandte Chemie International Edition* **43**, 3568-3571 (2004).

59. Creux, P., Lachaise, J., Graciaa, A., Beattie, J. K. & Djerdjev, A. M. Strong Specific Hydroxide Ion Binding at the Pristine Oil/Water and Air/Water Interfaces. *The Journal of Physical Chemistry B* **113**, 14146-14150 (2009).

60. Schweiss, R., Welzel, P. B., Werner, C. & Knoll, W. Dissociation of Surface Functional Groups and Preferential Adsorption of Ions on Self-Assembled Monolayers Assessed by Streaming Potential and Streaming Current Measurements. *Langmuir* **17**, 4304-4311 (2001).

61. Zimmermann, R., Freudenberg, U., Schweiß, R., Küttner, D. & Werner, C. Hydroxide and Hydronium Ion Adsorption — A Survey. *Current Opinion in Colloid & Interface Science* **15**, 196-202 (2010).

62. Preočanin, T. et al. Surface Charge at Teflon/Aqueous Solution of Potassium Chloride Interfaces. *Colloids and Surfaces A: Physicochemical and Engineering Aspects* **412**, 120-128 (2012).

63. Tian, C. S. & Shen, Y. R. Structure and Charging of Hydrophobic Material/Water Interfaces Studied by Phase-Sensitive Sum-Frequency Vibrational Spectroscopy. *Proceedings of the National Academy of Sciences* **106**, 15148-15153 (2009).

64. Kreuzer, H. J., Wang, R. L. C. & Grunze, M. Hydroxide Ion Adsorption on Self-Assembled Monolayers. *J. Am. Chem. Soc.* **125**, 8384-8389 (2003).

65. Zangi, R. & Engberts, J. B. F. N. Physisorption of Hydroxide Ions from Aqueous Solution to a Hydrophobic Surface. *J. Am. Chem. Soc.* **127**, 2272-2276 (2005).

66. Shull, K. R. Contact Mechanics and the Adhesion of Soft Solids. *Materials Science and Engineering: R: Reports* **36**, 1-45 (2002).

67. Maugis, D. Adhesion of Spheres: the JKR-DMT Transition using a Dugdale Model. *J. Colloid Interface Sci.* **150**, 243-269 (1992).

68. Kappl, M. & Butt, H. J. The Colloidal Probe Technique and its Application to Adhesion Force Measurements. *Particle & Particle Systems Characterization* **19**, 129-143 (2002).

69. Lahlou, M., Harms, H., Springael, D. & Ortega-Calvo, J.-J. Influence of Soil Components on the Transport of Polycyclic Aromatic Hydrocarbon-Degrading Bacteria through Saturated Porous Media. *Environmental Science & Technology* **34**, 3649-3656 (2000).

70. Israelachvili, J. & Wennerström, H. Role of Hydration and Water Structure in Biological and Colloidal Interactions. *Nature* **379**, 219-225 (1996).

71. Guleryuz, H., Røyset, A. K., Kaus, I., Filiàtre, C. & Einarsrud, M.-A. AFM Measurements of Forces between Silica Surfaces. *Journal of Sol-Gel Science and Technology* **62**, 460-469 (2012).

72. Poortinga, A. Electric Double Layer Interactions in Bacterial Adhesion to Surfaces. *Surface Science Reports* **47**, 1-32 (2002).

73. Adler, J. J., Rabinovich, Y. I. & Moudgil, B. M. Origins of the Non-DLVO Force between Glass Surfaces in Aqueous Solution. *J. Colloid Interface Sci.* **237**, 249-258 (2001).

74. Nalaskowski, J., Drelich, J., Hupka, J. & Miller, J. D. Adhesion between Hydrocarbon Particles and Silica Surfaces with Different Degrees of Hydration As Determined by the AFM Colloidal Probe Technique. *Langmuir* **19**, 5311-5317 (2003).

75. Cooper, K., Ohler, N., Gupta, A. & Beaudoin, S. Analysis of Contact Interactions between a Rough Deformable Colloid and a Smooth Substrate. *J. Colloid Interface Sci.* **222**, 63-74 (2000).

76. Jarvis, S. P., Yamada, H., Yamamoto, S. I., Tokumoto, H. & Pethica, J. B. Direct Mechanical Measurement of Interatomic Potentials. *Nature* **384**, 247-249 (1996).

77. Hayashi, K., Sugimura, H. & Takai, O. Force Microscopy Contrasts due to Adhesion Force Difference between Organosilane Self-Assembled Monolayers. *Appl. Surf. Sci.* **188**, 513-518 (2002).

78. Radtchenko, I. L., Papastavrou, G. & Borkovec, M. Direct Force Measurements between Cellulose Surfaces and Colloidal Silica Particles. *Biomacromolecules* **6**, 3057-3066 (2005).

79. Friedsam, C., Bécares, A. D. C., Jonas, U., Gaub, H. E. & Seitz, M. Polymer Functionalized AFM tips for Long-Term Measurements in Single-Molecule Force Spectroscopy. *ChemPhysChem* **5**, 388-393 (2004).

80. Raiteri, R., Grattarola, M. & Butt, H. J. Measuring Electrostatic Double-Layer Forces at High Surface Potentials with the Atomic Force Microscope. *The Journal of Physical Chemistry* **100**, 16700-16705 (1996).

81. Raiteri, R., Preuss, M., Grattarola, M. & Butt, H. J. Preliminary Results on the Electrostatic Double-layer Force between Two Surfaces with High Surface Potentials. *Colloids and Surfaces A: Physicochemical and Engineering Aspects* **136**, 191-197 (1998).

82. Rabinovich, Y. I., Adler, J. J., Ata, A., Singh, R. K. & Moudgil, B. M. Adhesion between Nanoscale Rough Surfaces. *J. Colloid Interface Sci.* **232**, 17-24 (2000).

83. Beach, E. R., Tormoen, G. W., Drelich, J. & Han, R. Pull-off Force Measurements between Rough Surfaces by Atomic Force Microscopy. *J. Colloid Interface Sci.* **247**, 84-99 (2002).

84. Götzinger, M. & Peukert, W. Particle Adhesion Force Distributions on Rough Surfaces. *Langmuir* **20**, 5298-5303 (2004).

85. Tormoen, G. W., Drelich, J. & Beach, E. R. Analysis of Atomic Force Microscope Pull-off Forces for Gold Surfaces Portraying Nanoscale Roughness and Specific Chemical Functionality. *Journal of Adhesion Science and Technology* **18**, 1-17 (2004).

86. Rumpf, H. & Bull, F. A. *Particle technology* (Chapman & Hall, London, 1990).

87. Rabinovich, Y. I., Adler, J. J., Ata, A., Singh, R. K. & Moudgil, B. M. Adhesion between Nanoscale Rough Surfaces. *J. Colloid Interface Sci.* **232**, 10-16 (2000).

88. Prokopovich, P. & Starov, V. Adhesion Models: From Single to Multiple Asperity Contacts. *Adv. Colloid Interface Sci.* **168**, 210-222 (2011).

89. Valtiner, M., Kristiansen, K., Greene, G. W. & Israelachvili, J. N. Effect of Surface Roughness and Electrostatic Surface Potentials on Forces Between Dissimilar Surfaces in Aqueous Solution. *Advanced Materials* **23**, 2294-2299 (2011).

90. Stuart, M. A. C. et al. Emerging Applications of Stimuli-Responsive Polymer Materials. *Nature materials* **9**, 101-113 (2010).

91. Yamamoto, Y. Self-Assembled Layers of Alkanethiols on Copper for Protection Against Corrosion. *J. Electrochem. Soc.* **140**, 436 (1993).

92. Gooding, J. J., Mearns, F., Yang, W. & Liu, J. Self-Assembled Monolayers into the 21st Century: Recent Advances and Applications. *Electroanalysis* **15**, 8196 (2003).

93. Folkers, J. P., Laibinis, P. E. & Whitesides, G. M. Self-Assembled Monolayers of Alkanethiols on Gold: Comparisons of Monolayers Containing Mixtures of Short- and Long-Chain Constituents with Methyl- and Hydroxymethyl Terminal Groups. *Langmuir* **8**, 1330-1341 (1992).

94. Love, J. C., Estroff, L. A., Kriebel, J. K., Nuzzo, R. G. & Whitesides, G. M. Self-Assembled Monolayers of Thiolates on Metals as a Form of Nanotechnology. *Chemical Reviews* **105**, 1103-1169 (2005).

95. Porter, M. D., Bright, T. B., Allara, D. L. & Chidsey, C. E. D. Spontaneously Organized Molecular Assemblies. 4. Structural Characterization of n-Alkyl Thiol Monolayers on Gold by Optical Ellipsometry, Infrared Spectroscopy, and Electrochemistry. *J. Am. Chem. Soc.* **109**, 3559-3568 (1987).

96.   Akkerman, H. B., Blom, P. W. M., De Leeuw, D. M. & De Boer, B. Towards Molecular Electronics with Large-Area Molecular Junctions. *Nature* **441**, 69-72 (2006).

97.   Vezenov, D. V., Noy, A., Rozsnyai, L. F. & Lieber, C. M. Force Titrations and Ionization State Sensitive Imaging of Functional Groups in Aqueous Solutions by Chemical Force Microscopy. *J. Am. Chem. Soc.* **119**, 2006-2015 (1997).

98.   Arai, T. & Fujihira, M. Effects of Electric Potentials on Surface Forces in Electrolyte Solutions. *Journal of Vacuum Science & Technology B: Microelectronics and Nanometer Structures* **14**, 1378-1382 (1996).

99.   Hillier, A. C., Kim, S. & Bard, A. J. Measurement of Double-Layer Forces at the Electrode/Electrolyte Interface Using the Atomic Force Microscope: Potential and Anion Dependent Interactions. *The Journal of Physical Chemistry* **100**, 18808-18817 (1996).

100. Hu, K., Chai, Z., Whitesell, J. K. & Bard, A. J. In Situ Monitoring of Diffuse Double Layer Structure Changes of Electrochemically Addressable Self-Assembled Monolayers with an Atomic Force Microscope. *Langmuir* **15**, 3343-3347 (1999).

101. Yokota, Y., Yamada, T. & Kawai, M. Force Curve Measurements between n-Decanethiol Self-Assembled Monolayers in Inert Solvent and in Electrochemical Environment. *e-Journal of Surface Science and Nanotechnology* **7**, 731-736 (2009).

102. Whitesides, G. M. & Laibinis, P. E. Wet Chemical Approaches to the Characterization of Organic Surfaces: Self-Assembled Monolayers, Wetting, and the Physical-Organic Chemistry of the Solid-Lquid Interface. *Langmuir* **6**, 87-96 (1990).

103. Hu, K. & Bard, A. J. Use of Atomic Force Microscopy for the Study of Surface Acid-Base Properties of Carboxylic Acid-Terminated Self-Assembled Monolayers. *Langmuir* **13**, 5114-5119 (1997).

104. Duval, J., Lyklema, J., Kleijn, J. M. & van Leeuwen, H. P. Amphifunctionally Electrified Interfaces: Coupling of Electronic and Ionic Surface-Charging Processes. *Langmuir* **17**, 7573-7581 (2001).

105. Duval, J., Kleijn, J. M., Lyklema, J. & van Leeuwen, H. P. Double Layers at Amphifunctionally Electrified Interfaces in the Presence of Electrolytes Containing Specifically Adsorbing Ions. *Journal of Electroanalytical Chemistry* **532**, 337-352 (2002).

106. Campbell, S. D. & Hillier, A. C. Nanometer-Scale Probing of Potential-Dependent Electrostatic Forces, Adhesion, and Interfacial Friction at the Electrode/Electrolyte Interface. *Langmuir* **15**, 891-899 (1999).

107. Bazant, M. Z., Kilic, M. S., Storey, B. D. & Ajdari, A. Towards an Understanding of Induced-Charge Electrokinetics at Large Applied Voltages in Concentrated Solutions. *Adv. Colloid Interface Sci.* **152**, 48-88 (2009).

108. Fréchette, J. & Vanderlick, T. K. Electrocapillary at Contact: Potential-Dependent Adhesion between a Gold Electrode and a Mica Surface. *Langmuir* **21**, 985-991 (2005).

109. Antelmi, D. A., Connor, J. N. & Horn, R. G. Electrowetting Measurements with Mercury Showing Mercury/Mica Interfacial Energy Depends on Charging. *The Journal of Physical Chemistry B* **108**, 1030-1037 (2004).

110. Raiteri, R. & Butt, H. J. Measuring Electrochemically Induced Surface Stress with an Atomic Force Microscope. *The Journal of Physical Chemistry* **99**, 15728-15732 (1995).

111. Gewirth, A. A. & Niece, B. K. Electrochemical Applications of in Situ Scanning Probe Microscopy. *Chemical Reviews* **97**, 1129-1162 (1997).

112. Serafin, J. M. & Gewirth, A. A. Measurement of Adhesion Force to Determine Surface Composition in an Electrochemical Environment. *The Journal of Physical Chemistry B* **101**, 10833-10838 (1997).

113. Kwon, H.-C. & Gewirth, A. A. AFM Force Measurements between SAM-Modified Tip and SAM-Modified Substrate in Alkaline Solution. *The Journal of Physical Chemistry B* **109**, 10213-10222 (2005).

114. Erdmann, M., David, R., Fornof, A. & Gaub, H. E. Electrically Controlled DNA Adhesion. *Nature nanotechnology* **5**, 154-159 (2010).

115. Hu, K., Fan, F. R. F., Bard, A. J. & Hillier, A. C. Direct Measurement of Diffuse Double-Layer Forces at the Semiconductor/Electrolyte Interface Using an Atomic Force Microscope. *The Journal of Physical Chemistry B* **101**, 8298-8303 (1997).

116. Döppenschmidt, A. & Butt, H. J. Measuring Electrostatic Double-Layer Forces on HOPG at High Surface Potentials. *Colloids and Surfaces A: Physicochemical and Engineering Aspects* **149**, 145-150 (1999).

117. Dedeloudis, C., Fransaer, J. & Celis, J. P. Surface Force Measurements at a Copper Electrode/Electrolyte Interface. *The Journal of Physical Chemistry B* **104**, 2060-2066 (2000).

118. Fréchette, J. & Vanderlick, T. K. Double Layer Forces over Large Potential Ranges as Measured in an Electrochemical Surface Forces Apparatus. *Langmuir* **17**, 7620-7627 (2001).

119. Wang, J. & Bard, A. J. Direct Atomic Force Microscopic Determination of Surface Charge at the Gold/Electrolyte InterfaceThe Inadequacy of Classical GCS Theory in Describing the Double-Layer Charge Distribution. *The Journal of Physical Chemistry B* **105**, 5217-5222 (2001).

120. Wang, J., Feldberg, S. W. & Bard, A. J. Measurement of Double-Layer Forces at the Polymer Film/Electrolyte Interfaces Using Atomic Force Microscopy: Concentration and Potential-Dependent Interactions. *The Journal of Physical Chemistry B* **106**, 10440-10446 (2002).

121. Barten, D., Kleijn, J. M., Duval, J. & Leeuwen, H. P. v. Double Layer of a Gold Electrode Probed by AFM Force Measurements. *Langmuir* **19**, 1133-1139 (2003).

122. Ge, C., Liao, J., Yu, W. & Gu, N. Electric Potential Control of DNA Immobilization on Gold Electrode. *Biosensors and Bioelectronics* **18**, 53-58 (2003).

123. Quinn, A., Sedev, R. & Ralston, J. Influence of the Electrical Double Layer in Electrowetting. *The Journal of Physical Chemistry B* **107**, 1163-1169 (2003).

124. Krämer, S., Fuierer, R. R. & Gorman, C. B. Scanning Probe Lithography Using Self-Assembled Monolayers. *Chemical Reviews* **103**, 4367-4418 (2003).

125. Miklavcic, S. J. & Said, E. Electrostatic Potential and Double Layer Force in a Semiconductor-Electrolyte-Semiconductor Heterojunction. *Physical Review. E.* **74**, 061606 (2006).

126. Taboada-Serrano, P., Vithayaveroj, V., Hou, C.-H., Yiacoumi, S. & Tsouris, C. Comparison between Effective Electrode/Electrolyte Interface Potential and Applied Potential for Gold Electrodes. *Industrial & Engineering Chemistry Research* **47**, 3525-3531 (2008).

127. Chan, D. Y. C. A Simple Algorithm for Calculating Electrical Double Layer Interactions in Asymmetric Electrolytes—Poisson–Boltzmann Theory. *J. Colloid Interface Sci.* **245**, 307-310 (2002).

128. Finklea, H. O., Yoon, K., Chamberlain, E., Allen, J. & Haddox, R. Effect of the Metal on Electron Transfer across Self-Assembled Monolayers. *The Journal of Physical Chemistry B* **105**, 3088-3092 (2001).

129. Finklea, H. O., Ravenscroft, M. S. & Snider, D. A. Electrolyte and Temperature Effects on Long Range Electron Transfer Across Self-Assembled Monolayers. *Langmuir* **9**, 223-227 (1993).

130. Janek, R. P., Fawcett, W. R. & Ulman, A. Impedance Spectroscopy of Self-Assembled Monolayers on Au (111): Evidence for Complex Double-Layer Structure in Aqueous $NaClO_4$ at the Potential of Zero Charge. *The Journal of Physical Chemistry B* **101**, 8550-8558 (1997).

131. Ulman, A. Formation and Structure of Self-Assembled Monolayers. *Chemical Reviews* **96**, 1533−1554 (1996).

132. Finklea, H. O., Bard, A. J. & Rubinstein, I. *Electroanalytical Chemistry: A Series of Advances*. (Marcel Dekker, Inc, New York, 1996).

133. Wagner, P., Hegner, M., Guentherodt, H. J. & Semenza, G. Formation and in situ Modification of Monolayers Chemisorbed on Ultraflat Template-Stripped Gold Surfaces. *Langmuir* **11**, 3867-3875 (1995).

134. Stamou, D. et al. Uniformly Flat Gold Surfaces: Imaging the Domain Structure of Organic Monolayers Using Scanning Force Microscopy. *Langmuir* **13**, 2425-2428 (1997).

135. Guo, L. H., Facci, J. S., McLendon, G. & Mosher, R. Effect of Gold Topography and Surface Pretreatment on the Self-Assembly of Alkanethiol Monolayers. *Langmuir* **10**, 4588-4593 (1994).

136. Škapin, S. D. & Matijević, E. Preparation and Coating of Finely Dispersed Drugs. *J. Colloid Interface Sci.* **272**, 90-98 (2004).

137. Kimmel, D. W., LeBlanc, G., Meschievitz, M. E. & Cliffel, D. E. Electrochemical Sensors and Biosensors. *Anal. Chem.* **84**, 685-707 (2012).

138. Dimitriadis, E. K., Horkay, F., Maresca, J., Kachar, B. & Chadwick, R. S. Determination of Elastic Moduli of Thin Layers of Soft Material Using the Atomic Force Microscope. *Biophys Journal* **82**, 2798-2810 (2002).

139. Lin, D. C., Shreiber, D. I., Dimitriadis, E. K. & Horkay, F. Spherical Indentation of Soft Matter Beyond the Hertzian Regime: Numerical and Experimental Validation of Hyperelastic Models. *Biomechanics and modeling in mechanobiology* **8**, 345-358 (2009).

140. Richert, L., Engler, A. J., Discher, D. E. & Picart, C. Elasticity of Native and Cross-Linked Polyelectrolyte Multilayer Films. *Biomacromolecules* **5**, 1908-1916 (2004).

141. Jiménez, A., Fabra, M. J., Talens, P. & Chiralt, A. Phase Transitions in Starch Based Films Containing Fatty Acids. Effect on Water Sorption and Mechanical Behaviour. *Food Hydrocolloids* **30**, 408-418 (2013).

142. Lisunova, M. O., Drachuk, I., Shchepelina, O. A., Anderson, K. D. & Tsukruk, V. V. Direct Probing of Micromechanical Properties of Hydrogen-Bonded Layer-by-Layer Microcapsule Shells with Different Chemical Compositions. *Langmuir* **27**, 11157-11165 (2011).

143. Tang, Z., Wang, Y., Podsiadlo, P. & Kotov, N. A. Biomedical Applications of Layer-by-Layer Assembly: From Biomimetics to Tissue Engineering. *Advanced Materials* **18**, 3203-3224 (2006).

144. Oliver, W. C. & Pharr, G. M. Measurement of Hardness and Elastic Modulus by Instrumented Indentation: Advances in Understanding and Refinements to Methodology. *J. Mater. Res.* **19**, 3-20 (2004).

145. Lin, D. C., Dimitriadis, E. K. & Horkay, F. Elasticity Models for the Spherical Indentation of Gels and Soft Biological Tissues. *Mater. Res. Soc. Symp. Proc.* **1060**, 1060-LL05-07 (2008).

146. Yang, L. & Paulson, A. T. Effects of Lipids on Mechanical and Moisture Barrier Properties of Edible Gellan Film. *Food Research International* **33**, 571-578 (2000).

3. Overview of the Thesis

In this thesis the direct force measurements has been applied for studying interfacial phenomena at electrodes and mechanical properties of ultrathin materials. In its framework four publications have been prepared, from which three have been published (two as co-author, one as contributing author). The fourth publication is ready for submission. These publications are compiled in the chapters 4-7.

3.1. A novel preparation method of mechanically stable colloidal probes by high-temperature sintering (Chapter 4)

The preparation of reliable and well-defined colloidal probes is essential for the accurate measurements of interaction forces as well as for the characterization of mechanical properties. Here a new approach is presented to fabricate robust, contamination-free colloidal probes. It allows obtaining a strong bond between an AFM cantilever and a colloidal particle, which can be effectively targeted by cleaning procedures. The bonding of colloids by high-temperature sintering solves the problem of organic contaminations, while the contact area determines the bonding strength (cf. **Figure 14**a). However, such sintering method has not been available for silica particles.

The mechanical stability of probes was tested by lateral force measurements using a lithographically patterned substrate with regular rectangular grooves. By applying a lateral force towards the colloidal probe a critical torque for the particle removal was reached. We found a way to incorporate small particles in a "neck" around a colloidal probe to increase probe-cantilever area. If some irregular-shaped silica particles obtained by pestle-grinding are used for this purpose, then the probe-cantilever bond strength increases two-three folds. If, however, the "neck" of silica nanoparticles (Ludox) is created (cf. **Figure 14**b, insert), then we were not able to remove the probe from the cantilever by pressing against the groove wall. As shown in **Figure 14**b the lateral force profile has characteristic force peaks, which correspond to twisting of the colloidal probe due to pressure against groove wall. If the critical torque is reached during the twisting, then the particles detaches from the cantilever and only one peak at lateral force profile is observed. Therefore, the continuous presence of peaks demonstrates that upon numerous twisting the cantilever bends, but the probe remains attached to it.
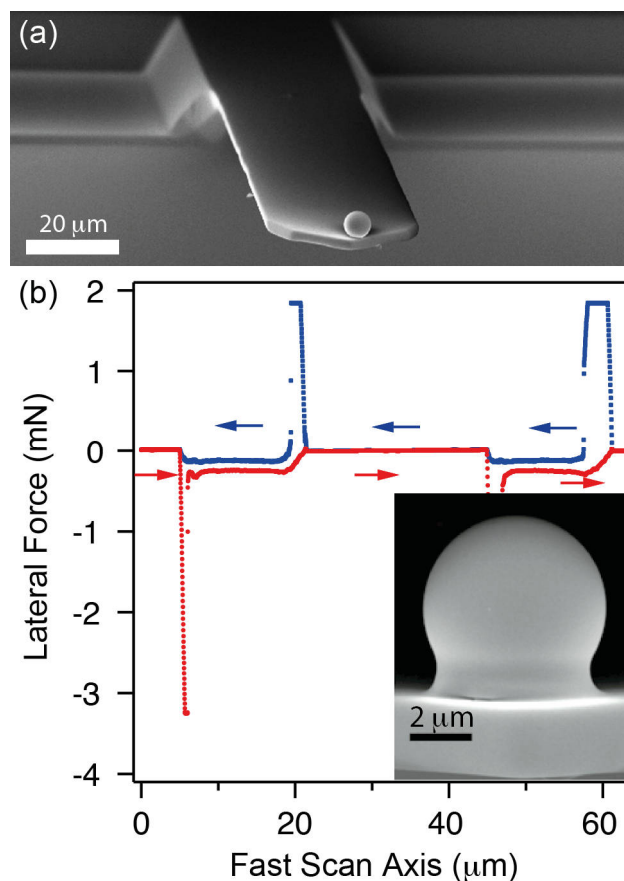
Figure 14: (a) SEM image of a typical colloidal probe obtained by sintering procedure. (b) Lateral force versus displacement graph captured by a cantilever with attached "unbreakable" colloidal particle during the movement against periodical structure. The peaks indicate on twisting of the cantilever, while the probe sustains the pressure against hard wall. For such a probe particle-cantilever connection was reinforces by the "neck" from nanoparticles (cf. insert)

the thermal renewal of sintered probe surface chemistry can be considered as another advantage of the method. Since in aqueous media the hydration of silicon oxide with silicic acid formation may occur, the possibility to reset the properties would be valuable. Indeed, at high temperature the dehydration occurs.[1]

3.2. Adhesion control at organic interfaces by electrochemistry (chapter 5)

Controlling adhesive properties by external stimuli such as potentials applied to an electrode is important for many applications like production of MEMS. As a model system electrodes covered with various non-ionizable SAMs were used here. Usage of stiff cantilevers with enhanced sensitivity suitable for aqueous solutions was essential to probe the full interaction range. Without loosing sensitivity it enabled to obtain interaction profiles without instabilities in the contact region. That in turn allowed

accurate detection of forces acting directly before the contact between the probe and a sample.

Non-ionizable SAMs, which were used in this work, differed only by the terminating groups, though their potentiostatically-mediated adhesive behavior appeared to be very different. We found that the adhesion towards silica colloidal probe for the hydrophilic OH-terminated SAM emerges at potentials above the potential of zero charge (pzc). Hence adhesive forces emerged only when the electrode became oppositely charged to the negatively charged probe. By contrast, for the hydrophobic CH_3-terminated SAM, a non-zero adhesion is present even at potentials below and above the pzc. Furthermore, flexible compensation of forces given by diffuse layer overlap enabled estimation of the solvent exclusion and van der Waals (vdW) forces.

Long-range forces due to diffuse layer overlap dominate the adhesion of rough colloidal particles to the flat electrode. In the top part of **Figure 15**a the dependence of maximal attractive forces recorded upon approach (F_i/R) and retraction, i.e. pull-off forces (F_a/R) are presented, where the values are normalized to the effective radius of interaction R. The interaction force profiles were acquired between a silica colloidal probe and CH_3-terminated electrode in electrolyte solutions. With increasing ionic strength the attractive forces generally decrease, while the increase in the applied potential leads to an increase of attractive forces. At low ionic strength the F_i/R given by DLVO forces accounts for the large part of F_a/R. Since we found very small vdW forces in the system, it is the electrostatic diffuse double layer contribution that dominates DLVO forces. Hence this contribution dominates the total adhesive forces at low ionic strength. Similar behavior has been demonstrated by hydrophilic SAM, where non-DLVO forces (e.i. solvent exclusion forces) are mediocre.
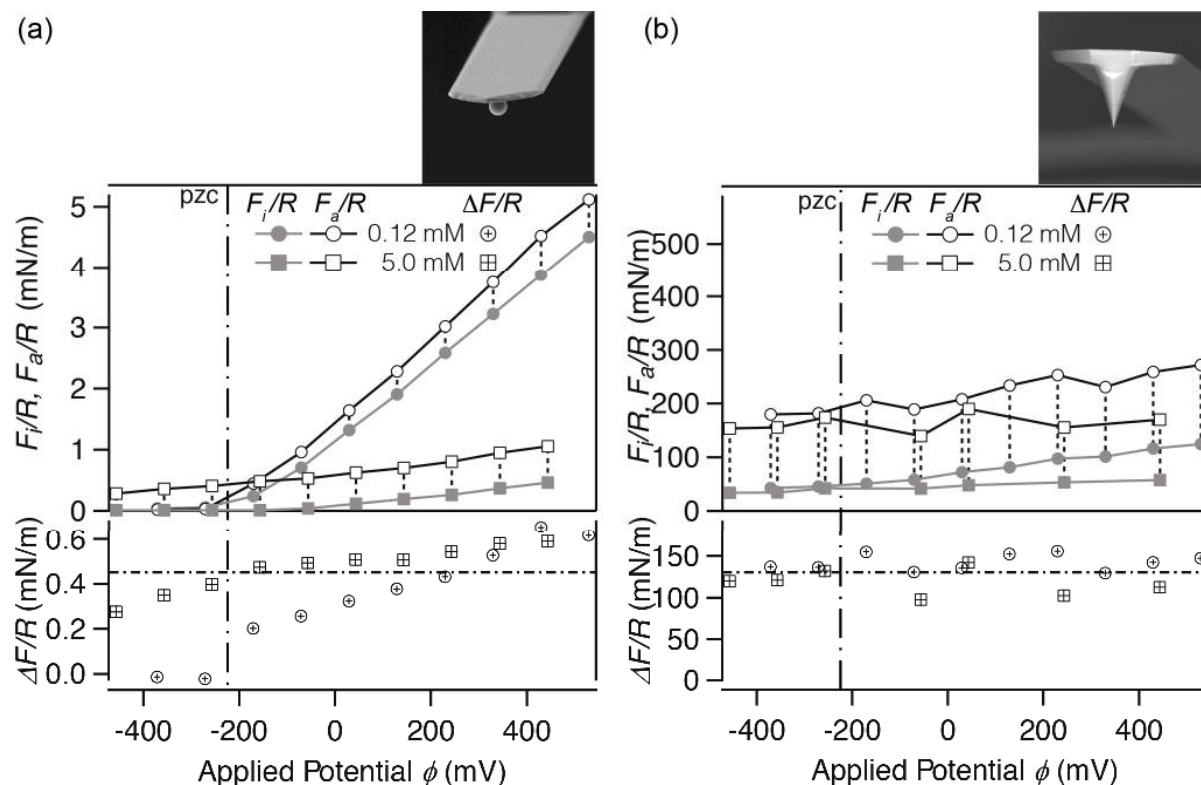
Figure 15: (a, top) Pull-off force F_a/R and maximal attractive force recorded upon approach F_i/R between CH$_3$-terminated electrode and silica colloidal probe as a function of applied potential (statistics of ca. 100 force curves for every point). The data series for two ionic strengths are presented (pH 4.7). (a, bottom) The difference $\Delta F/R$ between corresponding pull-off force and maximal attractive force recorded upon approach as a function of applied potential. Vertical line represents maximal difference observed at the potential of zero charge (pzc). (b) The top and bottom graphs are analogs to graph (a), but for a single-asperity silicon tip. In both graph statistics of ca. 100 force curves for every point is presented.

The difference $\Delta F/R$ between F_a/R and F_i/R determined by colloidal probe shows a slight dependence from the external potential (cf. **Figure 15**a, bottom). This behavior is not in line with solvent exclusion, but resembles more the electrocapillarity effect. However, that could be excluded by measurements with a single asperity on the same SAM (cf. **Figure 15**b, bottom). Moreover, the long-range forces have much less influence on the total adhesion force if probed by single asperity (cf. **Figure 15**b, top). Thus, the variation of $\Delta F/R$ with applied potential for colloidal probe results probably from the instability of the cantilever.

Besides force contributions, the role of surface roughness in the adhesion process has been quantified by solvent exclusion forces. The surface roughness leads to significant reduction of the theoretically predicted adhesion according to JKR theory. However,

detailed analysis of particle surface roughness using the Rabinovich model[2] provides a good quantitative description of the reduction factors. Thus, the increase in surface roughness results in a decrease of non-DLVO forces (i.e. solvent exclusion forces) and correspondingly of the total adhesive force.

3.3. Ion adsorption probed by direct force measurements (Chapter 6)

Modified electrodes provide also a versatile model system to study the ion adsorption on non-ionizable organic interfaces. Here the long-range interaction forces have been determined and analyzed quantitatively by fits to the full solution of the Poisson-Boltzmann equation. For SAM-modified electrodes the diffuse layer potential ψ^D can be tuned by external potential ϕ as shown in **Figure 16**a. Again, the hydrophilic and hydrophobic SAMs have been studied. Additionally to the electronic potential the pH of the electrolyte solution has been varied.
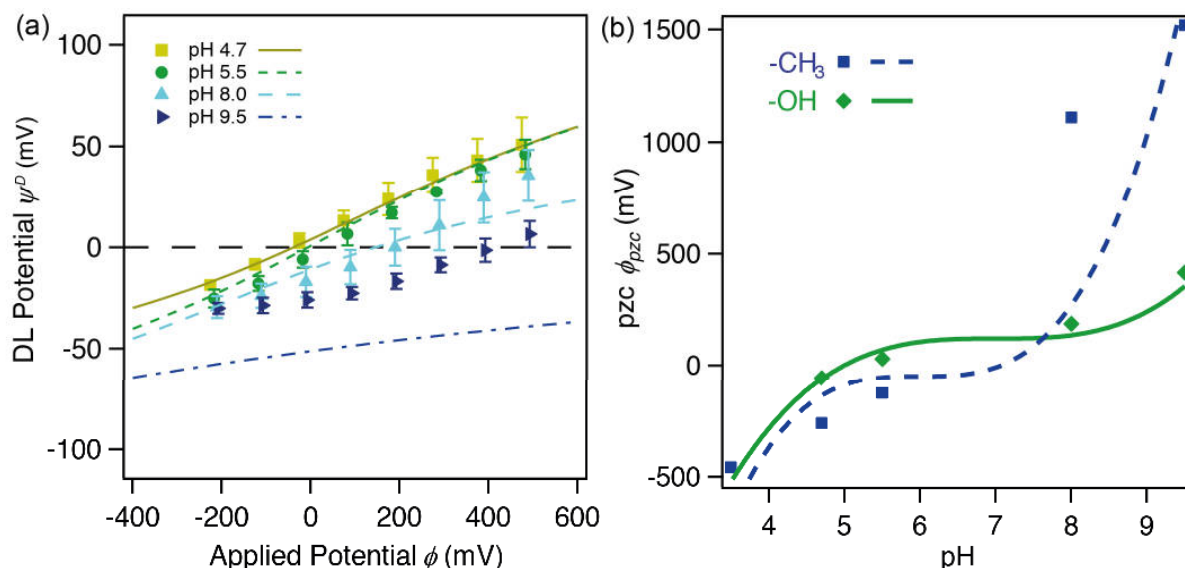
Figure 16: (a) Diffuse layer potential dependence of OH-terminated modified electrode on applied potential at various pH (I ca. 1 mM). Continuous curves represent global fit to the three-capacitor model.[3] (b) Dependence of potential of zero-charge (PZC) on pH of the solution for OH- and CH$_3$-terminated modified electrodes. The solid lines represent fits to the three-capacitor model.[3]

In this work we attempted to describe the modified electrode system with a model that includes blocking SAM, adsorbed ions, and the diffuse double layer. The dependence of the diffuse layer potential from external potential should be altered significantly if ion adsorption takes place. In particular the potential of zero charge (pzc) changes due to the additional charges located at the interface (cf. **Figure 16**b). Nevertheless, the pzc remains indifferent to the concentration of the background electrolyte (KCl).[4] We have been able

to provide a semi-quantitative description of this dependence based on a simple three-capacitor model that takes into account the adsorption of hydroxyl and hydronium ions.[3]

By fitting simultaneously the series $\psi^D(\phi)$ for different SAMs we determined the adsorption constants for hydroxide and hydronium ions. Data for both OH- and CH$_3$-terminated electrodes suggests the specific adsorption of those ions, while the surface remains indifferent to the ions of background electrolyte. The adsorption constants are higher for hydrophobic CH$_3$-terminated SAM, than for hydrophilic OH-terminated SAM. At the same time the adsorption of hydroxide ions is stronger than of hydronium.

This novel approach, described in chapter 7, has possible implications in the development of ion-selective electrodes, "smart" coatings, and surface plasmon resonance sensors.

3.4. Mechanical properties of ultrathin films by nanoindentation (chapter 7)

In chapter 7 the results on mechanical properties of ultrathin films determined by nanoindentation are reported. Within the project polyelectrolyte multilayer (PEM) films were prepared in the group of Prof. A. Fery by K. Trenkenschuh.[5] They were probed by colloidal probe technique at controlled humidity. The investigated PEM-films contained poly(allylamine hydrochloride) (PAH), poly(styrenesulfonate) (PSS), and poly(glutamic acid) (PGA). The latter tends to adsorb atmospheric water and change its conformation. As in similar systems the water in the PEM serves as plasticizer, hence increasing the plasticity and decreasing the stiffness of the multilayer film. We found that upon decreasing the relative humidity (RH) from 80% to 12,5% the Young's modulus of the film increases up to two orders of magnitude (cf. **Figure 17**). Furthermore, the process appears to be reversible, albeit with some hysteresis.
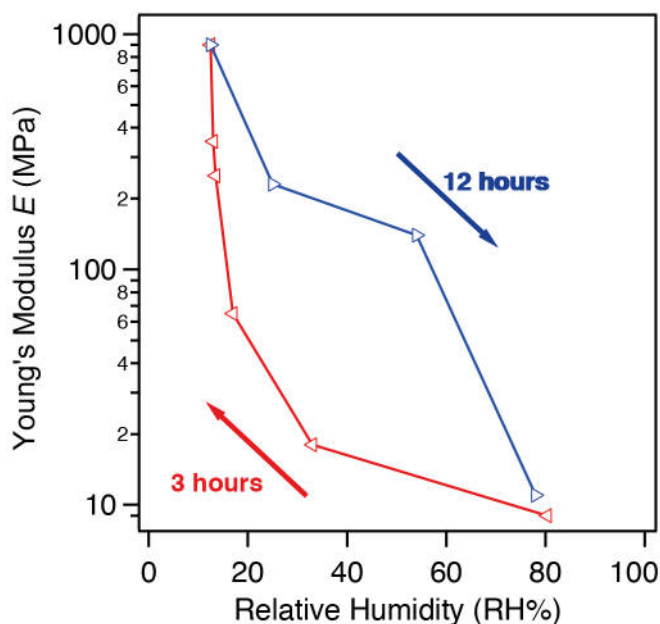
Figure 17: Dependence of Young's modulus of the (PAH/PGA$_{0.88}$-PSS$_{0.22}$) polyelectrolyte multilayer with polyglutamic acid as a function of relative humidity.

To analyze indentation data obtained by colloidal probe technique the measured force versus indentation profiles were compared to the modified Hertz model.[6] At low strain the indentation yields force profiles, which can be readily described by the model. Another prerequisite for compliance with the model is an indentation depth sufficiently larger than the surface roughness. The Young's moduli determined by direct force measurements agree well with data obtained by the wrinkling metrology method.[7]

References:

1. Nalaskowski, J., Drelich, J., Hupka, J. & Miller, J. D. Adhesion between Hydrocarbon Particles and Silica Surfaces with Different Degrees of Hydration As Determined by the AFM Colloidal Probe Technique. *Langmuir* **19**, 5311-5317 (2003).

2. Rabinovich, Y. I., Adler, J. J., Ata, A., Singh, R. K. & Moudgil, B. M. Adhesion between Nanoscale Rough Surfaces. *J. Colloid Interface Sci.* **232**, 17-24 (2000).

3. Duval, J., Lyklema, J., Kleijn, J. M. & van Leeuwen, H. P. Amphifunctionally Electrified Interfaces: Coupling of Electronic and Ionic Surface-Charging Processes. *Langmuir* **17**, 7573-7581 (2001).

4. Rentsch, S. *Direct Force Measurements Between Surfaces Under Potentiostatic Control*. PhD thesis (University of Geneva, Geneva, 2008).

5.   Trenkenschuh, K. *Buildup and Mechanical Properties of Multicomponent Polyelectrolyte films.* PhD Thesis (University of Bayreuth, Bayreuth, 2012).

6.   Lin, D. C., Dimitriadis, E. K. & Horkay, F. Elasticity Models for the Spherical Indentation of Gels and Soft Biological Tissues. *Mater. Res. Soc. Symp. Proc.* **1060**, 1060-LL05-07 (2008).

7.   Stafford, C. M. et al. A Buckling-Based Metrology for Measuring the Elastic Moduli of Polymeric Thin Films. *Nature materials* **3**, 545-550 (2004).

3.5. Individual Contributions to Joint Publications

In this part of the overview the individual contributions of the authors to each manuscript are specified.

Chapter 4

This chapter is published in Review of Scientific Instruments (2012, 83, 116103) under the title:

"Mechanically and Chemically Stable Colloidal Probes from Silica Particles for Atomic Force Microscopy"

by **Volodymyr Kuznetsov** and Georg Papastavrou

I performed the experiments as well as the data analysis and wrote the manuscript.

Georg Papastavrou supervised the project and participated in the writing of the manuscript.

Chapter 5

This chapter is published in Langmuir (2012, 28, 48, 16567-79) under the title:

"Adhesion of Colloidal Particles on Modified Electrodes"

by **Volodymyr Kuznetsov** and Georg Papastavrou

I performed the experiments as well as the data analysis and wrote parts of the manuscript.

Georg Papastavrou supervised the project and wrote the final version of the manuscript.

Chapter 6

This chapter is intended for submission to Journal of Physical Chemistry C under the tentative title:

"Ion Adsorption on Modified Electrodes as Determined by Direct Force Measurements under Potentiostatic Control"

by **Volodymyr Kuznetsov** and Georg Papastavrou

I performed the experiments as well as the data analysis and wrote the manuscript.

Georg Papastavrou supervised the project, was involved in the scientific discussion and corrected the manuscript.

Chapter 7

This chapter is published in Macromolecules (2011, 44, 8954–61) under the title:

"Tuning of the Elastic Modulus of Polyelectrolyte Multilayer Films built up from Polyanions Mixture"

by Katja Trenkenschuh, Johann Erath, **Volodymyr Kuznetsov**, Julia Gensel, Fouzia Boulmedais, Peter Schaaf, Georg Papastavrou, and Anreas Fery

Katja Trenkenschuh prepared samples with polyelectrolyte multilayers, characterized them by ellipsometry and wrinkling metrology method, did data analysis and wrote parts of the paper.

Johann Erath did nanoindentation experiments under ambient conditions, wrote a part of the manuscript, and was involved in the scientific discussion.

My contributions were the preparation of colloidal probes for all nanoindentation experiments, performed nanoindentation experiment at controlled humidity, wrote a part of the manuscript, and was involved in the scientific discussion.

Julia Gensel conducted initial experiments with ellipsometry and wrinkling metrology method, and was involved in the scientific discussion.

Fouzia Boulmedais performed Fourier transformed infrared spectroscopy in the attenuated total reflection mode, wrote a part of the manuscript, and was involved in the scientific discussion.

Peter Schaaf was involved in the scientific discussion concerning the results by infrared spectroscopy.

Georg Papastavrou was involved in the scientific discussion concerning the nanoindentation measurements and corrected the manuscript.

Anreas Fery supervised the project, was involved in the scientific discussion and corrected the manuscript.

4. Mechanically and chemically stable colloidal probes from silica particles for atomic force microscopy

Volodymyr Kuznetsov and Georg Papastavrou*

Department of Physical Chemistry II, University of Bayreuth,
Universitätstraße 30, 95440 Bayreuth, Germany

*E-mail corresponding author: Georg.Papastavrou@uni-bayreuth.de
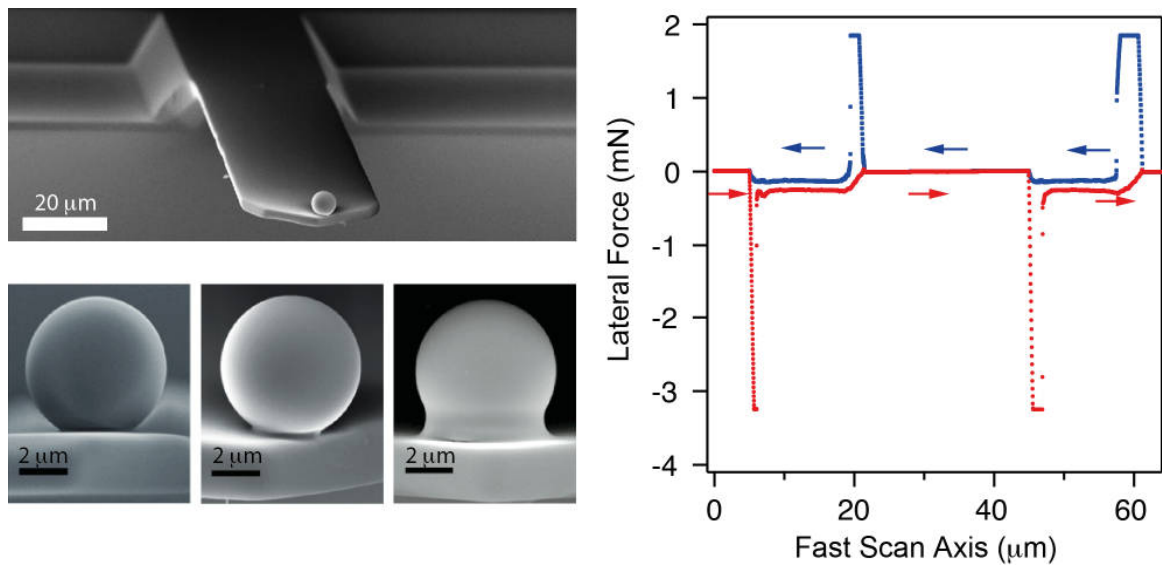
Abstract

In this note we present a novel approach to prepare colloidal probes for atomic force microscopy (AFM) by sintering. A central element of this procedure is the introduction of an inorganic 'fixation neck' between the cantilever and a micrometer-sized silica particle that is acting as probe. This procedure overcomes previous restrictions for the probe particles, which had to be low melting point materials, such as borosilicate glass or latex particles. The here-presented colloidal probes from silica can withstand large mechanical forces. Additionally, they have high chemical resistivity due to the absence of adhesives and the well-studied surface chemistry of colloidal silica.

Paper

Atomic force microscopy (AFM) has been invented in 1986 to image the surface topography of non-conducting samples. It was soon established that this technique is additionally highly suitable to probe locally the mechanical or electronic properties of sample and to measure surface forces with high sensitivity. However, a quantitative evaluation of force profiles requires defined interaction geometries, which cannot be easily obtained with the nm-sized AFM-tips used for imaging purposes. The attachment of colloidal particles to the end of a cantilever has been therefore an essential step in the development of direct force measurements by AFM. These so-called colloidal probes have been independently introduced by Ducker et al. and Butt about 20 years ago.[1,2] From then on, various types of colloidal probes have been used extensively to determine long-range interaction forces[3], also between single pairs of particles[4], as well as to study adhesion phenomena.[5] Additionally, colloidal probes are used increasingly in tribological[6] or micromechanical studies[7,8].

The preparation of colloidal probes has not changed much over the years, despite their widespread use: a colloidal particle is attached under ambient conditions to the end of an AFM-cantilever by means of a suitable glue and with the help of an optical microscope and a micromanipulator (for a comprehensive review see[9]). However, the stability of the glue against non-aqueous solvents as well as acids or bases limits the operational range for glued colloidal probes and represents a latent source of contamination. Furthermore, the interface with the glue is often the weakest mechanical element. Two recent developments aimed to overcome these limits: the introduction of sintering techniques to the preparation of colloidal probes[10-14] and the development of the multi-colloidal probe

technique[15]. Both approaches exclude the glue as fixation for the colloidal particles. However, the latter approach is intended for the reversible attachment of colloidal probes in a colloidal suspension and thus provides no mechanical stability for the probes. Instead, sintering of colloidal particles to the end of AFM-cantilevers allows for colloidal probes with increased mechanical stability and resistance. This technique has been described for colloidal polystyrene particles[10-12] as well as for borosilicate glass particles[13,14]. However, up to now sintering procedures for colloidal probes are based on probe particles with a lower melting point than the cantilever and thus exclude the use of silica as probe particles. Here, we present a new approach for preparing colloidal probes by sintering that overcomes this limitation and leads to superior mechanical and chemical stability of silica colloidal probes in comparison to the previously described procedures.
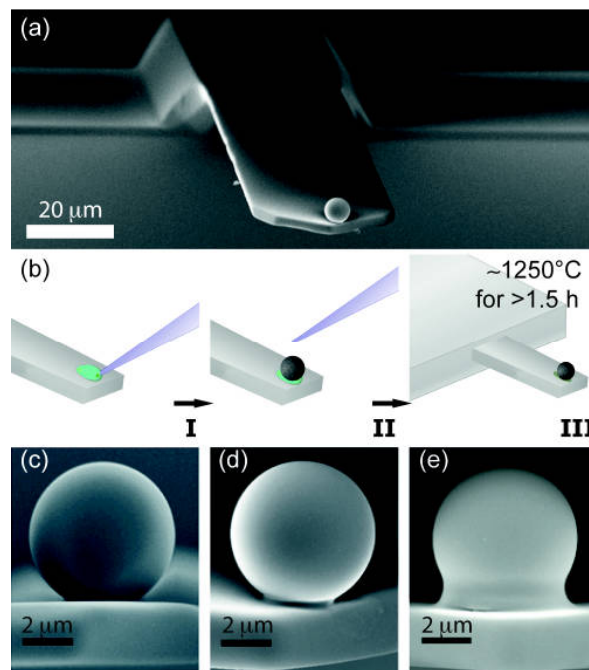
FIG. 1. (a) SEM image of a colloidal probe, i.e. colloidal silica particle attached to the end of a tipless AFM cantilever. (b) Steps for the preparation of colloidal probes. (c-e) Attachment point and neck, respectively, for here-examined sintering procedures (**A-C**): (c) no formation of neck (**A**) (d) neck by polydisperse silica pieces (**B**) and (e) neck formed by nm-sized Ludox-particles (**C**).

FIG. 1a) shows an overview-image of a representative colloidal probe prepared from a silica particle with a diameter of 6.8 μm that is attached to a tipless silicon cantilever (NSC12, Mikromasch, Lithuania). The images in FIG.1 were acquired by scanning electron microscopy (Zeiss 1530 FSEM) with a purposely-constructed holder for the cantilever. The cantilevers with the colloidal probes were rendered conductive by sputtering of 3-4 nm platinum (Sputter coater 208 HR, Cressington). The colloidal silica

particle shown in FIG 1a) has been attached to the tipless cantilever by sintering at > 1200°C. Sintering processes are well known in ceramic production[16] and lead also for silica particles to the formation of strong material bridges[17].

In this note we compare three different sintering procedures named in the following **A-C**. However, the main preparation steps are identical and are illustrated schematically in FIG. 1b.[18] The manipulation of the glue and the colloidal particles is carried out with an upright optical microscope quipped with a fixed stage (Zeiss Examiner) to which a motorized micromanipulator (Märzhäuser DC-3KS, Wetzlar, Germany) is attached. The handling is performed with etched tungsten wires (0.5 mm diameter, Sigma-Aldrich). First, a drop of a highly viscous organic liquid (either glycerol or glue) is placed on the end of the AFM cantilever (cf. FIG. 1b, step I). With another, freshly etched tungsten wire a colloidal silica particle is then picked up from a reservoir, prepared by drying a diluted silica particle suspension on a separate glass slide. This particle is then transferred on top of the liquid drop on the cantilever (cf. FIG. 1b, step II). The drop should have approximately the same lateral dimensions as the colloidal particles and serves two purposes: Firstly, it immobilizes the particle at a defined position due to capillary forces until the heat treatment (cf. FIG. 1c, step III), where it evaporates and decomposes, leaving only the silica particle and the cantilever (procedure **A**). Secondly, in the glycerol additional small silica pieces or nm-sized silica particles can be added (procedure **B** and **C**). During the sintering, these ingredients form a neck around the contact point of the µm-sized silica particle with the cantilever at the glycerol evaporates. The sintering process is taking place at a temperature of 1250 ± 50 °C for 1.5-2h and is followed by slow cooling overnight. Due to the high temperature necessary this procedure is only possible for silicon cantilevers and in absence of any metallic reflective coating.

FIG. 1c)-e) show SEM-images of colloidal probes prepared by the different sintering procedures **A-C**. The main difference between these procedures is the solid content in the glycerol drop. In the first procedure **A** (cf. FIG 1c) only glycerol is used and the procedure is analogous to the one previously described by Bonaccurso et al. for borosilicate particles[13,14]. However, in difference to borosilicate glass, the silica particles are not melting and thus sintering takes place only for a small area (cf. FIG. 1c). For procedure **B** we added silicon powder to the glycerol (approximately 10-20% w/w). This powder has been obtained by pestle grinding of silicon wafer pieces, where particles smaller than about 1 µm have been selected by sedimentation. This highly polydisperse

compound increases the number of contact points between the large silica particle and the cantilever and a small 'neck' around the colloidal particle is formed as the glycerol vanishes during the heat treatment (cf. FIG.1 d). This effect is significantly enhanced in procedure **C** by replacing the powder with small Ludox silica particles (Ludox AM-30, Sigma-Aldrich) with an average diameter of about 30 nm (approx. 40-60 w/w). The resulting neck is much more extended and homogenous compared to **B** (cf. FIG. 1e). We attribute this improvement to the reduced size of the Ludox particles, which can follow better the receding glycerol capillary during heating. Additionally, due to their reduced size more contact points are formed during sintering and the oxide layer formed on the cantilever is approximately of the same dimension as the Ludox particles diameter, leading to a dense bridge between the silica probe and the cantilever. In the following we demonstrate that the formation of the resulting neck leads to superior mechanical stability of the colloidal probes.
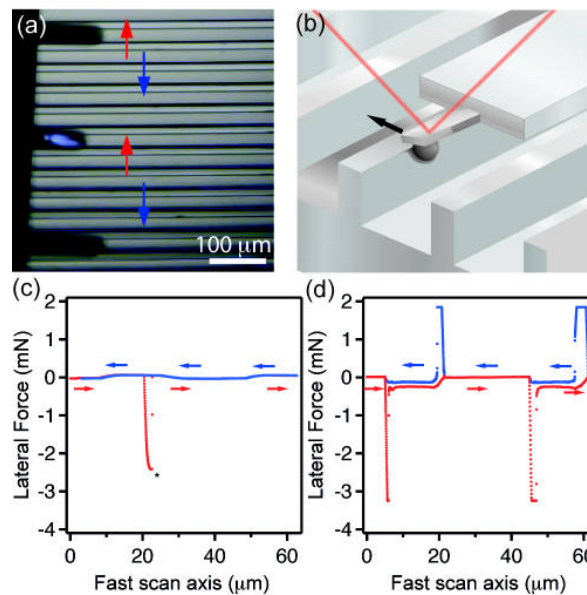

FIG. 2. (a) Optical microscopy image of a colloidal probe during particle detachment measurements on a structured substrate. (b) Schematic representation of measurement principle (c) Lateral force scan (both directions) on substrate for colloidal probe prepared by procedure B. At * the detachment of the probe particle occurs. (d) Instead, for colloidal probes prepared by procedure C (i.e. with Ludox particles) no detachment of the probe particles can be observed.

In order to quantify the mechanical stability of the colloidal probes, we determined the lateral forces at which the colloidal particles detach from the cantilevers. FIG. 2a) shows an optical microscopy image of the structured silicon substrate (GeSim, Germany, fabricated to custom design) used in these experiments. The trenches on the substrate are

periodically arranged (periodicity of 40 μm) and have a width of 30 μm and depth of 15 μm . The colloidal probe is scanned over the substrate as shown schematically in Fig. 2b). The fast scan direction of the cantilever is indicated. Upon entering a trench the colloidal particles touches the wall laterally, while at the same time it is not in contact with the trench bottom. Thus, it touches only the wall at one point. The colloidal probe is blocked during the further lateral movement of the cantilever and the cantilever bends in a torsional manner until either the particle detaches from the cantilever or the bending is so strong that the cantilever jumps out of the trench. The lateral forces acting on the colloidal probe are shown in FIG. 2c) and FIG. 2d), respectively. In FIG. 2c) a probe particle attached by procedure **B** detaches from the cantilever at a lateral force of approximately 2.5 mN (cf. * in FIG. 2c). Afterwards the bare cantilever scans over the surface, showing only a minimal torsional response, reflecting the trench profile. Instead, in FIG. 2 d) we show that for a colloidal probe prepared by procedure **C** it was practically impossible to remove the probe particle from the cantilever, even for highest load force and prolonged scanning. It should be noted that in FIG. 2d) the lateral bending of the cantilever is so strong that the saturation limit of the lateral photodetector is reached for one scan direction.

The quantitative determination of the lateral forces requires knowledge of the lateral cantilever spring constant that is calculated from the cantilever´s top-view dimensions and its spring constant in normal direction[19]. The latter is obtained from the thermal noise in air[20]. The sintering procedure does not lead to a significant change of the cantilever spring constants. The lateral sensitivity is determined by a previously described procedure[21]. Lateral force measurements are known to be prone to systematic errors and alternative methods to determine the lateral spring constant and sensitivity lead to slightly different lateral forces. However, they do not alter the relative difference between the presented preparation methods.
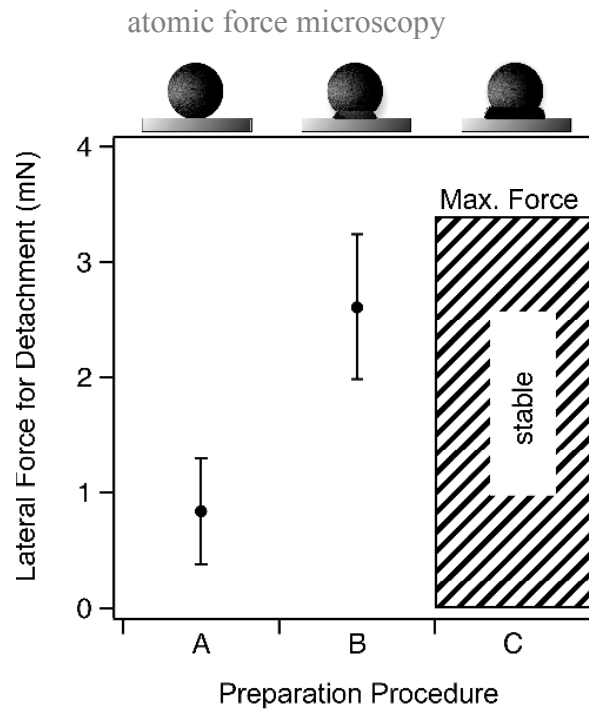
FIG. 3. Comparison of the lateral forces necessary for the detachment of colloidal probes prepared by different methods. In the case of procedure C with a neck of Ludox-particles practically no detachment could be observed in the accessible force range.

Figure 3 summarizes the lateral forces necessary to remove the colloidal probes from the tipless AFM cantilevers (NSC 12, MicroMasch, Lithuania). These cantilevers had spring constants in normal direction between 3-11 N/m. For each type of preparation at least 4 different colloidal probes have been examined. Colloidal probes prepared by method **A** have only a small contact area between the particles and cantilever (cf. FIG. 1c). In consequence, these colloidal probes show the lowest mechanical stability. Nevertheless, most of these colloidal probes are stable at lateral forces of up to 1.5 mN. For colloidal particles fixated by a sintered neck of polydisperse silicon pieces (i.e. procedure **B**) one can observe that significantly larger lateral forces are necessary for the detachment. For colloidal probe prepared by method C, i.e. a neck prepared by small silica particles (i.e. nm-sized Ludox particles), it was practically impossible to remove the colloidal particles from the cantilever in the force regime accessible. By applying uncontrolled shear forces, we broken often the cantilever at its fixation point rather than detaching the particle. Therefore, we assume that the stability of colloidal probes prepared by procedure **C** is comparable to the one of normal silicon cantilevers obtained by micromachining. The colloidal probes prepared by procedure **C** are thus highly suitable for micro-tribological or micro-indentation experiments, where large normal or lateral forces are exerted.

Since the silica colloidal probes are obtained by sintering processes, they are completely inorganic. Therefore they can be used in or cleaned by various aqueous solutions or organic solvents. Additionally they can be thermally treated at temperatures of above 800° C. Such a heat-treatment for silica particles is advantageous not only in terms of the removal of organic contaminants but to provide a well-defined surface chemistry[22]. The here-presented method of sintering with small Ludox-particle (i.e. procedure **C**) allows thus the preparation of highly stable colloidal probes with the well-known surface chemistry of colloidal silica. The introduction of a 'fixation neck' is not limited to silica particles and can be applied as well for organic or inorganic materials with lower melting points.

References:

[1] W. Ducker, T.J. Senden, and R.M. Pashley, Nature 353, 239 (1991).

[2] H. Butt, Biophys J 60, 1438 (1991).

[3] H. Butt, B. Cappella, and M. Kappl, Surf Sci Rep 59, 1 (2005).

[4] T. Muster, G. Toikka, R. Hayes, C. Prestidge, and J. Ralston, Colloid Surface A 106, 203 (1996).

[5] M. Kappl and H. Butt, Part Part Syst Char 19, 129 (2002).

[6] R. Cain, N. Page, and S. BIGGS, Phys Rev E 62, 8369 (2000).

[7] A. Fery, F. Dubreuil, and H. Mohwald, New J Phys 6, 18 (2004).

[8] K. Trenkenschuh, J. Erath, V. Kuznetsov, J. Gensel, F. Boulmedais, P. Schaaf, G. Papastavrou, and A. Fery, Macromolecules 44, 8954 (2011).

[9] Y. Gan, Rev Sci Instrum 78, 081101 (2007).

[10] E. Bonaccurso, *Investigation of Electrokinetic Forces on Single Particles*, PhD thesis, Universität-Gesamthochschule Siegen, 2001.

[11] O. Vinogradova, G. Yakubov, and H. Butt, J Chem Phys 114, 8124 (2001).

[12] J. Ally, E. Vittorias, A. Amirfazli, M. Kappl, E. Bonaccurso, C.E. McNamee, and H.-J. Butt, Langmuir 26, 11797 (2010).

[13] E. Bonaccurso, M. Kappl, and H. Butt, Phys Rev Lett 88, 076103 (2002).

[14] M. Indrieri, A. Podesta, G. Bongiorno, D. Marchesi, and P. Milani, Rev Sci Instrum 82, (2011).

[15] I. Popa, G. Gillies, G. Papastavrou, and M. Borkovec, J Phys Chem B 113, 8458 (2009).

[16] S.-J.L. Kang, Sintering (Butterworth-Heinemann, 2005).

[17] P.M. Ajayan and S. Iijima, J Am Ceram Soc 75, 999 (1992).

[18] S. Rentsch, R. Pericet-Camara, G. Papastavrou, and M. Borkovec, Phys Chem Chem Phys 8, 2531 (2006).

[19] cf. eq. (10) in M. Munz, J Phys D Appl Phys 43, (2010).

[20] J.L. Hutter and J. Bechhoefer, Rev Sci Instrum 64, 1868 (1993).

[21] R. Cannara, M. Eglin, and R. Carpick, Rev Sci Instrum 77, (2006).

[22] M. Kobayashi, M. Skarba, P. Galletto, D. Cakara, and M. Borkovec, J Colloid Interf Sci 292, 139 (2005).

5. Adhesion of Colloidal Particles on Modified Electrodes

Volodymyr Kuznetsov and Georg Papastavrou*

Department of Physical Chemistry II, University of Bayreuth,
Universitätstraße 30, 95440 Bayreuth, Germany

*E-mail corresponding author: Georg.Papastavrou@uni-bayreuth.de
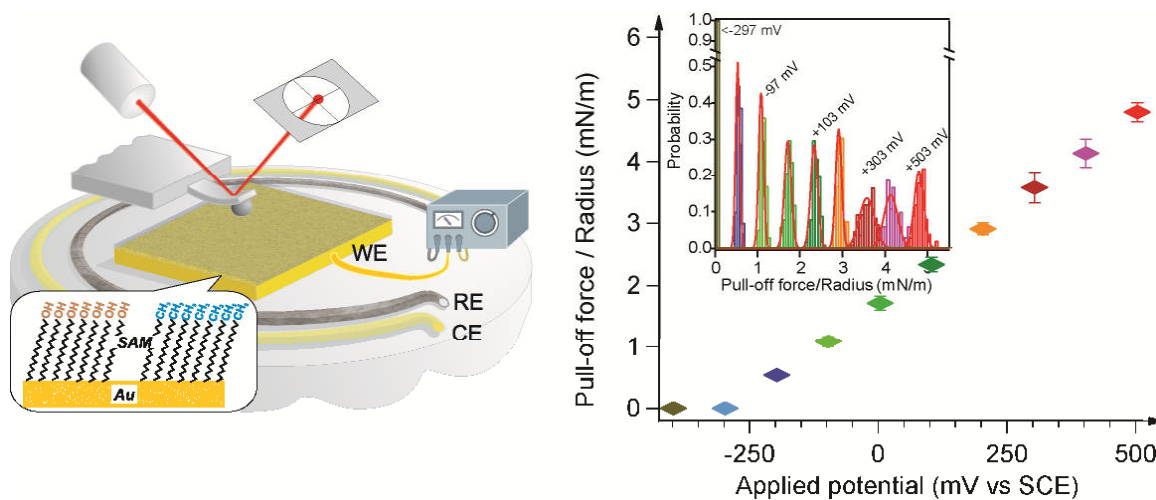
Abstract

The adhesion between colloidal silica particles and modified electrodes has been studied by direct force measurements with the colloidal probe technique based on the atomic force microscope (AFM). The combination of potentiostatic control of gold electrodes and their chemical surface modification by self-assembled monolayers (SAMs) allows for the decoupling of forces due to the electrical double layers and chemical functionality of the solid/liquid interface. Adhesion on such electrodes can be tuned over a large range in dependence of the externally applied potential and the aqueous solution's ionic strength. By utilizing cantilevers with a high force constant, it is possible to separate the various contributions to the adhesion in an unambiguous manner. These contributions comprise diffuse layer overlap, van-der Waals forces, solvent exclusion, and electrocapillarity. A quantitative description of the observed adhesion forces is obtained by taking into account the surface roughness of the silica particle. The main component in the adhesion, which is tuned by the external potential, originates from the overlap of the electrical double layers. By contrast, effects due to electrocapillarity are only of minor importance. Based on our quantitative analysis a new approach is proposed that allows tuning the adhesion force as a function of the externally applied potential. We expect this approach to have important applications for the design of microelectromechanical systems (MEMS), the development of electrochemical sensors as well as for micro- and nanomanipulation.

Introduction

Adhesion between surfaces has a strong influence on various processes such as colloidal transport in soils, wafer cleaning, colloidal aggregation, or friction between solids.[1-3] Adhesion is mediated by surface forces and represents a ubiquitous phenomenon in the colloidal domain. Typically, long-ranged interaction forces determine whether a colloidal particle can approach another surface closely enough to reach contact.[1] After this point, additional short-ranged interaction mechanisms have a strong influence on the sticking probability of a colloid or determine whether a given shear force is sufficient to remove an adhering colloidal particle. In order to tune the adhesion for industrial and technical applications, various approaches have been proposed. Most of these are based on permanently altering the surface properties, for example by polyelectrolyte coatings or monolayers of silanes or thiols.[4,5]

Interaction forces of various origins can mediate adhesion. The long-ranged force contributions are summarized in the theory of Derjaguin, Landau, Verwey, and Overbeek (DLVO) and result from the interaction of the diffuse layers as well as the van-der-Waals (vdW) forces.[2] Short ranged forces are only acting in the contact area. Such forces result from solvent exclusion as well as the formation of chemical bonds and have been studied by chemical force microscopy.[6-11] In the case of polymeric interfaces, additional force contributions can arise due to steric or bridging forces.[12]

With increasing miniaturization of mechanical devices down to the micro- and nanometer scale, the control of adhesive properties has become increasingly important for their performance and fabrication.[13] In particular, the possibility to control directly and instantaneously the adhesion would be important for many applications. Suitable external stimuli to trigger changes in adhesion can be for example electrical potential, illumination by light, or variation of the temperature. The latter two approaches have been studied extensively in recent years and typical examples are thin organic films based on PNIPAM or azo-benzene, respectively.[14,15] However, an electrode connected to a potentiostat provides for many applications a more direct and versatile approach to control surface properties. Additionally, it allows easily for computer control. Electrosorption has been studied for a long time in the field of electrochemistry.[16] By contrast, the concept of applying electric potentials to control adhesion processes on the nano- and micrometer level in the field of colloid science has been exploited only recently.[17]

The development of direct force measurement techniques, in particular the atomic force microscope (AFM) or the surface force apparatus (SFA), allowed in recent years to study these interaction forces for various systems in detail. While the SFA allows determining the interaction forces for a defined contact area, the atomic force microscope offers force resolution below 100 pN and thus can detect single bond ruptures as well as stretching and detachment of single polymer chains. By modifying the surface chemistry of the AFM tip, one can probe the interaction forces between well-defined functional groups.[11] This approach is commonly referred to as chemical force microscopy.[6-11] The development of the colloidal probe technique for the AFM allowed for a combination of well-defined interaction geometries with high force sensitivity.[18,19] The colloidal probe approach has been especially useful in adhesion studies due to its great versatility in choosing the probe surface.[20]

As the SFA and the AFM can be interfaced directly with an electrochemical setup, the corresponding adhesion processes can be studied in detail by direct force measurements.[21] Initial studies on bare noble metal electrodes show that the adhesion can be indeed tuned by the external potential.[22-26] Similar behavior has been observed for semi-conductors or organic interfaces.[27] However, a quantitative interpretation of the results and identification of the dominating interaction mechanism is still far from complete. Recent studies with the electrochemical SFA indicated the importance of electrocapillarity for the adhesion.[28] Furthermore, the effect of surface roughness does not only influence the interaction forces upon approach but also the adhesion.[29]

In this study we provide a new approach to study the adhesion mechanisms on electrode surfaces by determining the adhesion behavior not only as a function of the external potential but also the surface chemistry of the electrode. The latter is achieved by means of self-assembled monolayers on the electrode. The interaction force profiles are measured with the colloidal probe method and are evaluated quantitatively in order to separate the long-ranged force contributions to the adhesion from short ranged contributions arising only due to the contact of the surfaces. Adhesion to electrodes has been studied previously by AFM and SFA, in particular how besides the external potential other parameters such as roughness and surface chemistry influence the adhesion behavior.[17,23,24,24-32] However, by introducing a surface modification of the electrode with different ω-functionalized thiols it is possible to decouple chemical contributions from electrostatic ones. The latter can be varied instantaneously by the external potential applied to the electrode, while the former is given by the terminating functional groups of the SAM. Thus, in difference to the aforementioned studies the interdependence of these different contributions to the adhesion of colloidal objects can be determined in detail.

Experimental Methods

Materials. 16-mercaptohexadecanol-1 (99%, Frontier Scientific) and 1-hexadecanthiol (99%, Sigma Aldrich) were used for the electrode modification as received. Ethanolic solutions were prepared from ethanol of analytical grade. All aqueous solutions were prepared from deionized water of Milli-Q grade with a resistivity larger than 18MΩ. After regulating the pH of solution to pH 4.7 by addition of a traceable volume of 1M HCl (Sigma Aldrich), the total ionic strength has been adjusted to the

nominal values of 0.12 mM, 0.34 mM, 0.56 mM or 5 mM by addition of 1M KCl (Sigma Aldrich).

Preparation of flat gold electrodes. Smooth gold substrates were prepared by a modified 'template stripping' method.[33] We used as substrates p-doped (<20 Ohm/cm) silicon (100) wafers (CrysTec, Berlin, Germany), which have been cleaned beforehand by a modified RCA-procedure.[34] On these cleaned Si-wafers a layer of 60 nm Au (99.99% purity) has been deposited by thermal evaporation. Directly after evaporation RCA-cleaned glass slides of 11x11 mm are glued to the gold layer by means of a chemically resistant adhesive (EPO-TEK 377, Epoxy Technology Inc.), which was thermally cured for one hour at 150 °C.

For the preparation of the electrodes, these glass/glue/gold sandwiched slides were mechanically separated from the wafer and immediately rinsed copiously with ethanol and then transferred to the thiol solution. Surface modification by thiols was performed in 1mM ethanolic solution of 16-mercaptohexadecan-1-ol or 1-hexadecanthiol, respectively, for at least 12 hours. The electrodes with OH-terminated SAM were rinsed with copious amount of ethanol and then with water. The electrodes with CH_3-terminated SAM were rinsed with copious amount of ethanol and then sonicated twice in fresh ethanol in an ultrasonic bath. The electrodes were then immediately mounted in the electrochemical cell, covered with degassed electrolyte solution and AFM fluid cell has been closed.

Preparation of colloidal probes and AFM-cantilever for force measurements. Tipless AFM cantilevers (NSC12, Mikromasch, Lithuania) were cleaned consecutively in a series of solvents (ethanol, aceton, chloroform, aceton, and ethanol) and were then treated in O_2- plasma (Flecto10, Plasma Technology GmbH, Germany) at 100 W and 0.4 mbar for 90 sec. After this cleaning procedure they were coated by thermal evaporation (mini-coater, tectra, Germany) with a reflection layer consisting of 3 nm Cr (Sigma-Aldrich) as adhesion promoter and 60 nm Au. In order to avoid thermal drifts the tipless cantilevers have been coated from both sides. For the preparation of colloidal probes single silica particles (Bangs Laboratories, IN) with an approximate diameter of 6.8μm were attached to these cantilevers by means of a micromanipulator and UV-curable glue (Optical adhesive 63, Norland Products). We used cantilevers with nominal force constants in the range of 0.2 N/m and of 5.6 N/m. The spring constants of these cantilevers have been determined before the attachment of the colloidal particles by the

thermal noise method.[35] Directly before the force measurements the colloidal probes and normal AFM-cantilevers were cleaned by plasma treatment.

AFM imaging. The surface topography of the modified and unmodified electrodes as well as for heat-treated silica particles was determined by tapping mode AFM in air (Dimension 3100 equipped with a NanoScope V controller, Bruker). These measurements were performed with cantilevers (OMCL-AC160TS, Olympus) preselected for a tip radius below 10 nm. This selection has been performed by imaging a Nioprobe standard (Aurora Nanodevices, BC, Canada). The topography of colloidal silica particles was imaged with a scan size of 1x1 µm around the apex of the particle. The surface roughness has been determined after a 2nd-order plane fit of the height image with the software package belonging to the AFM (Bruker, Research NanoScope 7.30).
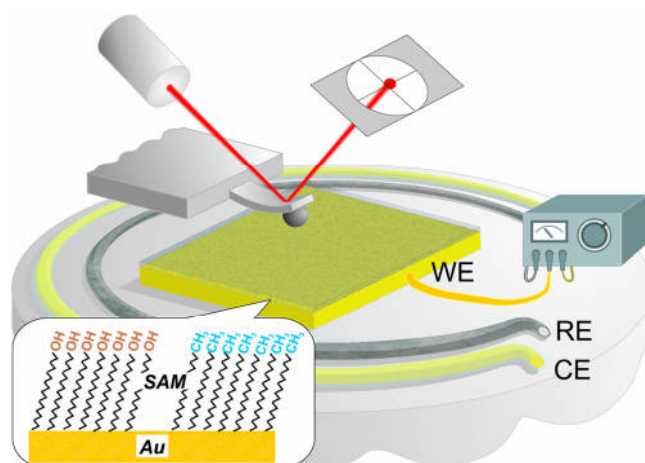
Figure 1: Schematic representation of the experimental setup to determine the adhesion between a colloidal silica particle attached to the end of an AFM-cantilever and a gold electrode modified by a self-assembled monolayer (SAM) terminating in non-ionizable functional groups. The electrode is connected to a potentiostat in a 3-electrode electrochemical cell with working (WE), counter (CE), and reference (RE) electrodes.

Combined setup for electrochemistry and AFM. In order to measure interaction forces under potentiostatic control we constructed a custom-made electrochemical cell, which could be adapted as semi-closed fluid cell to a MFP-3D (Asylum Research, Santa Barbara, CA).[36,37] The potentiostat for the 3-electrode electrochemical cell is custom-built and is based on a design from the group of H. Siegenthaler (University of Berne, Switzerland). Comparable potentiostats have been used in potentiostatically controlled direct force measurements and electrochemical scanning tunneling microscopy.[36,38] The working electrode is the thiol-modified gold electrode and the counter-electrode is a 100 mm gold wire with a diameter of 0.25 mm (Alfar-Aesar). As reference electrode we used

an Ag/AgCl-wire, which has been placed in a circular manner around the working electrode. Dissolution of AgCl has been neglected due to the small dissociation constant (2×10^{-6}M) in respect to the lowest concentration of Cl$^-$ (1.2×10^{-4} M). This pseudo-reference electrode has been calibrated against a commercial Ag/AgCl-reference electrode (Metrohm, Switzerland) in the same solutions as used for the direct force measurements. In order to allow comparison of our results with previous studies, we converted the potentials to the ones versus a standard calomel electrode (SCE). Immediately before the force measurements, the fluid cell was extensively rinsed with Milli-Q water. The gold counter-electrode was carefully annealed in a butane gas flame. All aqueous solutions for the electrochemical measurements have been degassed by means of nitrogen and consecutively with an HPLC-degassing unit directly before the measurements (FLOM Gastorr BG12).

The performance of the thiol-coated electrodes with the electrochemical AFM-cell and the potentiostat has been verified in an independent set of experiments by acquiring cyclic voltammograms in an aqueous solution of 10mM $[Fe(CN)_6]^{4-}$ and 250mM KCl at pH 6. In cyclic voltammograms the current is acquired as a function of the externally applied potential. In the case of hexacyanoferrat the position and area of the known oxidation and reduction peaks allow confirming that parameters like electrode surface and reference electrode potential are within the specifications. Cyclovoltammograms have been also been performed for the pure electrolyte solutions used for the measurements. These voltammograms are important to determine the potential window where the thiol layer remains stable on the electrode. The formation of defects at low or high potentials is accompanied by an increase of the current.

Before each set of force measurements the presence and quality of the thiol layer on the modified gold electrodes has been controlled by cyclic voltammetry. However, for these controls the same electrolyte solutions as for the acquisition of force profiles has been used and no $[Fe(CN)_6]^{4-}$ was present. During the force measurement the current in the electrochemical cell has been monitored to verify that no thiol desorption is taking place. The potential range that can be applied without occurrence of thiol desorption has been determined independent on the direct force measurements.

Direct force measurements. The interaction forces were measured with an AFM equipped with a closed loop control for all three axes (MFP-3D, Asylum Research, CA). For each applied potential, a series of at least 100 approach and retraction cycles with a

velocity of 0.8 μm/s were acquired. For the force profiles of one series, no differences between the first and the last curve could be observed. The maximum loading force was in the order of 10-12 nN.

The measured deflection versus piezo displacement curves were converted to force versus distance profiles by custom written procedures in IGOR PRO (Wavemetrics) based on standard algorithms.[39-41] In order to determine the diffuse layer potentials of the electrodes the series of force profiles attributed to one external potential has been averaged and then fitted. The averaged normalized force profiles F/R are fitted with the solution of the Poisson-Boltzmann equation for two infinite symmetric plates by means of a custom written program in FORTRAN and IGOR PRO (Wavemetrics).[39] Further details concerning the quantitative analysis of the interaction force profiles can be found elsewhere.[36] Routinely, the Debye-length obtained from these fits is compared to the nominal ionic strength of the electrolyte solutions in which the force profiles have been acquired. Commonly, deviations smaller than 10% for the ionic strength are observed and all data sets reported here fulfill this criterion.

The measurement of the interaction forces between two silica particles in the sphere-sphere geometry has been performed in a closed fluid cell (Asylum Research, Santa Barbara, CA) with a round glass cover slide as bottom. The two particles, one attached to the probe and one attached to the substrate, were first coarsely aligned by optical microscopy; the following fine alignment was achieved by a procedure similar to force volume plots. Further details are given elsewhere.[41] The data analysis was performed in an analogous manner to the one for the sphere-plate geometry.

Results and Discussion

In this study, we focus on SAMs terminating in non-ionizable functional groups, i.e. hydroxyl-groups (OH-terminated) and methyl-groups (CH$_3$-terminated). The former SAM is hydrophilic while the latter is hydrophobic. By performing the direct force measurements at a fixed pH-value of pH 4.7, the results can be directly compared with the ones of a previous study concentrating on the long-range interaction forces only.[36] Additionally, we varied the total ionic strength I of the electrolyte solution in order to tune the forces due to diffuse layer overlap.

Interaction forces under potentiostatic control. Figure 2 shows two representative force profiles acquired with colloidal probes made from silica particles with a diameter of

approximately 6.8 μm. However, the corresponding cantilevers have different force constants. The measurements have been performed under identical conditions (pH 4.7 and total ionic strength I=0.34 mM) on a CH_3-terminated electrode at external potentials of $\phi_1 = -397\,\text{mV}$ and $\phi_2 = +403\,\text{mV}$ (vs. SCE), respectively. The force profile in Figure 2a) has been acquired with a soft cantilever with a force constant of 0.38 N/m, while the force profile in Figure 2b) was measured with a much stiffer cantilever with a force constant of 3.78 N/m. Both force profiles show a single force versus distance curve upon approach (solid grey symbols) and retraction (open black symbols). In order to compare the force profiles with theoretical calculations the interaction forces have been normalized to the effective radius R of the interaction geometry according to the Derjaguin approximation. As we are measuring the interaction forces between a colloidal probe and a flat electrode (i.e. sphere/plane-geometry) the effective radius corresponds to the radius R of the colloidal probe. As the silica surface is negatively charged at pH 4.7 one finds repulsive long-ranged interaction forces upon approach for an applied potential of $\phi_1 = -397\,\text{mV}$ and attractive forces for $\phi_2 = +403\,\text{mV}$. Due to the low ionic strength of I=0.34 mM the diffuse layers are rather extended and the diffuse layer interaction is detectable for separation distances of more than 100 nm. As we will demonstrate in the following paragraph, the nominal ionic strength as calculated from the electrolyte composition, corresponds normally within less than 10% to the one obtained from the fits of the long-range interaction forces upon approach.
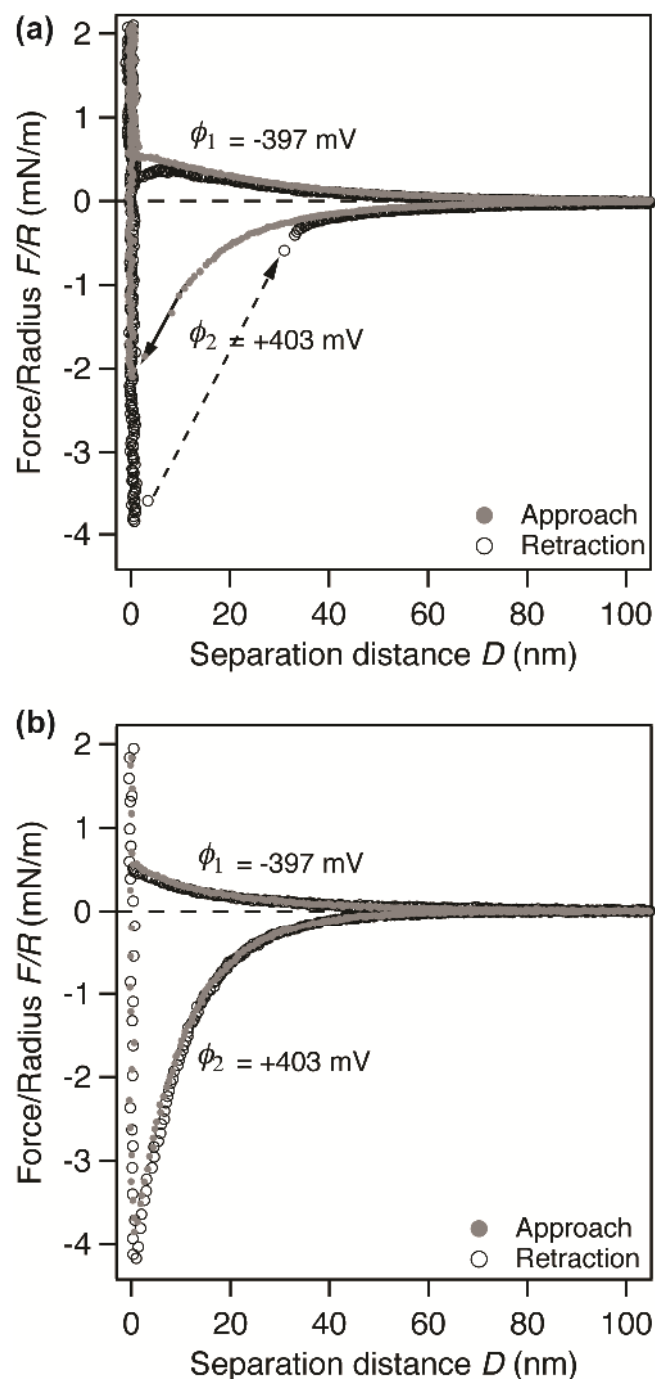
Figure 2: Exemplary force versus distance profiles between a silica colloidal probe and a CH_3-terminated SAM on a gold electrode under potentiostatic control. The externally applied potentials are -397 mV and $+403$ mV (vs. SCE), respectively. The force profiles have been acquired with different spring constants of (a) 0.38 N/m and (b) 3.78 N/m, respectively, but an identical diameter of the colloidal probes (i.e. 6.8 μm). Only for the soft cantilever instabilities are present in the force versus distance curves.

At large separation distances both force profiles in Figure 2 yield almost identical interaction forces, independently from the cantilever spring constant. However, for the

colloidal probe with the softer cantilever (cf. Figure 2a) a distinct instability occurs for ϕ_2 (i.e. the force profiles with long-ranged attractive forces) upon approach at a separation distance of about 15 nm. At this distance the attractive force gradient becomes comparable in magnitude to the cantilever spring constant and thus no static deflection of the cantilever is possible anymore. Due to this instability the cantilever jumps to the surface (indicated by the solid arrow in Figure 2a) and the 'true' interaction force profile cannot by acquired beyond this point. This effect is well known in direct force measurements.[42] Also for the retraction part, one observes a pronounced difference between the force profiles acquired with different cantilevers. The stiffer cantilever (cf. Figure 2b) allows sampling the interaction forces for nearly all separation distances. By contrast, the softer cantilever (cf. Figure 2a) shows a pronounced instability also upon retraction and jumps away from electrode (dashed arrow) the electrode. However, the pull-off force at which this separation is occurring is independent of the cantilever's spring constant. Instead, for the force profiles acquired at ϕ_1, where the long-range interaction is repulsive, both curves coincide to a large degree for approach part and no instabilities are present. Only, in the retraction parts one finds a small difference that occurs at separation of the colloidal probe from the electrode. Here, the softer cantilever shows a distinct but small pull-off force that is much less pronounced and barely traceable for the stiffer cantilever. As we will show later, one finds a greater variation in the pull-off forces as for the long-range forces during approach since in the former case small variation in the topography have a larger influence. Additionally, the block averaging for representing the force profiles as well as the higher force sensitivity for the soft cantilever are supposed to have an influence.

All measurements presented in the following have been performed with cantilevers having large cantilever force constants (e.g. in Figure 2b) in order to allow for a quantitative comparison of the interaction forces upon approach and retraction, in particular near to the electrode's surface. Such a comparison is essential in order to separate force contributions present only in the contact area from other interaction forces that are also long-ranged such as diffuse layer overlap and van-der-Waals forces.

Force profiles for different SAM-modified electrodes. Figure 3 shows force profiles acquired on electrodes modified by two different SAMs (i.e. CH_3- and OH-terminated). Otherwise the force profiles are acquired under identical conditions of pH 4.7 and I=0.34 mM. Each of the shown force profiles has been obtained by averaging a

series of about 100 force profiles. The force profiles have been selected from a more extensive set of force profiles at various applied potentials. Commonly, a potential regime ranging from -400 mV to + 530 mV vs. SCE has been sampled for different ionic strengths, which ranged from 0.12 mM to 5 mM. In this potential regime, we found the thiol-layers on the gold surface to be stable.[43] As previously reported, the differences between the force profiles for a given ionic strength and SAM result only from the externally applied potential.[36]

The essential changes in the force profiles with external potential ϕ are comparable for the CH_3-terminated (Figure 3a) as well as the OH-terminated SAM (Figure 3b). However, the transitions from repulsive (cf. ϕ_1) to attractive interactions (cf. ϕ_3) are occurring at different potentials.[36] During this transition the diffuse layer potential of the electrode drops to zero at the so-called "potential of zero charge" (pzc) where the electrode surface is nearly uncharged and the interaction forces upon approach are practically vanishing. The force profiles acquired near the pzc (cf. ϕ_2) are shown in Figure 3.
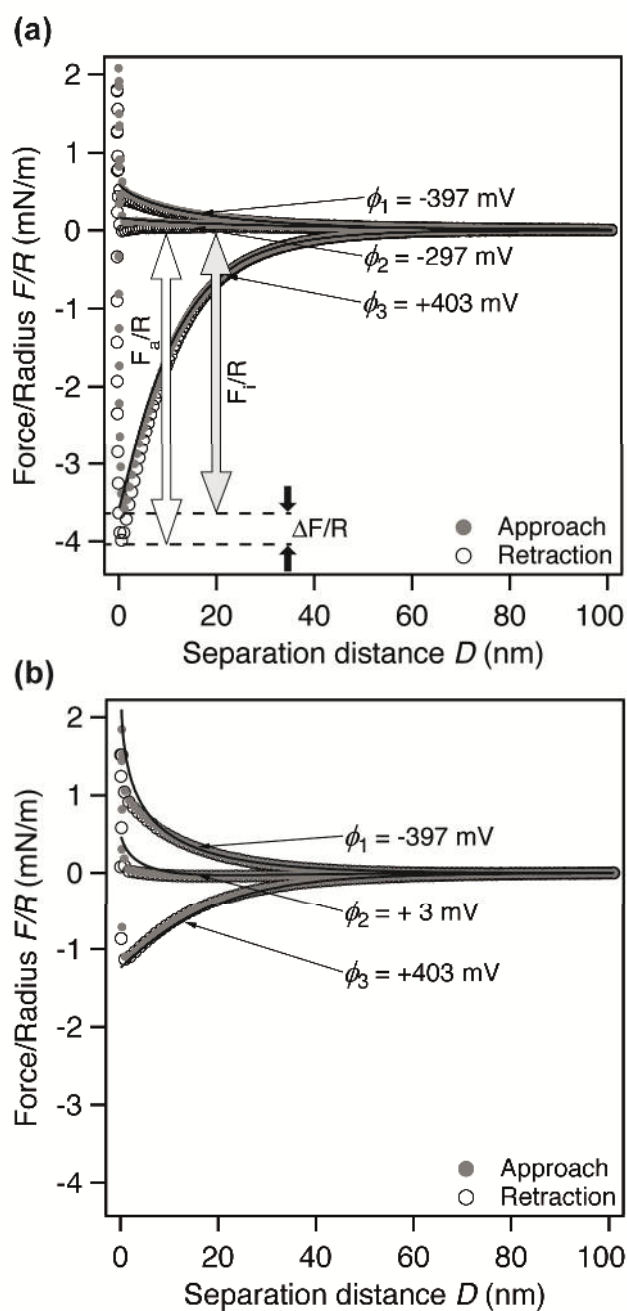
Figure 3: Averaged force profiles obtained during approach (closed symbols) and retraction (open symbols), respectively, on electrodes with (a) CH_3- and (b) OH-terminated SAMs at different applied potentials (I=0.34 mM). The solid lines indicate fits to full solutions of the Poisson-Boltzmann equation including the constant regulation approximation. The arrows indicate the interaction forces directly before contact between the surfaces F_i / R (approach) and the pull-off forces F_a / R (retraction), respectively. The corresponding difference $\Delta F / R = F_a / R - F_i / R$ results from force contribution acting only during contact (e.g. solvent exclusion).

The approach part of the force profiles is dominated at large separation distances by the force resulting from the overlap of the diffuse layers formed at the interfaces of the silica particle and the electrode, respectively. With increasing ionic strength this interaction is more short-ranged due to the reduced extension of the diffuse layers. The force profiles upon approach (i.e. open symbols in Figure 3) have been fitted to the full solutions of the Poisson-Boltzmann equation including charge regulation by means of the constant regulation approximation (full lines in Figure 3).[39] A quantitative evaluation of the diffuse layer properties as a function of the externally applied potential will be given in the following paragraph. For attractive interactions one can determine a force F_i / R directly before the probe makes contact with the electrode (cf. Figure 3a).

In the subsequent retraction of the colloidal probe, the silica particle is separated from the electrode surface and its adhesion to the electrode can be determined. Of special interest is in this respect the pull-off force necessary to separate the silica particle from the electrode. This force is indicated by F_a / R in Figure 3. For the negative potential the total interaction force upon separation is repulsive (i.e. positive sign) and thus the particle would not remain attached to the electrode without externally exerted force. Depending on the applied potential, the adhesion forces can be tuned from repulsive to attractive. However, one finds qualitative differences between the hydrophilic OH-terminated SAM and the hydrophobic CH_3-terminated SAM. For the former the force profiles upon approach and retraction coincide practically for the whole interaction range including the contact at approach and separation. By contrast, for the CH_3-terminated SAM, the force necessary to separate the colloidal probe after contact is larger than the force upon approach just before contact with the surface. This difference $\Delta F / R$ is attributed to the hydrophobicity of the surface and the resulting work of adhesion due to solvent exclusion in the contact area. [7-11] In order to quantify the different force contributions, we evaluate first the long-ranged DLVO forces and compare them afterwards with the pull-off forces.

Diffuse layer properties of the electrode. Figure 4 summarizes the diffuse layer potentials obtained from fits to the full solutions of the Poisson-Boltzmann equation including charge regulation as shown in Figure 3a) and b). In order to obtain the diffuse layer potential from these fits, we had to determine beforehand the diffuse layer potential and constant regulation parameter for the colloidal silica particles in a sphere/sphere geometry.[41] These values for the silica colloidal probes are compiled in the supplemental

information and are in good accordance with previously published results for the diffuse layer potential of silica surfaces.[27,44,45]

Each data point in Figure 4 results from a set of at least three independent measurements with different colloidal probes and electrodes. Around 100 single force profiles were acquired for each external potential and were then averaged. The diffuse layer potentials were determined from the averaged force profiles by fits to the full Poisson-Boltzmann equation. The fits have been performed by means of the so-called constant regulation approximation, which has been described in detail elsewhere.[39] Shortly, in this approximation the charge regulation between two interacting surfaces is summarized by two parameters: their diffuse layer potentials at infinite separation ψ^D and a regulation parameter p for each surface. The latter summarizes the complex surface chemistry (i.e. number of functional groups and their pK´s, Stern layer capacitance) by just one parameter. Typically, the interaction forces taking into account charge regulation are falling in between the classical boundary conditions of constant charge and constant potential. By measuring the interaction forces between two silica particles in the sphere/sphere geometry these values have been obtained first in a set of completely independent measurements for the silica colloidal probe. These data are compiled in the supporting information. Recently, we demonstrated that charge regulation should be taken into account to describe the interaction force profiles upon approach for small separation distances, even for SAM-modified electrodes under potentiostatic control.[36] However, at larger separation distances the values obtained for the diffuse layer potentials do not depend critically on the regulation parameter.

The first value obtained from the fits to the PB-equation is the Debye-length κ^{-1}, which is given by

$$\kappa^{-1} = \sqrt{\frac{\varepsilon\varepsilon_0 kT}{2N_A e^2 I}} \tag{1}$$

where $\varepsilon\varepsilon_0$ is the total permittivity of water, kT is the thermal energy at room temperature, N_A is Avogadro's number, e is the elementary charge and I is the ionic strength. The values obtained from the fits to the experimental data agree within less than 10% to the theoretical Debye-length calculated from the solution's ionic strength as stated during preparation. The fits have been restricted to separation distances larger than the solutions' theoretical Debye-length in order to exclude effects due to surface roughness, charge regulation, and electroviscous effects.[29,46] The dependence of the diffuse layer potential

ψ^D on the externally applied potential ϕ shows that for a given ionic strength the diffuse layer potential ψ^D of the modified electrodes varies monotonically with the externally applied potential. An increase of the ionic strength leads to a reduction of the diffuse layer potentials as can be seen most clearly for the highest ionic strength of 5mM. However, the potential of zero charge (pzc), i.e. the external potential where diffuse layer of an isolated electrode would vanish, does not depend on the ionic strength and concentration of KCl. The vertical dashed lines in Figure 4 indicate the pzc of $\phi_{pzc} = -225 \pm 15\,\text{mV}$ (vs. SCE) and $\phi_{pzc} = -86 \pm 24\,\text{mV}$ (vs. SCE) as determined for the CH$_3$-terminated electrode and the OH-terminated electrode, respectively.

The general dependence of the diffuse layer potential ψ^D from the externally applied potential ϕ can be described in terms of a simple model of two layers, attributing a capacitance to the SAM and the diffuse layer, respectively.[36] However, in order to describe the dependence at higher external potentials accurately, a more elaborate model has to be considered.[37,47] Additionally, the adsorption of hydroxyl- and hydronium ions to the SAMs has to be included.[48-50] Taking into account these contributions provides an explanation of the position and shift between the pzc's for the two different SAMs and leads to a significantly better model in describing the dependence of the diffuse layer potential on the externally applied potential.[36,37] However, such an elaborate model is outside the scope of this study and $\Delta F / R$ and pzc are sufficient for a quantitative analysis of the adhesion behavior.
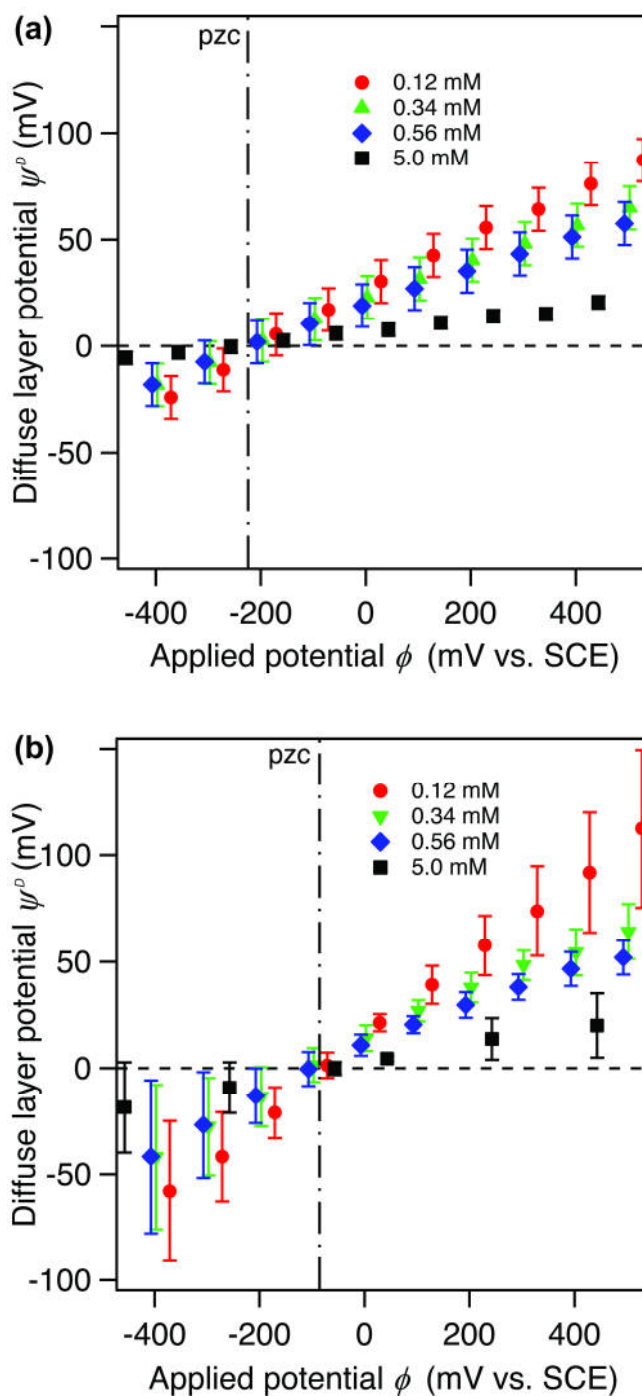
Figure 4: Diffuse layer potential versus externally applied potential for (a) CH_3- and (b) OH-terminated SAMs on gold electrodes. For each electrode the diffuse layer potentials obtained for different ionic strengths are shown. The dashed vertical lines indicate the position of the pzc.

Distribution of pull-off forces. Figure 5 a) shows a series of force versus distance profiles for the retraction part of the force profile when the colloidal probe is moved away from a CH_3-terminated electrode (I=0.34 mM). The retraction force profiles shown in Figure5a) are averaged from approximately 100 single retraction profiles in an analogous procedure as used for the force profiles of the approach part (cf. Figure 3). Again, the

interaction forces have been normalized to the effective radius R. Since a cantilever with a high spring constant has been used, the force profiles during retraction resemble closely the ones of the approach. In consequence, we observe the same dependence of the interaction forces from the externally applied potential as for the force profiles upon approach: Starting from a completely repulsive interaction at very negative potentials the overall interaction is tuned increasingly attractive by higher applied potentials.

In the following analysis of the adhesion we concentrate on the pull-off force F_a/R, which corresponds to the critical force necessary to separate the colloidal probe from the electrode surface. This force equals to the local minima for the retraction force profiles at about zero separation in Figure 5a and has been indicated as well in the force profiles of Figure 3. In contrast to the interaction forces that are detected several nanometers away from the electrode surface, one observes a larger scattering for the pull-off forces. This effect is well known from chemical force microscopy and can be attributed to a slight variations in contact due to surface roughness.[11] Instead, the absence of comparable scattering for the longer-ranged forces results from the larger surface area over which the interaction is averaged and thus small variations in the surface topography are smoothed out.

Figure 5b) summarizes the resulting distribution of the adhesion forces as determined from the single retraction profiles for different potentials. For each potential the pull-off forces scatter around a well-defined mean value. The solid lines indicate fits to the corresponding normal distribution for each potential ϕ. As expected, the pull-off forces F_a / R increase monotonically with the external potential. For potentials $\phi < 200\text{mV}$ the pull-off forces are positive, albeit a local minimum might be present at zero separation (cf. Figure 2a). Nevertheless, despite the local minimum of the interaction forces the sum of all interacting forces is still directed away from the surface and the particle would not adhere in a stable manner to the surface. In consequence an adhesion force of zero is attributed for the corresponding potentials (i.e. -297 mV and -397 mV). The variation of the mean pull-off forces F_a / R with the externally applied potential ϕ is summarized in the inset for the data of Figure 5b). The error bars correspond to the standard deviations of the normal distribution.
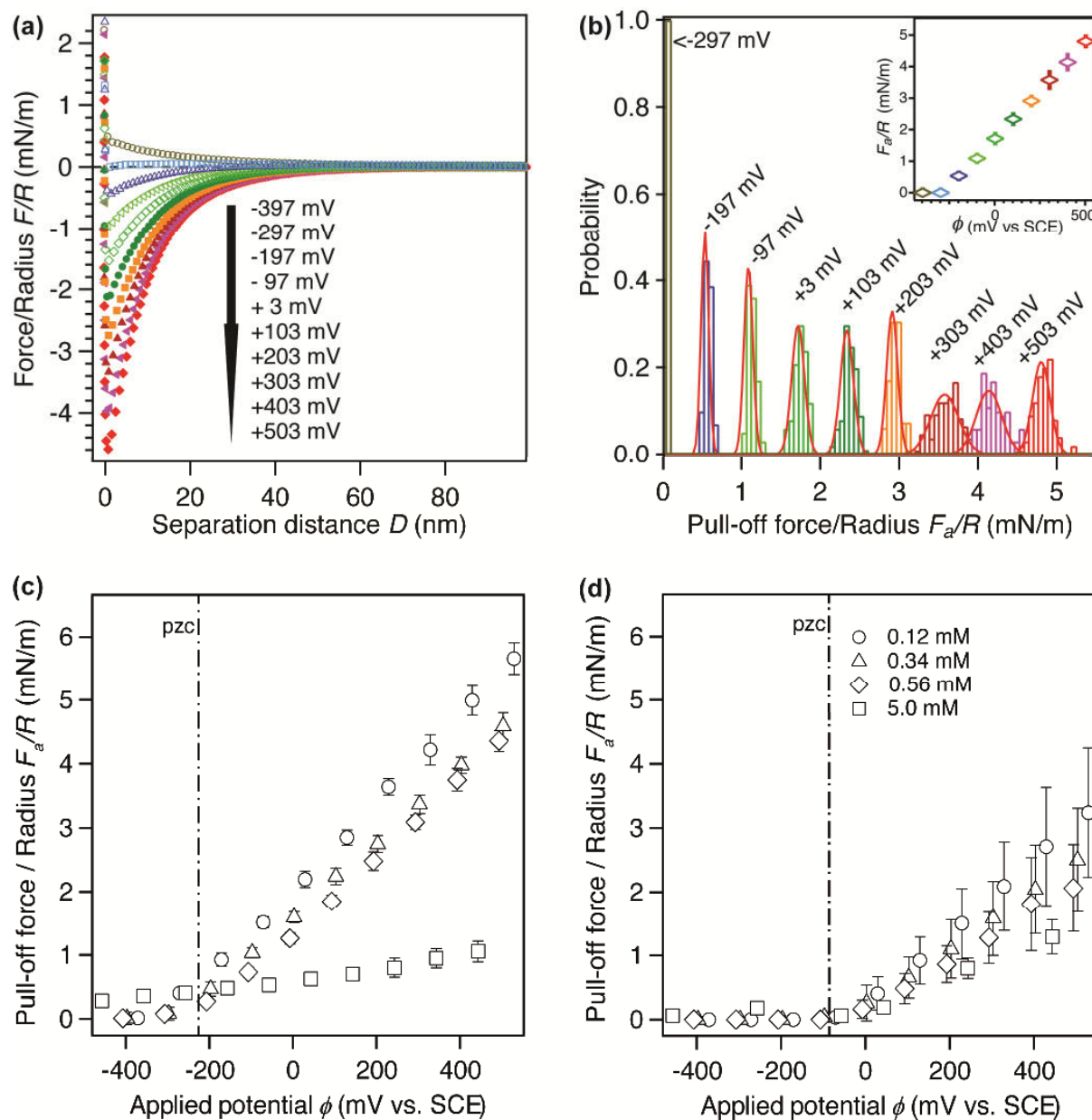
Figure 5: (a) Averaged interaction force profiles upon retraction for an electrode modified by a CH_3-terminated SAM for different applied potentials (I=0.34 mM). The minima in these profiles correspond to the pull-off forces, which is the force necessary to separate the colloidal particle from the electrode surface. (b) Distributions of the pull-off forces for a series of about 100 forces curves for each potential. The solid lines indicate fits to a normal distribution. (c) Compilation of the average pull-off forces at different potentials and different ionic strengths for a CH_3-terminated electrode compiled from three independent data sets in terms of electrode and colloidal probe. (d) Analogous compilation for an OH-terminated electrode.

Adhesion versus externally applied potential. In Figure 5c)-d) we compiled the dependence of the pull-off forces F_a / R on the applied potential ϕ for at least three data sets (different combinations of colloidal probes and electrodes) and various ionic

strengths. Figure 5c) shows the data for the electrodes modified by CH_3-terminated SAMs and Figure 5d) for OH-terminated SAMs, respectively. For both SAMs, one observes a monotonic increase of the pull-off forces and thus of the adhesion with increasing external potential after the pzc. By contrast, increase of the ionic strength by addition of the background electrolyte leads to a reduction of the pull-off forces. At high ionic strengths of about 5 mM (data not shown) the adhesion shows only a small dependence on external potential that is in agreement with diffuse layer potential shown in Figure 4. Thus, we can state that the forces due to diffuse layer overlap represent the most significant contribution to the adhesion. The diffuse layer potential ψ^D depends critically on ionic strength and varies otherwise strongly with the external potential ϕ (cf. Figure 4) but to a smaller extent with increasing ionic strength.

For both SAMs we find a clear transition from non-adhesive to adhesive behavior with increasing potential. The potentials for the transitions are independent of ionic strength. For the OH-terminated SAM, the change from adhesive to non-adhesive behavior occurs at approximately 100 mV vs. SCE (cf. Figure 5d) and thus coincides approximately with the pzc ($\phi_{pzc} \approx -86\,\text{mV}$) indicated by the vertical dashed line in Figure 5d). As for all potentials smaller than the pzc the overall interaction becomes repulsive (cf. Figure 4b), the transition from adhesive to non-adhesive interaction is expected to occur around the pzc. By contrast, for the CH_3-terminated SAM one has to apply much more negative potentials (i.e. $\phi < -300\,\text{mV}$) than the pzc ($\phi_{pzc} \approx -225\,\text{mV}$) in order to switch from adhesive to non-adhesive behavior. Solvent exclusion in the contact area leads to additional adhesion for the hydrophobic (i.e. CH_3-terminated) SAM as reported previously in studies by chemical force microscopy.[6-11] Thus, one finds that much more negative potentials than the pzc on the hydrophobic SAM have to be applied in order to reach the region where no overall adhesion is taking place, as the repulsive diffuse layer forces have to compensate for the additional adhesive component by solvent exclusion.

Influence of DLVO-forces on adhesion. As illustrated in Figure 3a), two types of contributions to the adhesion forces can be distinguished. Firstly, long-ranged interactions that are accounted for by DLVO-theory, namely vdW-forces and diffuse layer overlap. Secondly, short-ranged contributions, which are only present in the contact area, namely solvent exclusion and electrocapillarity. The long-ranged interaction forces are present during approach as well as during retraction of the colloidal probe. By contrast,

contributions of forces related to the contact area can be neglected as soon as the contact between the two solid surfaces is broken. Such a partition of force contributions has been proposed previously and can be approximated by simple models assuming that the interactions inside and outside of the contact area can be separately taken into account.[24,51] Here, we pursued a more direct approach, which does not require a theoretical model taking into account in a separate manner short- as well as long-ranged forces. By comparing the forces directly before contact (i.e. F_i / R) and at pull-off (i.e. F_a / R), one can separate contributions to the pull-off force originating short-ranged interactions from ones due to long-ranged forces (cf. Figure 3a) without any underlying assumptions. However, a prerequisite for this method is that the force profiles have been acquired with a cantilever of sufficiently high spring constant (cf. Figure 2)

In Figure 6 we compiled a number of exemplary data sets of the interaction forces F_i / R directly before contact during the approach and the corresponding pull-off forces F_a / R during the retraction for various ionic strengths and both SAMs (cf. top graphs). The bottom graphs show the resulting difference $\Delta F / R = F_a / R - F_i / R$. For the hydrophobic CH_3-terminated electrode, $\Delta F(\phi) / R$ varies between 0.2 to 0.6 mN/m with applied potential ϕ. By contrast, for the hydrophilic OH-terminated electrode one finds significantly smaller values with $\Delta F / R(\phi) < 0.06$ mN/m.
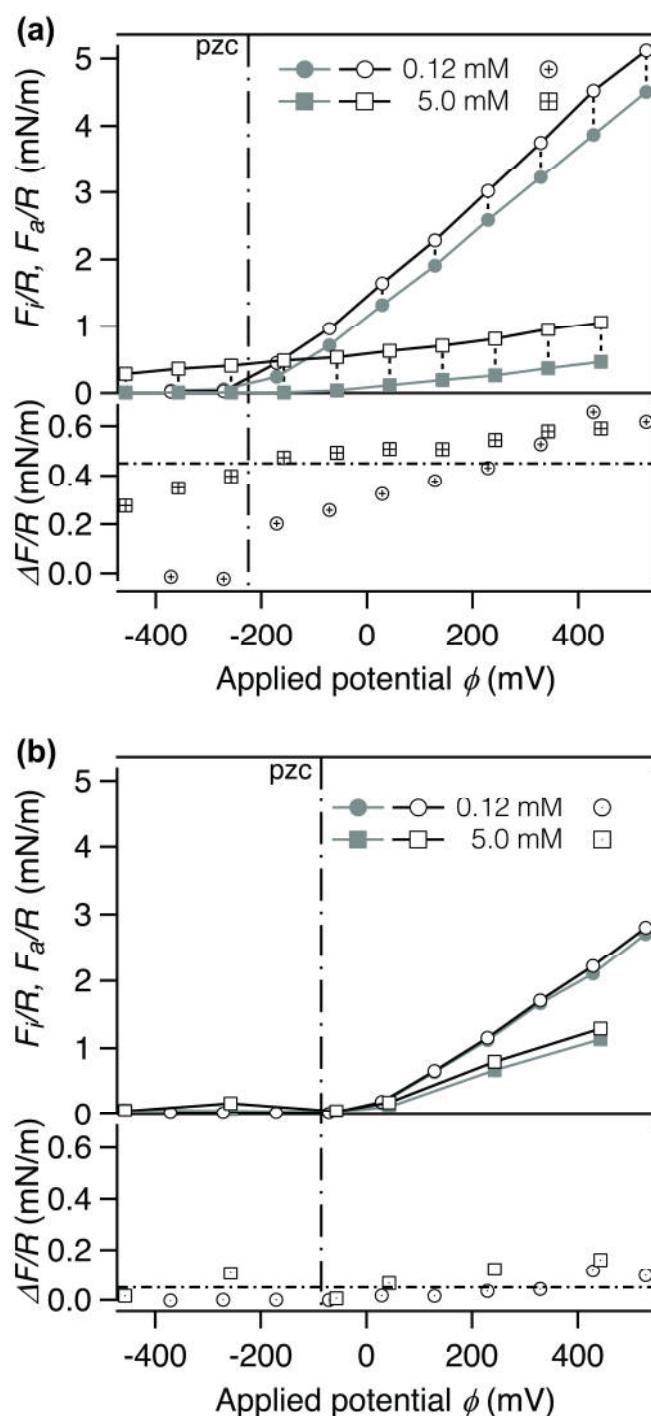
Figure 6: (a) Interaction forces before contact (F_i / R, filled symbols) and corresponding pull-off forces (F_a / R, open symbols) as a function of the applied potential for a CH$_3$-terminated electrode. The bottom graph shows $\Delta F / R = F_a / R - F_i / R$. The dashed line corresponds to $\Delta F / R$ at pzc for $I = 5$ mM. (b) Analogous data set for an OH-terminated electrode.

Work of adhesion at potential of zero charge. The influence of solvent exclusion can be best studied at the pzc. At this potential the electrode's diffuse layer practically vanishes and interaction forces due to diffuse layer overlap are minimal. However, due to

charge regulation between the surfaces a small interaction force induced by the diffuse layer of the silica particle is present. Force profiles at external potentials near the pzc show that the remaining interaction forces upon approach are extremely small (cf. force profiles for ϕ_2 in Figure 3a and 3b). Therefore, additional contributions to the pull-off force, such as solvent exclusion, can be best quantified at the pzc. The work of adhesion due to solvent exclusion is given by:[2]

$$W_{solv} = \gamma_{SAM/H_2O} + \gamma_{SiO_x/H_2O} - \gamma_{SAM/SiO_x} \tag{2}$$

where γ_{SAM/H_2O}, γ_{SiO_x/H_2O}, and γ_{SAM/SiO_x} are the interfacial energies of the two solid/liquid and the solid/solid interface, respectively.

The interfacial energies γ_{-CH_3/H_2O} and γ_{-OH/H_2O} of the two SAMs have been reported previously and corresponding values are compiled in Table 1. The here-measured static contact angles of $\theta_{-CH_3/H_2O} = 108°$ and $\theta_{-OH/H_2O} = 21°$ on the electrodes are in agreement with reported values.[4] The interfacial energy γ_{SiOx/H_2O} for the silica surface has been reported to be in the range of 1-15 mN/m (cf. Table 1).[54-56] It has been approximated here by $\gamma_{SiO_x/H_2O} \approx 1.6 \, \text{mN/m}$ as for both hydrophilic surfaces (i.e. OH-terminated SAM and silica) a closely bound layer of interfacial water is supposed to exist, which is controlling the interfacial properties as determined by adhesion studies.[10,56] This interfacial water layer is also responsible for the reduced adhesion between silica surfaces[55,56] or OH-terminated SAMs[10] as determined by the colloidal probe techniques or chemical force microscopy, respectively. The observation that adhesion forces between OH-terminated SAMs in nonpolar solvents are much larger than in water further supports the assumption of a closely bound interfacial water layer.[7,10]

Table 1: Compilation of interfacial energies

	γ_{-CH_3/H_2O} (mN/m)	γ_{-OH/H_2O} (mN/m)	γ_{SiO_x/H_2O} (mN/m)	$\gamma_{SiO_x/-CH_3}$ (mN/m)	$\gamma_{SiO_x/-OH}$ (mN/m)
γ in eq. (2)	46.0 [a]	1.6 [a]	1.6 [b]	19.6 [c]	1.6 [b]
γ reported	44-55 [d]		2.0 [e], 7.5 [f], 1-15 [g]	(20-35) [h]	-

[a] taken from ref.[10], [b] approximated by γ_{-OH/H_2O}, [c] calculated from $W_{-OH/H_2O/-CH_3}$ in ref.[10]

[d] cf. review[11], [e] cf. ref.[54], [f] cf. ref.[55], [g] cf. ref.[56].

[h] cf. $W_{PE/H_2O/SiO_x}$ =20-35 mN/m for poly(ethylene) particles and heat treated silica.[57]

Adhesion phenomena related to solvent exclusion are commonly described in terms of the theory of Johnson-Kendall-Roberts (JKR).[2] This theory assumes that the interaction is limited to the contact area and elastic deformation due to surface force can be approximated in terms of the Hertz model. For the JKR-theory one finds a finite contact area at separation of the surface and a corresponding pull-force F^{JKR}/R of

$$F^{JKR}/R = \frac{3}{2}\pi W_{solv} \tag{3}$$

where R is the effective radius, which corresponds due to the sphere/plane geometry to the radius of the colloidal probe and W_{solv} as work of adhesion. In consequence F^{JKR}/R can be directly compared to $\Delta F(\phi_{pzc})/R$ at the pzc, when W_{solv} is calculated by eq. (2) from the interfacial energies compiled in Table 1. The resulting theoretical values for F^{JKR}/R are compiled in Table 2.

These theoretical values are compared to experimental values for $\Delta F(\phi_{pzc})/R$ that have been acquired at the highest ionic strength (i.e. 5 mM). In this way residual forces due to diffuse layer overlap are strongly reduced if the condition $\phi \approx \phi_{pzc}$ is not completely fulfilled (cf. data for I=5 mM in Figure 4). Furthermore, by evaluating the difference $\Delta F/R$ rather than F_a/R only contributions from the contact area (cf. Figure 3a) are taken into account. The dashed vertical lines in the bottom graphs of Figure 6a) and b) indicate $\Delta F/R$ at pzc and I=5 mM for the CH$_3$- and OH-terminated electrode, respectively. The corresponding values are also summarized in Table 2. The large difference for $\Delta F/R$ between the OH-terminated electrode and the CH$_3$-terminated electrodes (cf. Figure 6) is in line with the difference of the interfacial energies and thus W_{solv}. Comparison with the experimental data shows that the JKR-model overestimates the forces upon separation to a large extent. Such discrepancies are commonly observed for adhesion between rough interfaces and factors of 20× - 200× compared to ideally flat surfaces have been reported.[52,58-60]

Table 2: Experimental pull-off forces, work of adhesion due to solvent exclusion, and calculated pull-off forces for the JKR-theory and the Rabinovich-model[a]

	$\Delta F(\phi_{pzc})/R$ exp. (mN/m)	W_{solv}[b] (mN/m)	F^{JKR}/R (mN/m)	$\tilde{F}^{rough}/R$ (mN/m)
-CH$_3$	0.45	28.00	131.88	0.79
-OH	0.05	1.60	7.54	0.04

[a] the parameters for the surface roughness in the Rabinovich-model[52,53] were determined by AFM-imaging as r_{rms}=2.1 nm and λ= 50 nm. [b] calculated for SAM/H$_2$O/SiO$_x$

Roughness and adhesion. The roughness of the colloidal probes and of the electrodes is illustrated in Figure 7. Figure 7a) shows an AFM-image of the surface topography of an electrode. Its surface can be considered as smooth compared to the one of a colloidal particle as shown in Figure 7b). It should be noticed that in Figure 2b) the curvature due to the particle radius R has been removed by flattening of the AFM image. Figure 7c) shows in a 3-dimensional representation how the ultrastructure of the silica particle prepared by Stöber-like processes is superimposed to the particle's curvature. The here-reported pronounced roughness of the μm-sized silica particle is found frequently for large silica particles prepared by Stöber- processes.[41] In the following, we consider the electrodes as smooth in comparison to the silica particles. This approximation is supported by the root-mean-square (rms) roughness of r_{rms} = 0.3 nm and r_{rms} = 2.1 nm for the electrodes and silica particles (after flattening), respectively.
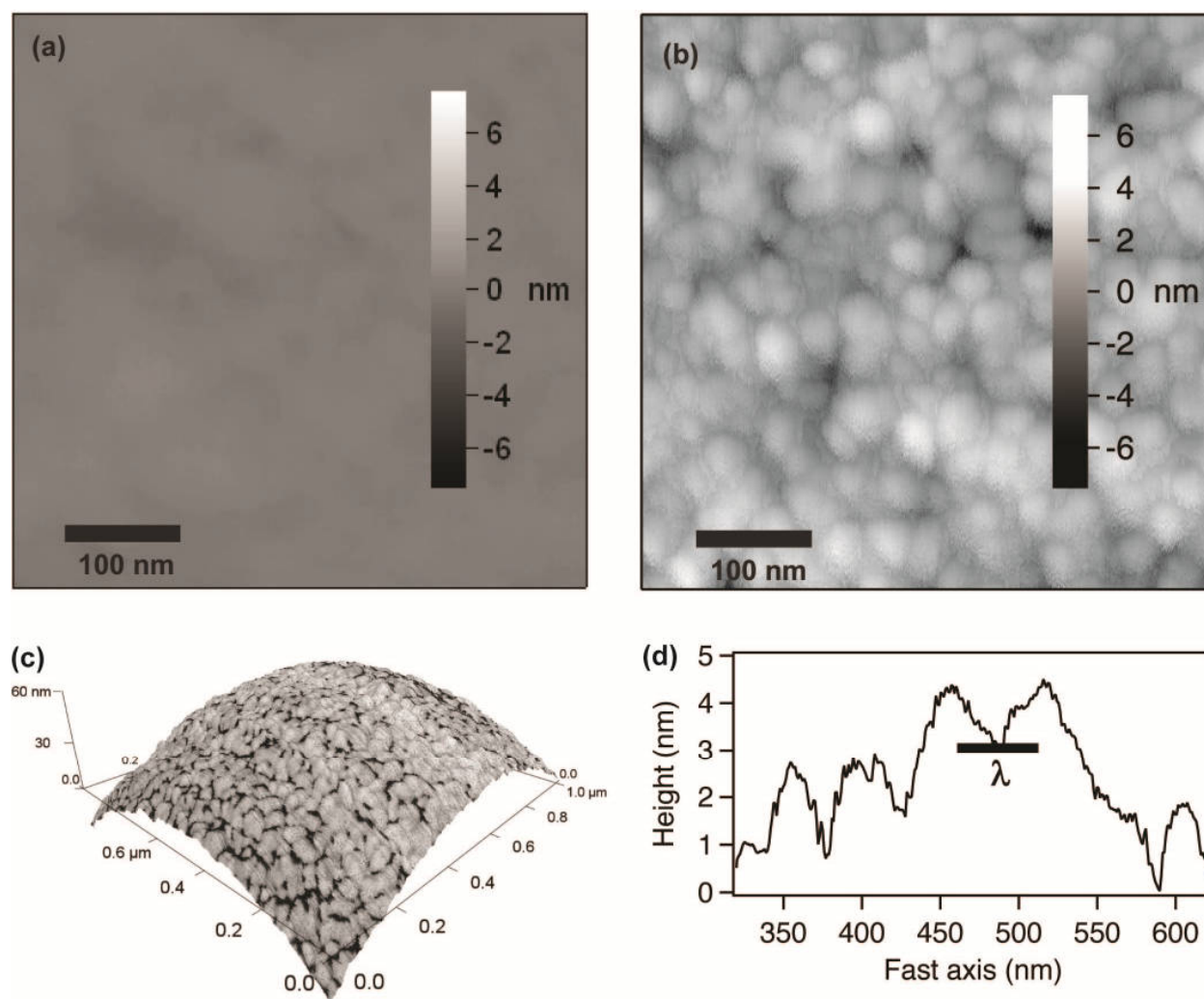
Figure 7: (a) Surface topography of a SAM-modified gold electrode and (b) a colloidal silica particle. (c) The silica particle's ultrastructure is superimposed to its curvature radius R as shown in the 3-dimensional representation. A section through the height image (after flattening) is shown in (d). The roughness parameter $\lambda = 50\,\text{nm}$, which describes the average distance between the single asperities, is indicated.

A quantitative approach to incorporate the effect of surface roughness on adhesion has been given by Rabinovich et al.[52] This model has been developed from the so-called Rumpf-model that has been the first approach to study the influence of small asperities on the adhesion. In the Rabinovich-model this methodology has been extended to periodically rough surfaces whose roughness is described by means of few parameters. This model can be further simplified when only one of the two surfaces shows significant surface roughness, as it is here the case. The surface roughness is described in this case by the following two parameters: a roughness parameter r and a characteristic distance λ between the asperities. The latter parameter is indicated in Figure 7d), which

represents a section through the surface topography of a silica colloidal probe as shown in Figure 7b). The roughness parameter r is given by $r = \lambda^2 / 32k_1 r_{rms}$, where r_{rms} is the rms-roughness of the surface and k_1 is a dimensionless constant with $k_1 = 1.817$. From the AFM-images we obtained $r_{rms} = 2.1\,\text{nm}$ and $\lambda = 50\,\text{nm}$ for the silica particles, which have an average radius R of 3.4 µm. In the framework of the JKR-model one obtains for the pull-off force including roughness effects: [53]

$$F_a^{rough} / R = \frac{3}{2}\pi W_{sol}\frac{r}{R+r} + \left[2\pi \frac{A}{12\pi D_0^2}\frac{1}{\left(1+y/D_0\right)^2} \right] \tag{4}$$

with $y = k_1 r_{rms}$ and the Hamaker constant A. The first term in equation (4) describes the contributions in the various contact points, while the second term in square brackets results from the van-der-Waals forces during contact but integrated over the entire surfaces. The nearest distance between the surfaces is given by D_0, which is commonly set to $D_0 \approx 0.16\,\text{nm}$. [2] The Hamaker constant A for the vdW-interaction between the silica particle and the SAM-modified gold electrode is here only estimated in a very approximate manner. Assuming that the Hamaker constant of the composite system electrode/water/silica probe can be approximated by $A = A_{(Au/SAM)/H_2O/SiO_x} = \sqrt{A_{(Au/SAM)/H_2O/(SAM/Au)}A_{SiO_x/H_2O/SiO_x}}$, thus neglecting the complicated interdependence of polarizabilities of gold and water, one obtains with $A_{(Au/SAM)/H_2O/(SAM/Au)} \approx 5\cdot10^{-20}\,\text{J}$ (cf. ref.[61]) and $A_{SiO_x/H_2O/SiO_x} \approx 0.77\cdot10^{-20}\,\text{J}$ (cf. ref. [62]) a Hamaker constant of $A \approx 1.9\cdot10^{-20}\,\text{J}$. Thus, the term in square brackets in eq. (4) leads to an attractive vdW-force of about 0.21 mN/m. This value should be approximately the same for both electrodes and is in the order of the experimentally determined F_i / R of $0.01 - 0.05\,\text{mN/m}$ for the electrodes at pzc and I=5mM. As the contributions due to vdW-forces are present during approach and have thus not to be taken into account for the evaluation of $\Delta F / R$, equation (4) reduces to:

$$\tilde{F}^{rough} / R = \frac{3}{2}\pi W_{sol}\frac{r}{R+r} \tag{4a}$$

With the interfacial energies compiled in Table 1 and including surface roughness according to equation (4a), we see that solvent exclusion is significantly reduced due to the surface roughness for both SAMs. The resulting values are compiled in Table 1. One finds a very good correspondence with the experimental data, considering that no free

parameters were adjusted since the roughness parameters as well as the interfacial energies were obtained by independent measurements. The remaining discrepancies at pzc can be expected since the roughness of the surfaces is summarized only by two statistical parameters and the surface topography for some particles might show significant deviations from this statistical mean.

Influence of electrocapillarity. Despite the good correspondence of $\Delta F / R$ at pzc with the calculated values, one finds a variation of $\Delta F / R$ with the external potential ϕ as shown in the bottom graph of Figure 6a). One possible explanation would be that γ_{SAM/H_2O} and γ_{SAM/SiO_x} are not independent on the applied potential. The influence of electrocapillarity effects on adhesion has been reported by Frechette et al. for studies with the electrochemical SFA.[32] Commonly, the change of the interfacial energy by the external potential is described by means of the well-known Lippmann equation, which has been originally used to describe the potential dependent rise of mercury in a capillary. For a SAM-covered electrode it reads:[63]

$$\gamma_{SAM/H_2O}(\phi) = \gamma_{SAM/H_2O}^{pzc} - \frac{1}{2} C_{SAM/H_2O} (\phi - \phi_{pzc})^2 . \tag{5}$$

In consequence, the interfacial energy of the solid/liquid interface γ_{SAM/H_2O} varies from the one at pzc γ_{SAM/H_2O}^{pzc} as a function of the externally applied potential ϕ. The interfacial capacitance C_{SAM/H_2O} for similar modified electrodes is in the order of 7.8-8.0 µF/cm^2.[64] However, the applied potentials ranges of $\phi_1 \approx -400\,\text{mV}$ to $\phi_2 \approx +400\,\text{mV}$ (vs. SCE) and are small compared to the typical potentials applied in electrowetting experiments in air.[63] With this capacitance one obtains for the CH$_3$-terminated electrode a maximal change by 21% for $\gamma_{SAM/H_2O}(\phi_2)$ in comparison to γ_{SAM/H_2O}^{pzc}. However, the Lippmann equation predicts a reduction of the interfacial energy if the potential is not identical to the pzc. Thus, equation (5) alone in combination with equation (2) fails to explain the observed increase of $\Delta F / R$ (and thus $F_a^{JKR/rough} / R$) with higher applied potentials ϕ.

Horn and coworkers demonstrated by wetting experiments that the interfacial energy between mica and mercury varies with the external potential.[65] Frechette et al. applied these results for the interface between mica and a gold electrode.[32] If we adapt their approach for the interface between the silica particle and the SAM-modified electrode one obtains:

$$\gamma_{SiO_x/SAM}\left(\phi\right)=\gamma_{SiO_x/SAM}^{pzc}-\sigma_0\left(\phi-\phi_{pzc}\right)-C_{SiO_x/SAM}\left(\phi-\phi_{pzc}\right)^2 \tag{6}$$

Here, $\gamma_{SiO_x/SAM}^{pzc}$ is the interfacial energy between the colloidal probe and the SAM-modified electrode at pzc and σ_0 is the charge density of the silica surface during contact with the SAM. This charge density σ_0 in contact is here approximated in a very coarse manner from the diffuse layer potentials by the Grahame equation[40,41] (i.e. from long-ranged interaction forces) and we obtain $\sigma_0 = 1.82$ mC/m^2 (at pH 4.7 and $I = 0.12$mM). For the most negative ($\phi_1 = -400\,\text{mV}$) or positive ($\phi_2 = +400\,\text{mV}$) potentials, the variation of the work of adhesion W_{solv} on the CH$_3$-terminated electrode can be calculated by inserting equations (5) and (6) in (2). One obtains $W_{solv}\left(\phi_1\right)/W_{solv}\left(\phi_{pzc}\right)\cong 1.00$ and $W_{solv}\left(\phi_2\right)/W_{solv}\left(\phi_{pzc}\right)\cong 1.19$, respectively, for the CH$_3$-terminated electrode. Thus, electrocapillarity due to eq. (6) could essentially account for the observed changes in $\Delta F/R$ as function of ϕ. A higher charge density of the silica particle in contact with the electrode due to charge regulation would amplify this effect and would lead to larger ratios $W_{solv}\left(\phi\right)/W_{solv}\left(\phi_{pzc}\right)$.

However, as we determine the long-ranged interaction forces independently it is clear that the dominant change in the pull-off forces originates from the forces due to diffuse layer overlap. Furthermore, we do not find the same variations of $\Delta F/R$ with ϕ at all on the OH-terminated electrode or at high ionic strengths on the CH$_3$-terminated electrode (cf. Figure 6). The absence of pronounced changes of $\Delta F/R$ as function of ϕ might be explained by charge regulation. However, a more likely explanation for the increase of $\Delta F/R$ with ϕ might be that with increasingly attractive interaction forces small instabilities near contact are taking place and the colloidal probe jumps to the surface. In consequence F_i/R would progressively underestimated with increasing potential ϕ and one would observe an apparent growth of $\Delta F/R$ (cf. Figure 2).

Adhesion of a single asperity on electrode. The above interpretation in regard to adhesion originating from electrocapillarity effects on the SAM-modified electrodes is not further supported by the adhesion behavior of a single asperity. For a single asperity of few nanometers no effects due to roughness are expected and the attractive as well as repulsive forces are too small for cantilever instabilities. A suitable single asperity is readily available from silicon cantilevers normally used for AFM contact-mode imaging.

Their tip has dimensions comparable to the ultrastructure on the silicon particle (cf.
Figure 7). Figure 8 shows the F_a / R for such a nm-sized tip (cf. inset in Figure 8) as a
function of the applied potential on a hydrophobic CH_3-terminated electrode. In order to
normalize the interaction forces for sphere/plane geometry, the effective tip radius R is
determined indirectly by the forces $F_a = 0.42\,nN$ and $\Delta F = 0.32\,nN$ at pzc and I=5mM.
The interfacial energies used in the calculation are the same as given in Table 1. This
approach is commonly followed in chemical force microscopy and equation (3) gives R.
The resulting tip radius of $R_{tip} \approx 2.5\,nm$ is in good agreement with scanning electron
microscopy (SEM) images obtained after the force measurements (cf. inset in Figure 8),
which show that the tip diameter is smaller than 10 nm.
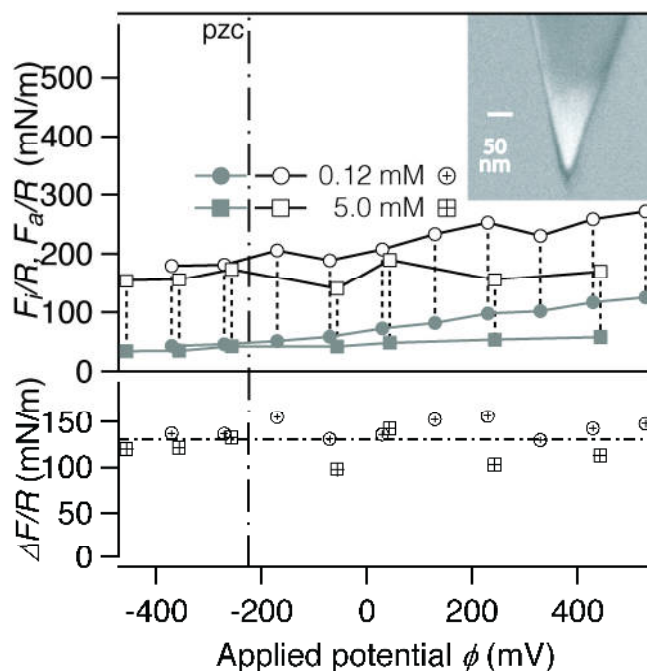
Figure 8: In the top graph: Interaction forces as measured by a nanometer-sized AFM-tip (i.e. single
asperity). Compilation of interaction forces before contact (F_i / R, filled symbols) and pull-off forces
(F_a / R, open symbols) as a function of the applied potential for different ionic strengths. In the
bottom graph: Compilation of $\Delta F / R = F_a / R - F_i / R$ as function of the applied potential. The inset
shows a SEM-image of the tip with which these measurements have been performed.

The general dependence of the pull-off forces is analog to the one found for the
colloidal probes (cf. Figure 6). However, with the single asperity a smaller scattering of
the pull-off forces is observed, as roughness does lead to variation of the contact area.
The lower graph shows the corresponding difference $\Delta F / R$ for each series. Within the
accuracy of our measurements, no variation of $\Delta F / R$ is observed with ϕ and the values

scatter around $\Delta F / R\left(\phi_{pzc}\right)$. Thus, any variation of γ_{-CH_3/H_2O} and γ_{-CH_3/SiO_x} with ϕ must be small and does not contribute significantly to the observed variation of the pull-forces with the external potential.

Conclusions

In this study we identified the main parameters that allow tuning the adhesion of colloidal particles on modified electrodes by an external potential. It is primarily the interplay between surface roughness and interfacial energy that establishes the extent to which the adhesion can be altered by the external potential. Especially, if one of the surfaces is highly hydrophobic, solvent exclusion contributes strongly and results in an adhesion 'offset'. This offset has to be compensated by repulsive diffuse layer forces to switch from adhesive to a non-adhesive behavior. On the other hand, a high surface roughness reduces the 'true' contact area with the particle and thus diminishes the influence of surface hydrophobicity. This effect has been demonstrated by comparing the adhesion between a sharp AFM-tip and colloidal probes of comparable surface chemistry.

Electrocapillarity effects do not play a major role in the adhesion on SAM-modified electrodes. It is primarily the long-ranged force due to the overlap of the electrical double layers, which provides the control of the adhesion as a function of the external potential. The charge density of the colloidal particles is in this respect an important parameter as it generates one of the two diffuse layers involved in the interaction. The presence of additional intrinsic charges from the SAM or by specifically adsorbed ions influences the diffuse layer of the electrode and additionally shifts the position of the potential of zero charge (pzc). Thus, both parameters directly influence the slope of the pull-off force in respect to the externally applied potential (cf. Figure 5). An additional parameter, albeit of less importance, is the thickness of the modification layer (i.e. SAM). The thicker this layer is, the larger is the potential drop in respect to the external potential and thus the smaller is the variation of the electrode's diffuse layer.

By tuning the composition of the SAM, e.g. by mixed SAMs, it is possible to adapt the electrode's adhesion behavior for a given batch of colloidal particles in a rational manner to prevised applications, not also in terms of the adhesive strength but also terms of the window of electrochemical potentials. Therefore, our results should be not only of importance for electrochemical sensors but also for the design of micro-electromechanical systems (MEMS) such as grippers.[66] Another feasible application

would be a new approach for the nano- and micromanipulation by AFM that would be based on switching the adhesion behavior rather than applying shear forces.

Acknowledgments

Supporting Information Available

The supporting information contains an example for a force profile between silica particles in the sphere/sphere geometry and summarizes the parameters obtained from the corresponding fits to the full solutions of the Poisson-Boltzmann equation including the constant regulation approximation. This information is available free of charge via the Internet at http://pubs.acs.org/.

References:

(1)   Williams, R. H.; Elimelech, M. *Particle Deposition & Aggregation*; Butterworth-Heinemann, 1998.

(2)   Israelachvili, J. N. *Intermolecular and surface forces*; American Press, 1992; pp. 1–470.

(3)   Gao, J.; Luedtke, W.; Gourdon, D.; Ruths, M.; Israelachvili, J.; Landman, U. *J Phys Chem B* **2004**, *108*, 3410–3425.

(4)   Love, J.; Estroff, L.; Kriebel, J.; Nuzzo, R.; Whitesides, G. *Chem Rev* **2005**, *105*, 1103–1169.

(5)   Claesson, P.; Dedinaite, A.; Rojas, O. *Adv Colloid Interfac* **2003**, *104*, 53–74.

(6)   Noy, A.; Frisbie, C.; Roznyai, L.; Wrighton, M.; Lieber, C. *Journal of the American Chemical Society* **1995**, *117*, 7943–7951.

(7)   Sinniah, S.; Steel, AB; MILLER, C.; Reutt-Robey, J. *Journal of the American Chemical Society* **1996**, *118*, 8925–8931.

(8)   Papastavrou, G.; Akari, S.; Mohwald, H. *Europhys Lett* **2000**, *52*, 551–556.

(9)   Papastavrou, G.; Akari, S. *Colloid Surface A* **2000**, *164*, 175–181.

(10)   Warszynski, P.; Papastavrou, G.; Wantke, K. D.; Mohwald, H. *Colloid Surface A* **2003**, *214*, 61–75.

(11)   Vezenov, D.; Noy, A.; Ashby, P. *J Adhes Sci Technol* **2005**, *19*, 313–364.

(12)   Maeda, N.; Chen, N.; Tirrell, M.; Israelachvili, J. *Science* **2002**, *297*, 379–382.

(13)   Laboriante, I.; Bush, B.; Lee, D.; Liu, F.; Liu, T.-J. K.; Carraro, C.; Maboudian, R. *J Adhes Sci Technol* **2010**, *24*, 2545–2556.

(14)   Raduge, C.; Papastavrou, G.; Kurth, D.; Motschmann, H. *Eur Phys J E* **2003**, *10*, 103–114.

(15)   Schmidt, S.; Zeiser, M.; Hellweg, T.; Duschl, C.; Fery, A.; Moehwald, H. *Adv Funct Mater* **2010**, *20*, 3235–3243.

(16)   Gileadi, E. *J Electroanal Chem* **1966**, *11*, 137–&.

(17)   Frechette, J.; Vanderlick, T. K. *Ind Eng Chem Res* **2009**, *48*, 2315–2319.

(18)   Butt, H. *Biophys J* **1991**, *60*, 1438–1444.

(19)   Ducker, W.; Senden, T. J.; Pashley, R. M. *Nature* **1991**, *353*, 239–241.

(20)   Kappl, M.; Butt, H. *Part Part Syst Char* **2002**, *19*, 129–143.

(21)   Papastavrou, G. *Colloid Polym Sci* **2010**, *288*, 1201–1214.

(22)   Ishino, T.; Hieda, H.; Tanaka, K.; Gemma, N. *Jpn J Appl Phys 2* **1994**, *33*, L1552–L1554.

(23)   Hillier, A.; Kim, S.; Bard, A. *J Phys Chem-Us* **1996**, *100*, 18808–18817.

(24)   Campbell, S.; Hillier, A. *Langmuir* **1999**, *15*, 891–899.

(25)   Raiteri, R.; Preuss, M.; Grattarola, M.; Butt, H. *Colloid Surface A* **1998**, *136*, 191–197.

(26)   Barten, D.; Kleijn, J.; Duval, J.; Leeuwen, von, H.; Lyklema, J.; Stuart, M. *Langmuir* **2003**, *19*, 1133–1139.

(27)   Hu, K.; Fan, F.; Bard, A.; Hillier, A. *J Phys Chem B* **1997**, *101*, 8298–8303.

(28)   Frechette, J.; Vanderlick, T. *Langmuir* **2001**, *17*, 7620–7627.

(29)   Valtiner, M.; Kristiansen, K.; Greene, G. W.; Israelachvili, J. N. *Adv Mater* **2011**, *23*, 2294–.

(30)   Serafin, J. M.; Gewirth, A. A. *J Phys Chem B* **1997**, *101*, 10833–10838.

(31)   Kwon, H.; Gewirth, A. *J Phys Chem B* **2005**, *109*, 10213–10222.

(32)   Frechette, J.; Vanderlick, T. *Langmuir* **2005**, *21*, 985–991.

(33)   Stamou, D.; Gourdon, D.; Liley, M.; Burnham, N.; Kulik, A.; Vogel, H.; Duschl,

C. *Langmuir* **1997**, *13*, 2425–2428.

(34)   KERN, W.; PUOTINEN, D. *Rca Rev* **1970**, *31*, 187–&.

(35)   Hutter, J. L.; Bechhoefer, J. *Rev Sci Instrum* **1993**, *64*, 1868–1873.

(36)   Rentsch, S.; Siegenthaler, H.; Papastavrou, G. *Langmuir* **2007**, *23*, 9083–9091.

(37)   Rentsch, S. Direct Force Measurements Between Surfaces Under Potentiostatic Control, Ph.D. thesis, University of Geneva, Faculty of Sciences, 2008.

(38)   Ammann, E.; Beuret, C.; Indermuhle, P.; Kotz, R.; de Rooij, N.; Siegenthaler, H. *Electrochim Acta* **2001**, *47*, 327–334.

(39)   Pericet-Camara, R.; Papastavrou, G.; Behrens, S.; Borkovec, M. *J Phys Chem B* **2004**, *108*, 19467–19475.

(40)   Pericet-Camara, R.; Papastavrou, G.; Behrens, S.; Helm, C.; Borkovec, M. *J Colloid Interf Sci* **2006**, *296*, 496–506.

(41)   Rentsch, S.; Pericet-Camara, R.; Papastavrou, G.; Borkovec, M. *Phys Chem Chem Phys* **2006**, *8*, 2531–2538.

(42)   Butt, H.; Cappella, B.; Kappl, M. *Surf Sci Rep* **2005**, *59*, 1–152.

(43)   Munakata, H.; Oyamatsu, D.; Kuwabata, S. *Langmuir* **2004**, *20*, 10123–10128.

(44)   Hartley, P.; Larson, I.; SCALES, P. *Langmuir* **1997**, *13*, 2207–2214.

(45)   Giesbers, M.; Kleijn, J.; Fleer, G.; Stuart, M. *Colloid Surface A* **1998**, *142*, 343–353.

(46)   Guriyanova, S.; Mairanovsky, V. G.; Bonaccurso, E. *J Colloid Interf Sci* **2011**, *360*, 800–804.

(47)   Duval, J.; Kleijn, J.; Lyklema, J.; van Leeuwen, H. *J Electroanal Chem* **2002**, *532*, 337–352.

(48)   Kreuzer, H.; Wang, R.; Grunze, M. *Journal of the American Chemical Society* **2003**, *125*, 8384–8389.

(49)   Luetzenkirchen, J.; Preocanin, T.; Kallay, N. *Phys Chem Chem Phys* **2008**, *10*, 4946–4955.

(50)   Zimmermann, R.; Freudenberg, U.; Schweiss, R.; Kuettner, D.; Werner, C. *Curr Opin Colloid In* **2010**, *15*, 196–202.

(51)   Schwarz, U. *J Colloid Interf Sci* **2003**, *261*, 99–106.

(52)   Rabinovich, Y.; Adler, J.; Ata, A.; Singh, R.; Moudgil, B. *J Colloid Interf Sci* **2000**, *232*, 17–24.

(53)   Segeren, L.; Siebum, B.; Karssenberg, F.; Van den Berg, J.; Vancso, G. *J Adhes*

Sci Technol **2002**, *16*, 793–828.

(54)   Tsukruk, V. V.; Bliznyuk, V. N. *Langmuir* **1998**, *14*, 446–455.

(55)   Batteas, J.; Quan, X.; Weldon, M. *Tribol Lett* **1999**, *7*, 121–128.

(56)   Guleryuz, H.; Royset, A. K.; Kaus, I.; Filiatre, C.; Einarsrud, M.-A. *J Sol-Gel Sci Techn* **2012**, *62*, 460–469.

(57)   Nalaskowski, J.; Drelich, J.; Hupka, J.; Miller, J. *Langmuir* **2003**, *19*, 5311–5317.

(58)   Beach, E.; Tormoen, G.; Drelich, J.; Han, R. *J Colloid Interf Sci* **2002**, *247*, 84–99.

(59)   Gotzinger, M.; Peukert, W. *Langmuir* **2004**, *20*, 5298–5303.

(60)   Tormoen, G.; Drelich, J.; Beach, E. *J Adhes Sci Technol* **2004**, *18*, 1–17.

(61)   Ederth, T. *Langmuir* **2001**, *17*, 3329–3340.

(62)   Senden, T.; Drummond, C. *Colloid Surface A* **1995**, *94*, 29–51.

(63)   Mugele, F.; Baret, J. *J Phys-Condens Mat* **2005**, *17*, R705–R774.

(64)   Ekeroth, J.; Konradsson, P.; Bjorefors, F.; Lundstrom, I.; Liedberg, B. *Anal Chem* **2002**, *74*, 1979–1985.

(65)   Antelmi, D.; Connor, J.; Horn, R. *J Phys Chem B* **2004**, *108*, 1030–1037.

(66)   Dejeu, J.; Bechelany, M.; Rougeot, P.; Philippe, L.; Gauthier, M. *ACS nano* **2011**, *5*, 4648–4657.

Supporting information

Interaction forces between silica particles in the sphere/sphere geometry. In order to determine unambiguously the diffuse layer potential of the modified electrodes, we determined first the diffuse layer properties of the silica colloidal probe. These measurements have been performed in a completely symmetric system, which consists of two silica spheres. Thus, these measurements have been performed in the sphere/sphere geometry as presented in a previous publication.[1]
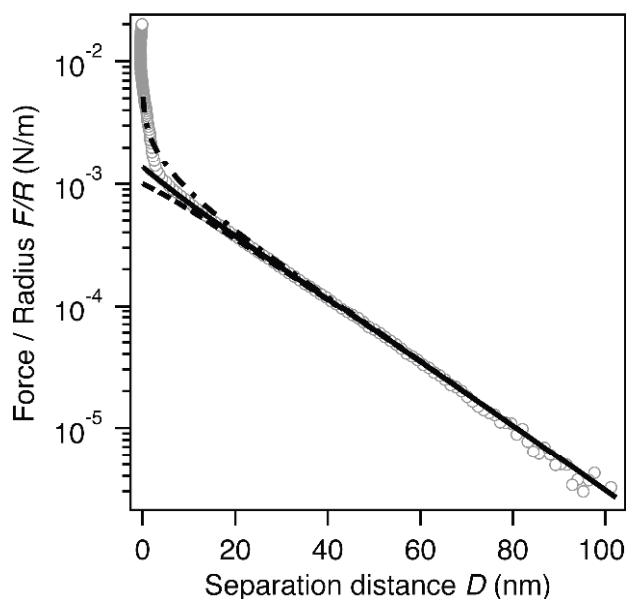

Figure S1: Exemplary force versus distance profiles upon approach between a silica colloidal probe and a colloidal silica particle immobilized on a glass slide. The force profile has been averaged from about 50 single force profiles. The solid line indicates the fit to the full Poisson-Boltzmann equation including the charge regulation. By contrast, the dashed lines represent the solution to classical boundary conditions of constant charge (top) and constant potential (bottom), respectively.

Figure S1 shows an exemplary interaction force profile for two silica particle at pH 4.7 and a total ionic strength of I=0.34 mM. Before acquiring the force profiles the colloidal particles are aligned axially by optical microscopy and so-called force volume plots, where the lateral position of the colloidal probed is varied on a lattice. Both colloidal particles are prepared in an identical manner. Thus, a comparable surface chemistry of both particles is ensured.

Fitting Poisson-Boltzmann equation with constant regulation approximation. The force average force profiles acquired in the sphere/sphere geometry have been fit to the full solutions of the Poisson-Boltzmann equation. Here, we included besides the classical boundary conditions of constant charge and constant potential also the so-called constant

regulation approximation.[2] This approximation summarizes the charge regulation of the interacting surface by the diffuse layer potentials of the isolated surfaces ψ^D and a regulation parameter p, which is defined as:

$$p = \frac{C_d}{C_d + C_i} \tag{S-1}$$

where C_i is the inner layer capacitance and C_d is the diffuse layer capacitance given by

$$C_d = \varepsilon\varepsilon_0 \kappa \cosh(e\psi^D / 2k_B T)$$

where $\varepsilon\varepsilon_0$ is the total permittivity of the water, $k_B T$ the thermal energy and e the elementary charge. The inverse Debye-length κ is given by equation (1).

The regulation parameter takes typically values between 0 and 1. The former value corresponds to the boundary condition of constant potential ($p=0$) and the latter to the one of constant charge ($p=1$). The values for the regulation parameter obtained from the fits scatter substantially. However, here we limited the fit interval to separations larger than one Debye-length κ^{-1}. Therefore, the regulation parameter has no substantial effect on the diffuse layer potentials obtained from the fits to the constant-regulation approximation. We find that the diffuse layer potentials are in general agreement with the inverse Grahame-equation:

$$\psi^D = \frac{2k_B T}{e} \operatorname{asinh}\left(\frac{e\sigma}{2k_B \varepsilon\varepsilon_0 \kappa}\right) \tag{S-2}$$

where σ is the diffuse layer charge density of the isolate silica particles.

The values for ψ^D and p resulting from the fits are compiled in Table S1. The obtained diffuse layer potentials are in good general agreement with values reported in other studies. In order to determine the diffuse layer potentials of the electrodes at different external potentials, we used the values compiled in Table S1 as fixed parameters for the silica particles and fitted the diffuse layer potential ψ^D (and the regulation parameter) of the electrode at a given ionic strength. Further details concerning this approach, in particular in respect to the regulation parameter for an electrode under potentiostatic control, can be found elsewhere.[3,4]

Table S1: Compilation of diffuse layer potential and regulation parameters for silica colloidal probes at different ionic strengths

| Ionic strength	0.12 (mM)	0.34 (mM)	0.56 (mM)	5.0 (mM)
ψ^D (mV)	-58.0	-57.3	-53.0	-37.6
p	0.80	0.70	0.60	0.10

References:

(1)   Rentsch, S.; Pericet-Camara, R.; Papastavrou, G.; Borkovec, M. *Phys Chem Chem Phys* **2006**, *8*, 2531–2538.

(2)   Pericet-Camara, R.; Papastavrou, G.; Behrens, S.; Borkovec, M. *J Phys Chem B* **2004**, *108*, 19467–19475.

(3)   Rentsch, S.; Siegenthaler, H.; Papastavrou, G. *Langmuir* **2007**, *23*, 9083–9091.

(4)   Rentsch, S. *Direct Force Measurements Between Surfaces Under Potentiostatic Control*, Ph.D. thesis, University of Geneva, Faculty of Sciences, 2008.

6. Ion Adsorption on Modified Electrodes as Determined by Direct Force Measurements under Potentiostatic Control

Volodymyr Kuznetsov and Georg Papastavrou*

Department of Physical Chemistry II, University of Bayreuth,

Universitätstraße 30, 95440 Bayreuth, Germany

*E-mail corresponding author: Georg.Papastavrou@uni-bayreuth.de
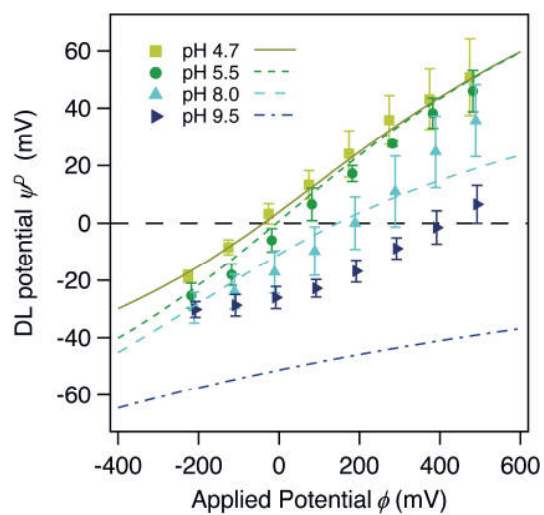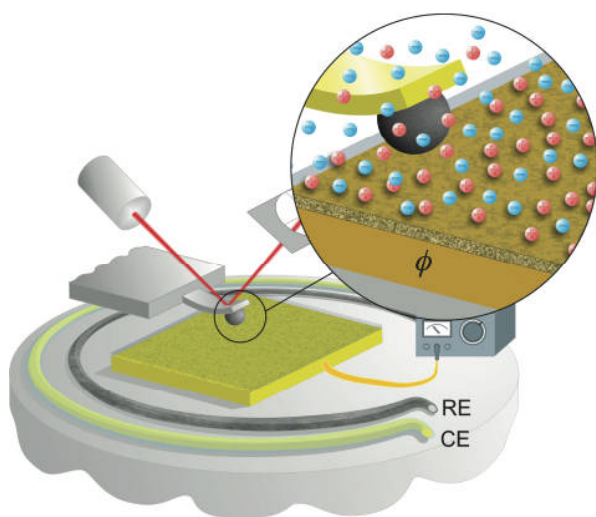
Abstract:

The existence and the scope of interfacial charging behavior of inert polymers due to contact with aqueous solutions remain under discussion, though such polymers are widely used for contamination-sensitive applications. A novel sensitive method to quantify ion adsorption on non-ionizable organic interfaces was developed. It is based on direct force measurements between a colloidal probe and an electrode modified with self-assembled monolayer (SAM) terminated in a defined group. To describe the charging of methyl- and hydroxyl-terminated SAMs in electrolyte solutions, diffuse layer properties were determined as a function of externally applied potential and solution pH. The observed variations qualitatively support the notion of specific charge accumulation in the Stern layer. Based on the assumption about the specific adsorption of hydronium and hydroxide ions the three-capacitor model was used to describe the data. Generally, it provides semi-quantitative description of charging, though improvements are envisaged.

Introduction

The interfaces of water with gases, solids or other immiscible liquids are ubiquitous on this planet and belong certainly to the most important ones. Interfaces with water are of central importance not only for life or environment but also for many industrial processes.[1-3] However, only recently a number of theoretical and experimental studies addressed them on the molecular level. Of particular interest has been the interface between water and hydrophobic phases, such as the water/oil, water/lipid layer, or water/air interfaces. The charge accumulation at such interfaces has been under discussion since different experimental techniques provided apparently contradicting data. In this respect it has been of central interest to which extent hydroxyl and hydronium ions adsorb preferentially at hydrophobic interfaces.[4-6] Some spectroscopic techniques that are sensitive to the interfacial layer of molecules provided evidence that a preferential adsorption of hydronium ions is taking place.[7-9] However, studies based on electrophoretic techniques that probe the diffuse layer of the interface indicated an overall negative sign for the diffuse layer potential and hence suggested the adsorption of hydroxyl-ions.[10-18] However, molecular dynamics simulations appeared controversial in their results.[7,19-21]

Here, we provide a new experimental approach to study ion adsorption at hydrophobic and hydrophilic interfaces. Our approach is based on direct force measurements on modified electrodes and thus provides different approach in regard to electrokinetic techniques. Firstly, the diffuse layer potentials determined by direct force measurements are unambiguous concerning the position of the plane of shear. Secondly, the external potential applied to the modified electrode, which corresponds to the potential of zero charge (pzc) where the diffuse layer potential of the electrode is vanishing depends critically on the presence of adsorbed ions at the interface. A corresponding theoretical model that quantitatively describes the diffuse layer potential as a function of the externally applied potential can be easily adapted to this configuration.

Direct force measurements on electrodes under potentiostatic control have been reported previously.[22-27] However, here the electrode is additionally modified by a self-assembled monolayer (SAM) that allows to render the surface of a gold electrode in a very defined manner either hydrophobic or hydrophilic. The SAMs examined in this study comprise only functional groups that do not show ionization behavior as a function of pH, namely hydroxyl and methyl groups. In previous studies with this type of electrodes we concentrated on the diffuse layer properties as a function of thiol-length and ω-functionalization[28] or the adhesion behavior.[29] Instead, here we determine the diffuse layer properties not only as a function of the external potential but also of the pH in order to probe the ion adsorption at the interface to the SAM. Previously for comparable SAMs the streaming potential has been determined as a function of pH and ionic strength.[17,30,31] This potential is comparable to the open-circuit potential obtained by direct force measurements, where the potentiostat is disconnected from the electrode. Furthermore, Kreuzer et al.[21] provided a theoretical study of the diffuse layer potential of thiol-SAMs terminating in hydroxyl- or methyl-groups.

Materials and methods

Materials. 16-mercaptohexadecanol-1 (99%, Frontier Scientific) and 1-hexadecanthiol (99%, Sigma Aldrich) were used for the electrode modification as received. Solutions with these thiols were prepared with ethanol of analytical grade. All aqueous solutions were prepared with deionized water of Milli-Q grade with a resistivity larger than 18MΩ. The pH and total ionic strength of working solutions were adjusted

with 1M HCl or 1 M KOH, and 1 M KCl (all analyitical grade and purchased from Sigma Aldrich) solutions correspondingly. The pH for solutions in the basic regime has been adjusted directly before the measurements by adding an specifically calculated amount of KOH of the already degassed solutions containing the appropriate amount of KCl. The total ionic strength of all aqueous solutions was 1.2 mM if not stated otherwise.

Preparation of flat gold electrodes. The electrodes were prepared as reported recently.[29] The modification was carried out by a modified 'template stripping' method.[32,33] On RCA-cleaned Si-wafers (CrysTec, Berlin, Germany) a 60 nm layer of gold (99.99% purity) was deposited by thermal evaporation (mini-coater, tectra, Germany). After evaporation the glass slides of 11x11 mm were glued to the gold layer by means of a chemically resistant adhesive (EPO- TEK 377, Epoxy Technology Inc.), with subsequent thermal cure (1 h, 150 °C).

The electrodes were prepared by separating mechanically the glass-slides (glass/glue/gold) from the wafer. The former were immediately rinsed copiously with ethanol and then transferred to the appropriate thiol solutions. Surface modification by thiols was performed in 1mM ethanolic solution of 16-mercaptohexadecan-1-ol or 1-hexadecanthiol, respectively, for at least 12 hours. The electrodes with OH-terminated SAMs were rinsed with copious amount of ethanol and then with water. The electrodes with CH_3-terminated SAMs were rinsed with copious amounts of ethanol and then sonicated twice in fresh ethanol in an ultrasonic bath. The electrodes were then immediately mounted in the electrochemical cell, covered with degassed electrolyte solution. Directly afterwards the AFM fluid cell has been closed.

Preparation of colloidal probes and AFM-cantilever for force measurements. Tipless AFM cantilevers (NSC12, Mikromasch) were cleaned consecutively in a series of solvents (ethanol, aceton, chloroform, aceton, and ethanol) and were then treated by in oxygen plasma (90 s, 100 W, 0.4 mbar) in a commercial plasma cleaner (Flecto10, Plasma Technology GmbH, Herrenberg, Germany). Afterwards they were coated by thermal evaporation with a reflection layer consisting of 3 nm chromium (Sigma-Aldrich) as adhesion promoter and 60 nm gold (99.99%). In order to avoid thermal in liquid the tipless cantilevers have been coated from both sides. For the preparation of colloidal probes silica particles (Bangs Laboratories, IN) with an average diameter of 6.8 μm were attached to these cantilevers by means of a micromanipulator and UV-curable glue

(Optical adhesive 63, Norland Products). We used cantilevers with nominal force constants in the range of 0.17 N/m and 4.14 N/m. The force constants of these cantilevers have been determined by the thermal noise method before the attachment of the colloidal particles.[34] Directly before the force measurements the colloidal probes were cleaned consecutively in a series of solvents alike bare cantilevers and were then treated in oxygen plasma (90 s, 100 W, 0.4 mbar).

Combined setup for electrochemistry and AFM. To measure interaction forces under potentiostatic control a custom-made electrochemical cell has been constructed for a commercial atomic force microscope (MFP-3D, Asylum Research, Santa Barbara, CA).[35] The setup is shown schematically in Figure 1. The electrode modified by a SAM is acting as working electrode and is connected to a custom-built potentiostat that is based on a design from the group of H. Siegenthaler (University of Berne, Switzerland).[28,29,36] In this 3-electrode electrochemical cell a 100 mm gold wire with a diameter of 0.25 mm used as counter-electrode (Alfar-Aesar) and silver wire coated with Ag/AgCl, which was placed in a circular manner around the working electrode was used as reference electrode. All aqueous solutions were degassed, firstly, by purging with nitrogen for 15 min and then with an HPLC-degassing unit directly placed before the inlet of the electrochemical cell (Gastorr BG12, Flom). The electrolyte solutions degassed in this way were exchanged by a peristaltic pump (Reglo Analog C MS-2/08-160, ISMATEC) and the pH was controlled at the outlet by means of a special pH-electrode for low ionic strengths (Aquatrode Plus 6.0253.100, Metrohm) in a specially constructed flow-through cell from polypropylene that allowed working under inert atmosphere.
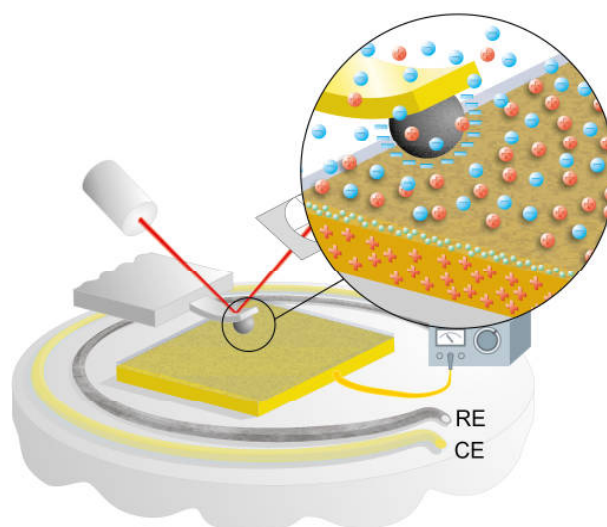
Figure 1: Schematic representation of the experimental setup to determine the interacting forces between a colloidal probe and a gold electrode modified by a self-assembled monolayer (SAM) terminating in non-ionizable functional groups. The electrode is connected as working electrode (WE) to a potentiostat in a 3-electrode electrochemical cell with counter (CE) and reference (RE) electrodes.

Before each set of force measurements the SAM on the modified gold electrodes has been controlled by cyclic voltammetry (CV). The applied potential range, where no thiol desorption occurs, has been determined in a series of experiments independently from the direct force measurements presented here.[29,37]   Additionally, during the force measurements the current was monitored to verify that no thiol desorption is taking place.

Direct force measurements. The force measurements were performed with an AFM equipped with a closed loop control for all three axes (MFP-3D, Asylum Research, CA). For each applied potential, a series of at least 100 approach and retraction cycles with a velocity of 0.8 μm/s has been acquired. For the force profiles of one series, no significant differences between the first and the last curve could be observed. The maximum loading force was in the order of 12-15 nN.

The measured deflection versus piezo displacement curves were converted to force versus distance profiles by custom written procedures in IGOR PRO (Wavemetrics) based on standard algorithms.[38] In order to determine the diffuse layer potentials of the electrodes the series of force profiles attributed to one external potential has been averaged and then fitted.[28,29]The force profiles are normalized by effective radius and are fitted to the full solutions of the Poisson- Boltzmann equation by means of a custom written program in FORTRAN and IGOR PRO (Wavemetrics).[39] Further details concerning the quantitative analysis of the interaction force profiles can be found elsewhere.[38] Routinely, the Debye length obtained from these fits has compared to the nominal ionic strength of the electrolyte solutions. Commonly, deviations smaller than 10% for the ionic strength are observed and all data sets reported here fulfill this criterion.

The measurement of the interaction forces between two silica particles in the sphere-sphere geometry has been performed in a closed fluid cell (Asylum Research, Santa Barbara, CA) with a round glass cover slide as bottom. The two particles, one attached to the probe and one attached to the slide, were coarsely aligned by optical microscopy; the following fine alignment was achieved by a procedure similar to force volume plots. Further details are given elsewhere.[40,41] The data analysis has been performed in an

analogous manner to the one for the measurements on the electrodes.

Results and discussion

In this study we have determined the diffuse layer properties of SAM-modified electrodes as a function of the pH of the electrolyte solution and varied additionally the external potential of the electrode. We used two types of SAMs with non-ionizable terminating groups, which are either hydrophobic (CH_3-terminated) or hydrophilic (OH-terminated) properties, The electrode´s diffuse layer potentials are obtained from fits to the interaction force profiles that are acquired by the colloidal probe technique based on the AFM. However, a prerequisite for a quantitative evaluation of the interaction force profiles is to determine first the diffuse layer properties of the colloidal probe in the examined pH-range. The force profiles on the electrodes are then fit to the full solutions of the Poisson-Boltzmann equation. The resulting electrodes' diffuse layer potentials can be semi-quantitatively described as a function of pH and applied potential in the framework of a recently published model that takes ion adsorption of hydronium and hydroxide ions to the SAM into account.[42]

Diffuse layer properties of the colloidal probe.   Figure 2 shows exemplary interaction force profiles between a colloidal silica probe and identical silica spheres attached to a flat substrate. Such direct force measurements in the sphere-sphere geometry are necessary for determining the diffuse layer properties of the colloidal probe in a completely symmetric system before using the probes under identical conditions to evaluate the diffuse layer properties of electrodes.[28,29]   Each force profile shown results from the averaging of about 50 single force curves. All measurements have been performed at different pH-values but constant ionic strength of $I = 1.2$ mM.
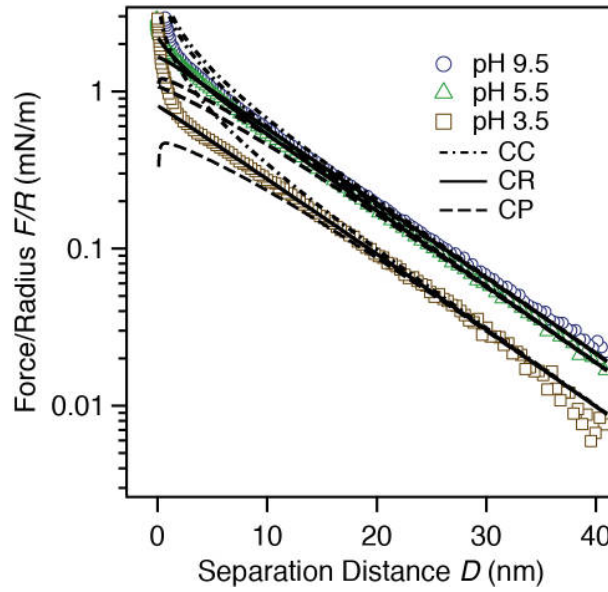
Figure 2: Interaction forces between silica particles in the sphere geometry for different pH-values but constant ionic strength (I=1.2 mM). The fits to the PB-equation with different boundary conditions are represented by the dashed (CC constant charge, CP constant potential) and full (CR charge regualtion approximation) lines.

The force profiles for the interaction between two silica particles show for all pH-values repulsive forces over the full separation distance and can be described by the overlap of the two diffuse layers originating from the particles. At separations larger than about 10-15 nm, the interaction force decays exponentially as indicated by the straight lines in the semi-logarithmic representation of Figure 2. The decay constant is given by the by the inverse of the Debye-length κ^{-1} with

$$\kappa^{-1} = \sqrt{\frac{\varepsilon\varepsilon_0 kT}{2N_A e^2 I}} \tag{1}$$

where $\varepsilon\varepsilon_0$ is the total permittivity of water, kT is the thermal energy at absolute temperature, N_A is Avogadro's number, e is the elementary charge and I is the ionic strength. The interaction force in Figure 2 have been normalized to the effective radius R_{eff}

$$\frac{1}{R_{eff}} = \frac{1}{R_{CP}} + \frac{1}{R_S} \tag{2a}$$

with the radii R_{CP} and R_S, of the colloidal probe and the immobilized particle, respectively. In the case of sphere-plane geometry, as for the electrodes, equation (2) reduces to $R_{eff}=R_{CP}$, where R_{CP} is the radius of the colloidal probe. In this manner the

experimental force profiles $F(D)/R_{eff}$ can be evaluated quantitatively by the Derjaguin equation with the free interaction energy $W_{int}(D)$ of two infinite plates at separation D by

$$F(D) = 2\pi R_{eff} W_{int}(D) \tag{2b}$$

where $W_{int}(D)$ for the silica surface results from overlap of their diffuse layers and is thus given by the solutions of the Poisson-Boltzmann (PB-) equation.

The dashed lines in Figure 2 represent fits to the full solutions of the PB-equation with the classical boundary conditions of constant charge (CC) and constant potential (CP). The solid lines represent fits to the constant regulation approximation (CR) that takes into account the charge regulation between the two surfaces.[39] In this approximation the influence of surface chemistry of the surfaces is summarized by the diffuse layer potential ψ^P at infinite separation and a regulation parameter p that is defined by[39]

$$p = \frac{C^D}{C^I + C^D} \tag{3}$$

Here, C^I is the inner layer capacitance and C^D is the diffuse layer capacitance. The latter is given by

$$C^D = \varepsilon\varepsilon_0\kappa \cosh\left(\frac{e\psi^D}{2kT}\right) \tag{4}$$

where ψ^P is the diffuse layer potential at infinite separation of the surfaces.[39] Commonly, the regulation parameter ranges from 0 to 1, where the $p=0$ corresponds to CP and $p=1$ to CC. In order to describe the interaction profiles over the full range of separations, one has to take into account charge regulation. Charge regulation is also important to describe the interaction force between a silica colloidal probe and an electrode.[28] However, the diffuse layer potentials obtained from the fits are not significantly influenced from p as long as the interaction force profiles are evaluated at separation distances larger than about κ^{-1}. The absence of attractive force at small separations due to van-der-Waals forces results from the surface roughness of colloidal silica particles and has been observed previously.[40,41]

Variation of colloidal probe properties with pH. By fitting interaction force profiles like the ones shown in Figure 2, the diffuse layer potentials ψ^P and the regulation parameters p can be determined for the different pH-values. Hover, the sign of the diffuse layer potentials cannot be inferred from the interaction forces in a symmetric system but

it is known to be negative.[43,44] In Table 1 the results from at least 5 pairs of particles and two different colloidal probes are summarized.

Table 1: Diffuse layer potentials and regulation parameters for the silica colloidal probes at different pH.values and I = 1.2 mM

pH	3.5	4.7	5.5	8.0	9.5
ψ^D (mV)	-30.2 ± 2.3	-44.2 ± 4.2	-44.9 ± 6.0	-45.7 ± 3.8	-47.4 ± 3.1
p	0.60 ± 0.10	0.50 ± 0.05	0.50 ± 0.20	0.60 ± 0.25	0.60 ± 0.20

The diffuse layer potentials in Table 1 are in good general agreement with the values reported by other groups.[45,46] However, the silica surface chemistry is highly susceptible to preparation history and conditions. Thus, diffuse layer potentials reported in the literature vary significantly. The increase and successive leveling-off of ψ^D for high pH-values follows the trend expected from surface chemistry of silica according to 1-pK or 2-pK dissociation models for the ionization behavior.[47] In the pH-range studied here the regulation parameter changes only slightly and the observed variations are within the accuracy of the method. The values for the regulation parameter of p = 0.3-0.8 are in general agreement with   calculations based on a 1-pK model.[39] The average values summarized in Table 1 for ψ^D and p are used in the following for the quantitative analysis the interaction force profiles on the SAM-modified electrodes.

Interaction profiles over SAM-modified electrodes. Figure 3 shows a selection of exemplary force profiles on SAM-modified electrodes acquired with colloidal probes whose diffuse layer properties have been determined previously. The measurements compiled in Figure 3 have performed on two different electrodes that were either modified by OH-terminated SAMs (cf. Figure 3a,b) or a CH$_3$-terminated SAMs (cf. Figure c,d). The measurements have been performed in solutions of different pH and additionally the potential applied to the electrodes has been varied over a wide range. From the full range of pH-values ranging from pH 3.5 to pH 9.5 examples slightly acidic (i.e. pH 5.5, cf. Figure a,c) and slightly basic (i.e. pH 8.0, cf. Figure b,d) pH-regime are shown.. For each pH-value a series of different potentials ϕ_i has been applied to the electrode, ranging from approximately ϕ_1=-225mV (vs. SCE) to ϕ_8=+475mV (vs. SCE). Each force profile shown for a given potential ϕ_i is obtained by averaging about 100

single force curves acquired at this protential. These potentials may vary slightly (<5%) for the reference electrode used in the study (Ag/AgCl-wire). Its potential against commercial Ag/AgCl-electrode was *in-situ* determined in the AFM cell before and after the experiments under used solution conditions.
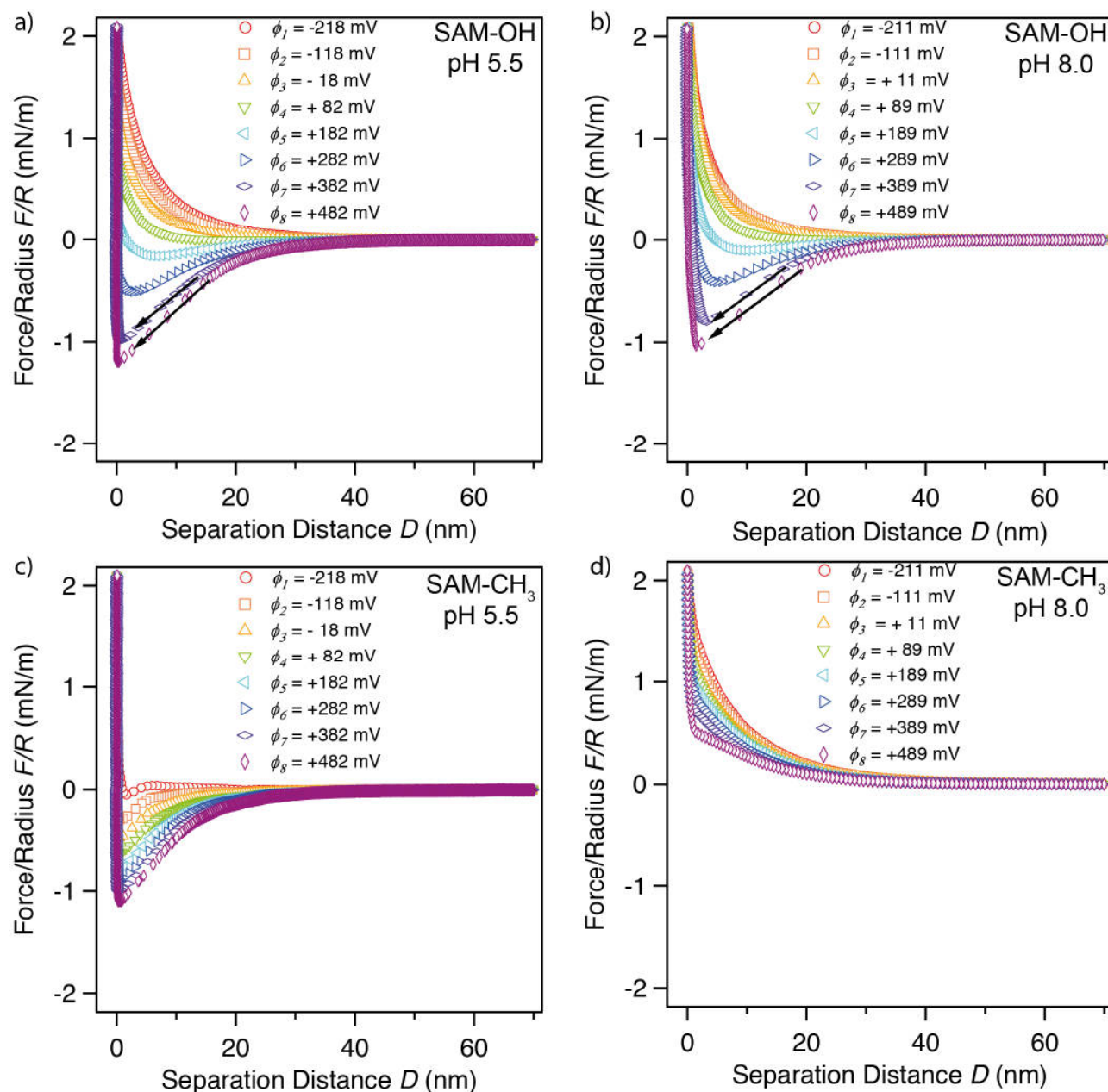
Figure 3: Exemplary force versus distance profiles upon approach between a silica colloidal probe and an electrode with (a, b) OH- and (c, d) CH3-terminated SAMs at different applied potentials. They were acquired in acidic (pH 5.5: a, c) and basic (pH 8.0: b, d) solutions. The force profiles have been averaged from about 100 single force-distance curves. The applied potentials ϕ are given versus a saturated calomel electrode (SCE).

Let us first consider the electrode modified by the OH-terminated SAM. At pH 5.5 the force profiles show qualitatively a similar behavior as reported previously for pH 4.7.[28,29] At very negative potentials ϕ the interaction is repulsive (cf. ϕ_1- ϕ_3 in Figure 3a). Due to the negative charge of the colloidal probe such repulsive interaction is expected. With increasing ϕ the interaction becomes always less repulsive until finally a transition from repulsive to attractive behavior (cf. ϕ_4- ϕ_5 Figure 3a) takes place. In this potential interval one find also the potential of zero charge ϕ_{pzc}, which corresponds to the potential that leads to a vanishing diffuse layer. Upon further increase of ϕ the interaction becomes progressively attractive (i.e. ϕ_6- ϕ_8 Figure 3a). The arrows in Figure 3 indicate instabilities of the cantilever where it jumps directly to the electrode´s surface,. It occurs if the gradient of acting attractive force becomes larger than the spring constant. Figure 3b) shows the interaction force profiles for the same electrode modified by an OH-terminated SAM at pH 8.0. The dependence of the profiles under these slightly basic conditions is comparable to the one under the slightly acidic conditions discussed before (i.e. pH 5.5). However, the forces profiles at comparable potentials are slightly different and seem to be shifted to more negative potentials. This is most clearly visible for ϕ_5 and ϕ_6 near to the ϕ_{pzc}, which is shifted. In terms of diffuse layer potential this shift will be discussed later in detail.

For the electrode modified with the CH$_3$-terminated SAM the pH of the solution has a much stronger influence on the interaction force profiles. Under acid conditions at pH 5.5 (cf. Figure 3c) the interaction force profiles are generally attractive (i.e. ϕ_2- ϕ_8 in Figure 3c), only for the lowest potential of ϕ_1=-218 mV a slightly repulsive interaction between the electrode and the negatively charged silica probe can be observed. The ϕ_{pzc} for the electrode with the CH$_3$-terminated SAM is shifted to more negative potentials at pH 4.7 in respect to the OH-terminated SAM as previously reported.[28,29] Thus, the same effect can be observed also at pH 5.5 for these two types of modified electrodes. By contrast, under basic conditions the interaction profiles are completely repulsive, independently from the applied potential. Therefore, a ϕ_{pzc} is not reached and even at the highest positive ϕ_8=+475mV the interaction force profiles remain completely repulsive, albeit reduced in strength compared to the smaller potentials (i.e. ϕ_1- ϕ_7 in Figure 3d).

Diffuse layer potentials of the electrodes. The force profiles as a function of the applied potential and pH have been analyzed quantitatively. The procedure is analogous

to the one presented for the silica particles (cf. Figure 2) and is illustrated in an exemplary manner in Figure 4. The combination of silica colloidal probes and SAM-modified electrodes represents an asymmetric combination of surfaces. Therefore, the parameters ψ_{CP}^{D} and p_{CP} for the colloidal probe are fixed according to the values compiled in Table 1 and the diffuse layer potential ψ^{D} and the regulation parameter p of the electrode are determined by the fit to the full PB-equation with the charge regulation approximation.

Figure 4 demonstrates the fit quality to PB-equation at the different boundary conditions of the interaction force profiles obtained at pH 8.0 for an electrode with an OH-terminated SAM. The two boundary conditions of constant charge (CC, $p=1$) or constant potential (CP, $p=0$) for the electrode's surface show large deviations from the force profiles at small separations. As previously reported,[29,35] one has also to take charge regulation for the electrodes surface into account, despite the fact that it is connected to a potentiostat and therefore CP boundary condition would be expected (cf. solid line in Figure 4). The occurrence of charge regulation at the surface of an electrode connected to a potentiostat is compatible with the presence of a layer of adsorbed ions at its interface. However, the three boundary conditions give practically the same result at large separation (i.e. 1-2 $\times$ κ^{-1}) between the probe and the electrode and thus have no large influence on the diffuse layer potentials ψ^{D} of the electrode as obtained from the fits. From the fits to the PB-equation with the charge regulation approximation shown in Figure 4 one obtains diffuse layer potentials of ψ (ϕ_{1})= -16.8 mV, $\psi(\phi_{5})$= +14.3 mV, and $\psi(\phi_{8})$= +61.2 mV, respectively.
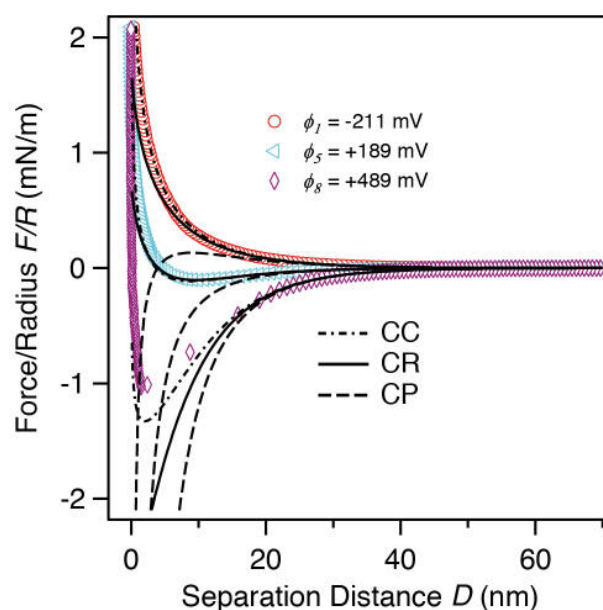
Figure 4: Exemplary force versus distance profiles upon approach between a silica colloidal probe and an OH-terminated electrode (I = 1.2mM, pH 8.0) with fits to the full PB equation with different boundary conditions. The solid lines represent the charge regulation approximation (CR), while the dashed lines represent constant charge (CC) and constant potential (CP) boundary conditions, respectively.

Diffuse layer potentials vs. pH. Figure 5 summarizes the diffuse layer potentials obtained from the fits of the single interaction force profiles as shown in Figure 4. Figure 5a) shows the results for the electrode modified by an OH-terminated SAM and Figure 5b) for the ones for an electrode with a CH_3-terminated SAM, respectively. Both graphs plot the diffuse layer potential as a function of the applied potential. The different pH-values are represented by different symbols, while ionic strength is constantly I=1.2 mM. Each data point has been obtained from the diffuse layer potentials of at least three different data sets with different colloidal probes.
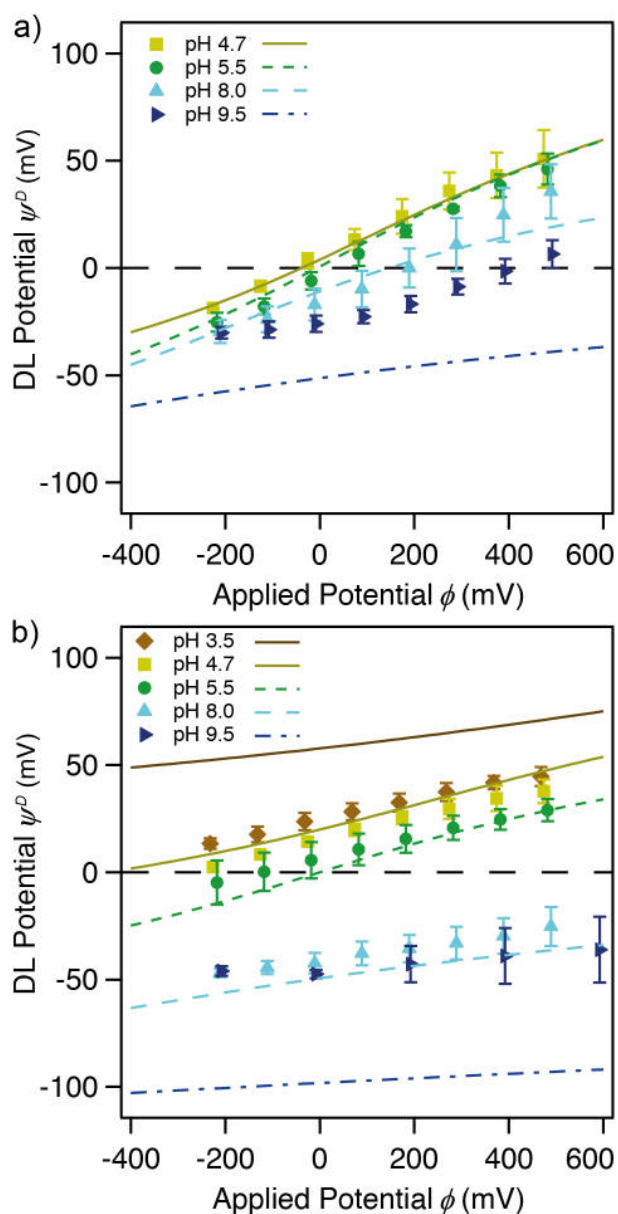
Figure 5: Diffuse layer potential versus externally applied potential for electrodes modified by an OH-(a) and a CH3- (b) terminated SAM, respectively. The data points correspond to the diffuse layer potentials determined at different applied potentials and pH-values. The lines represent global fits simultaneous at all pH-values according to three-capacitor model for each SAM. The resulting fit parameters are compiled in Table 2.
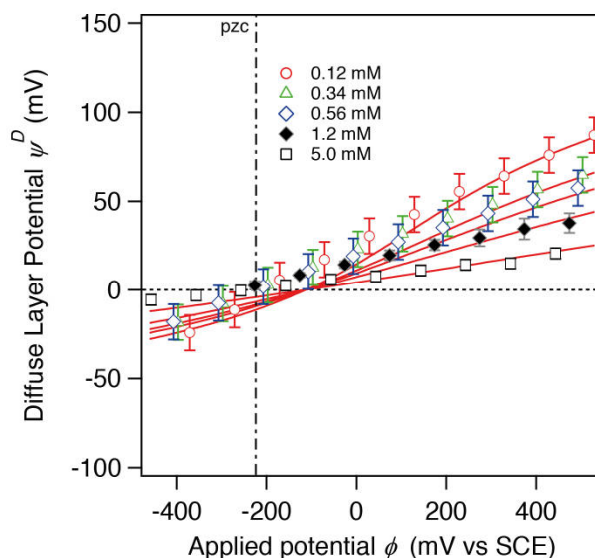
The diffuse layer potentials on the electrode with the OH-terminated SAM increase monotonically with applied potential for all pH-values. Such monotonic behavior is expected from the force profiles in Figure 3 a),b) and the general shape of curves for ψ^D vs. ϕ are similar to the ones reported previously for OH-terminated electrodes at pH 4.7 and different ionic strength.[28,29] However, the values for the potential of zero charge ϕ_{pzc}

shift to higher potentials with increasing pH and thus OH⁻-concentration. In the case of pH 4.7 (and I=1.2 mM) ϕ_{pzc}=230 ± 7 mV (vs. SCE) is in good agreement with the one reported previously for the same type of electrode and pH.[29]

For the electrodes with a CH$_3$-terminated SAM one finds instead a more pronounced variation of ψ^D vs. ϕ as a function of of pH. Only for a small regime of pH-values (3.5 < pH < 8.0) one can observe the presence of ϕ_{pzc} in the potential regime accessible in the experiments as otherwise desorption of the SAM is occuring. In this regime ϕ_{pzc} is shifting with pH to higher values but for more acidic (*i.e.* < pH 4.7) or basic conditions (*i.e.* > pH 5.5) no reversal of the sign of ψ^D can be obtained for the CH$_3$-terminated SAM. For the acidic regime the interaction is in these cases either completely attractive and for the basic regime completely repulsive. Under the most basic conditions at pH 9.5 the diffuse layer potential ψ^D remains practically constant and independent from the applied potential ϕ.

The main trends of ψ^D vs. ϕ in Figure 5 are in good agreement with preferential ion adsorption of hydronium- or hydroxide-ions on SAM-modified electrodes[4,21,48]: At low pH, i.e. high concentration of OH$_3^+$ and low concentration of OH⁻, a net positive charge is resulting on the interface due to adsorption of OH$_3^+$. By contrast, at high pH, i.e. high OH⁻ and low OH$_3^+$- concentration, one observes a negatively charged ion layer at the interface. The adsorption of hydronium- as well as hydroxyl-ions is clearly pronounced for the hydrophobic interface, which is in agreement with theoretical studies.[21]

Influence of the background electrolyte. At this point it is important to verify that the background electrolyte does not adsorb preferentially to the SAM-modified electrodes. Figure 6 summarizes the dependence of the diffuse layer potential ψ^D on the applied potential ϕ for various total ionic strengths at pH 4.7 for the CH$_3$-terminated electrode. $\psi^D(\phi)$ becomes weaker with increasing ionic strength and thus KCl-concentration. This behavior is expected on basis of the Gouy-Chapman-Stern theory[49] and has been observed for the same SAM-modified electrodes previously.[28,29] It is evident that the potential of zero charge remains constant at 224 ± 15 mV, independently from the total ionic strength. Thus, we can conclude that adsorption of potassium (K$^+$) or chloride (Cl⁻) ions to the SAM can be neglected in comparison to hydronium- or hydroxyl-ions.

Figure 6: Diffuse layer potential versus externally applied potential for CH3-terminated electrode at pH 4.7 and different ionic strengths. The full symbols are determined at I=1.2 mM, while the open symbols at different ionic strengths have been reported elsewhere.29 The lines indicate calculations based on the three-capacitor model with the parameters compiled in Table 2.

Model for diffuse layer properties of SAM-modified electrodes. In the following we are presenting a simple model for the electrode/SAM/solution interface in order to describe preferential ion adsorption to SAM-modified electrodes under potentiostatic control. Despite its simplicity this model allows to capture the essential features outlined in the previous paragraphs. This model has been presented in similar form first by Duval et al. in order to describe ion adsorption at oxide layers of metal electrodes.[42] It has been then adapted to SAM-modified electrodes.[35] Figure 7 outlines in a schematic manner the composition of the different layers at the interface: (i) the gold electrode connected to the potentiostat with an electronic charge σ_e at its interface, (ii) the self assembled monolayer (SAM) with thickness d_{SAM} dielectric constant ε_{SAM}, (iii) the layer of preferentially adsorbed ions with a charge density σ_{ion} at the interface between SAM and electrolyte solution, and (iv) the diffuse layer with the diffuse layer charge density σ_D. With these layers different potentials are associated, where ϕ corresponds to the externally applied potential, ψ^a the potential at the interface of the SAM and ψ^D the diffuse layer potential.
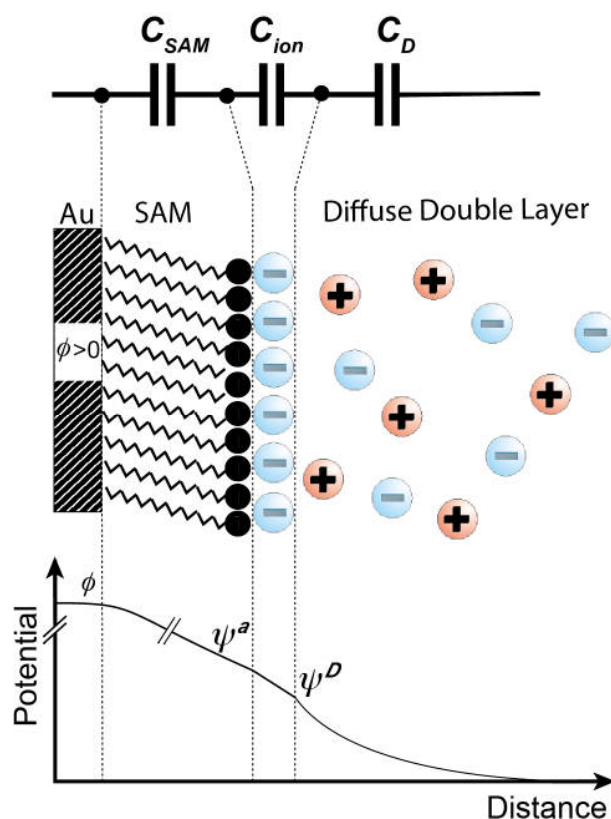
Figure 7: The schematic representation of the three capacitor model consisting of the electrode with a self-assembled monolayer (SAM), an adsorbed layer of ions and the diffuse layer.

The layer structure can be described by three capacitances in series, namely C_{SAM} of the SAM, the Stern layer capacitance of the adsorbed ion layer C_{ion}, and the diffuse layer capacitance C_D. The capacitance of the SAM is about $C_{SAM} = \varepsilon_0 \varepsilon_{SAM} / d_{SAM}$. Here, we used the values of $C_{SAM(OH)}$ = 1.1 µF·cm^{-2} and $C_{SAM(CH_3)}$ = 0.8 µF·cm^{-2}, respectively, that have been determined previously from direct force measurements.[28] The capacitance of the adsorbed ion layer C_{ion} is approximated by C_{ion} = 80 µF·cm^{-2},[50] which is in the range of values reported for similar solution conditions.[22,51,52]

In the direct force measurements we determine the diffuse layer potential, which results from the charge density of the diffuse layer σ_D by

$$\sigma_D = -\sqrt{8 I \varepsilon_0 \varepsilon_{SAM} RT} \sinh\left(y^D / 2\right) \tag{5}$$

where the dimensionless potentials y^D and alike are given by

$$y^d = F\psi^d / RT; \quad y^a = F\psi^a / RT; \quad y^e = F\psi^e / RT \tag{6a-c}$$

This diffuse layer charge density depends additionally on the potential drop over the adsorbed ion layer according to

$$\sigma_D(\psi^D) = -C_{ion}(\psi^a - \psi^D) \tag{7}$$

and analogously one obtains for the potential drop of ϕ over the SAM

$$\sigma_e(\psi^D, \phi) = C_{SAM}(\phi - \psi^a(\psi^D)) \tag{8}$$

where the potential of the inner Helmholtz plane ψ^a at the SAM is given by

$$\psi^a(\psi^D) = \psi^D + ((8I\varepsilon\varepsilon RT)^{1/2} / C_{ion})\sinh(y^D/2) \tag{9}$$

The charge densities at the interfaces between the different layers have to fulfill overall electroneutrality condition by

$$\sigma_e + \sigma_{ion} + \sigma_D = 0 \tag{10}$$

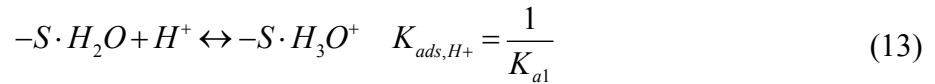Assuming a Langmuir-type adsorption of an ion monolayer in the Stern-layer with a total number of adsorption sites N_S, the charge density σ_{ion} in the Stern layer can be directly related to the ion adsorption. If the total number of adsorption sites is given by $N_s = [-S \cdot H_2O] + [-S \cdot OH^-] + [-S \cdot H_3O^+]$ where [-S·H_2O] are the unoccupied adsorption sites, while [-S·OH] and [-S·H_3O^+] are sites occupied by hydronium- and hydroxyl-ions, respectively; then the charge density of the Stern layer is given by:

$$\sigma_{ion} = eN_S(\theta_{OH_3^+} - \theta_{OH^-}) \tag{11}$$

where F is the Faraday constant and $\theta_{OH_3^+/OH^-}$ is the fraction of sites occupied by hydronium- and hydroxyl-ions, respectively:

$$\theta_{OH_3^+} = \frac{[-S \cdot OH_3^+]}{[-S \cdot OH_3^+] + [-S \cdot H_2O] + [-S \cdot OH^-]}; \quad \theta_{OH^-} = \frac{[-S \cdot OH^-]}{[-S \cdot OH_3^+] + [-S \cdot H_2O] + [-S \cdot OH^-]} \tag{12a,b}$$

The ion adsorption is described by the following two chemical equilibria with the adsorption constants $K_{ads,H+}$ and $K_{ads,OH-}$ for hydronium- and hydroxyl-ions, respectively:

$$-S \cdot H_2O + H^+ \leftrightarrow -S \cdot H_3O^+ \quad K_{ads,H+} = \frac{1}{K_{a1}} \tag{13}$$

$$-S \cdot H_2O + OH^- \leftrightarrow -S \cdot OH^- + H_2O \quad K_{ads,OH-} \tag{14a}$$
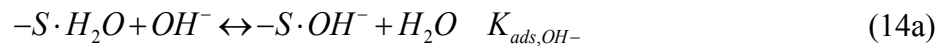
$$K_{ads,OH-} = \frac{[-S \cdot OH^-][H_2O]}{[-S \cdot H_2O][OH^-]} = K_{a2} \cdot K_{Wa} = \frac{K_{a2} \cdot 55.6(mol/l)}{K_W} \tag{14b}$$

where K_W and K_{Wa} are the ionic product and association constant of water, respectively; and [H_2O] is about 55.6 mol/l in diluted electrolyte solution. The two constants, K_{a1} and

K_{a2}, used in numerical calculations, are matching those defined by Duval et al.[42] and can be converted to $K_{ads,H+}$ and $K_{ads,OH-}$ by equations (13) and (14b) by means of the ionic product of water K_w and the number of water molecules per liter. The values for K_{a1} and K_{a2} are given by

$$K_{a1} = [-S \cdot H_2O] \cdot C_{H^+}^{bulk} \exp(-y^a) / [-S \cdot H_3O^+] \tag{15a}$$

$$K_{a2} = [-S \cdot OH^-] \cdot C_{H^+}^{bulk} \exp(-y^a) / [-S \cdot H_2O] \tag{15b}$$

where $C_{H^+}^{bulk}$ is the hydronium concentration in the bulk.[42]

Semi-quantitative model for ion adsorption. By solving numerically the system of equations (5)-(12) and (15), the diffuse layer potential ψ^D can be calculated as a function of the external potential ϕ at a given pH. For these calculations only the parameters related to preferential ion adsorption are not known *a priori* and have to be determined. We determined pK_{ads,H^+}, pK_{ads,OH^-}, and N_S from simultaneous χ^2-fits to the complete datasets of $\psi^D(\phi)$ for all pH-values on the OH- (cf. Fig. 5a) and the CH3-terminated SAMs (cf. Figure 5b), respectively. The results are compiled in Table 2 and have been used to calculate the dashed lines in Figure 5.

Table 2: Parameters for three-capacitor model with ion adsorption

SAM	N_s	C_{SAM}	C_{ion}	$lgK_{ads,H}^+$	$lgK_{ads,OH}^-$
	(cm^{-2})	(μF cm^{-2})	(μF cm^{-2})	(L mol)	(L mol)
16-Mercapto-hexadecanol	5×10^{14}	1.1	80	1.4	5.0
1-Hexadecanethiol	0.9×10^{14}	0.8	80	2.5	6.7

The simple 3-capacitance model with ion adsorption given by equations (5) – (15) provides a surprisingly good semi-quantitative description of the experimental data on ψ^D obtained by direct force measurements on SAM-modified electrodes as a function of the applied potential. The resulting values for the number of adsorption sites N_S as well as the adsorption constants are falling in reasonable quantitative regimes. The number of adsorption sites N_S ranging from 0.9×10^{14} to 5.0×10^{14} cm^{-2} (cf. Table 2) can be compared to the area per thiol in a closely-packed SAM and the distance given by the Bjerrum length. For the number of thiols one finds $N_{SAM} \sim 4.6 \times 10^{14}$ cm^{-2} based on an area per group of 21.6 Å^2 as determined by various methods.[53-55] Another length scale

relevant for ion adsorption is the Bjerrum length of l_B, i.e. the distance between ions, where the interaction energy is in the order of thermal energy (kT). In aqueous solution at standard conditions $l_B = 0.7$ nm, which would correspond to a surface area of 38.5 Å^2 per ion with an upper limit for adsorption capacity of $N_S \sim 2.6 \times 10^{14}$ cm^{-2}. In a similar manner, one can consider the ion radii for the hydroxide ion with a radius of ca. 6.7 Å including the solvation shell[56,57] and for the hydronium[58,59] with an effective radius of ca. 1.44 Å[58,59] resulting in $N_S = 0.71 \times 10^{14}$ cm^{-2} and $N_S = 15.4 \times 10^{14}$ cm^{-2}, respectively.

The adsorption constants for hydronium and hydroxyl-ions tabulated in Table 2 to hydrophobic SAMs are in very good agreement with values reported for comparable interfaces but determined by completely different techniques.[5,12,14,15,48] Lützenkirchen et al. report values of $\lg K_{ads,OH^-}$ in the range of 6.7-8.3 on various hydrophobic interfaces based on electrokinetic and spectroscopic data obtained at the air/water, oil/water, Teflon/water, and diamond/water interfaces.[14] It should be noted that these authors introduce an additional 'ice-like' water layer at the hydrophobic interface, resulting in a more refined model. Healy and Fuerstenau estimate $\lg K_{ads,OH^-} > 8.0$ for a nonpolar solid/liquid or liquid/gas interface,[12] which is comparable to the value is reported by Leroy et al.[13] with $\lg K_{ads,OH^-} = 8.94 \pm 0.02$ for water/gas bubble interface obtained by electrokinetic measurements. In comparison, the values of $\lg K_{ads,OH^-} \sim 4.8\text{-}6.2$ for the air/water interface as determined by Manciu and Ruckenstein are somewhat lower and thus in better agreement with our data.[15] The adsorption constant of hydronium $\lg K_{ads,H^+}$ to hydrophobic interfaces found here is also consistent with other studies, where values of $\lg K_{ads,H^+} \sim 1\text{-}3$ are reported.[13,18] Leroy et al. determined from the electrophoretic mobility of air bubbles a value of $\lg K_{ads,H^+} = 2.54 \pm 0.02$, which is in good agreement with the value of $\lg K_{ads,H^+} = 2.5$ found here for the CH$_3$-terminated SAM.[13] It has to be pointed out that some of the adsorption constants for $\lg K_{ads,OH^-}$ cited here have been converted from dissociation constant of interfacial water in the literature according to equation (14b). There are no comparable data available for the adsorption constants $\lg K_{ads,H^+}$ and $\lg K_{ads,OH^-}$ for the hydrophilic SAM. However, the here observed difference between the hydrophobic and hydrophilic SAMs has been predicted previously by simulations of Kreutzer and Grunze.[21]

Limitations of the simple adsorption model. Various studies, either theoretical or by spectroscopic techniques, indicate that a more refined model for the interface between

SAM and the electrolyte has to be applied in order to account better for the interfacial properties. However, a more refined description of the interface, which takes its molecular properties into account, is beyond the scope of this study. The shortcoming of the simple model, which has been applied here becomes obvious if one replaces the global fit of ψ^P vs. ϕ for all pH-values by fits of ψ^P vs. ϕ for each pH. For these fits C_{SAM} and C_{ion} were the same as in Table 2, as they have no large influence on the fits. The fits of single pH-series provide a superior match between experimental data and calculations, when NS as well as $lgK_{ads,H}^+$ and $lgK_{ads,OH}^-$ are allowed to vary for each pH-value independently. The number of adsorption sites is varying with pH for both SAMs, with values ranging from 5×10^{14} cm^{-2} (pH 4.7) to 1×10^{14} cm^{-2} (pH 9.5) for the OH-terminated SAM and 5×10^{14} cm^{-2} (pH 3.5) to 0.5×10^{14} cm^{-2} (pH 9.5) for the CH$_3$-terminated SAM. Taking into account different effective radii for the hydronium- and hydroxyl-ions this decrease in available adsorption sites on the SAM with pH seems reasonable.

In a similar manner the adsorption constants for hydronium- and hydroxyl-ions determined for single pH-series vary significantly with the pH. For the CH$_3$-terminated SAM we find the hydronium adsorption constant $lgK_{ads,H}^+$ in a range of 1.5-3.5 and $lgK_{ads,OH}^-$ in the range of 5-8.6 for the hydroxide-ion adsorption. For the OH-terminated electrode the hydronium adsorption remains practically constant at $lgK_{ads,H}^+$ =1.4 for all pH-vlaues. By contrast, $lgK_{ads,OH}^-$ varies in the wide range of 3.8-6.2. This apparent variation of N_S and lgK_{ads} is in our opinion a clear sign of the shortcomings of the here-applied simple model. A more appropriate description might include the introduction of an 'ice-like' layer at the interface, especially for the hydrophobic SAM. Such a layer has different properties in comparison with bulk water.[14,60] It extends to about 3-6 layers of water molecules in solution and has been also observed by spectroscopic studies.[8,61,62] Nevertheless, the model given by equations (5)-(15) provides a satisfactory semi-quantitative description of ψ^P vs. ϕ, especially for the hydrophilic SAM and confirms that the observed variations with pH have indeed to be attributed to the adsorption of hydronium and hydroxyl-ions to the SAM.

Variation of the pzc with pH. The effect of ion adsorption is most pronounced if one considers the variation of the potential of zero charge (pzc). Figure 8 shows the variation of pzc with pH for both SAMs. The data for the pzc have been determined by

interpolating the experimental data for each pH with a fit to the three-capacitor model including ion adsorption at the corresponding pH. Solid data points indicate that a pzc can be verified experimentally (cf. Figure 5), while open symbols indicate that the pzc would be outside the range experimentally accessible due to the stability of the SAM. This stability of the SAM is also indicated by the dashed horizontal lines based on data for the stability of thiol-SAMs on gold under external potentials.[37] The lines are based on the three-capacitor model as given by equations (5)-(15) and the values summarized in Table 2. These curves have been shifted in such a way that they cross the experimental values of pzc at pH 5.5 for each SAM correspondingly, because those pzc-values are the most near to the iso-electric point.[50]

Figure 8 demonstrates that the pzc shifts to more positive potentials with increasing pH for both SAMs. However, the pzc variation range is much higher for methyl- than for hydroxyl-terminated SAM. This behavior of the pzc is in line with the adsorption of hydronium- and hydroxyl-ions to the SAMs. With increasing charge in the Stern layer increasing potentials of opposite sign have of to be applied in order to compensate for this charge. The determination of pzc is also possible by classical electrochemical techniques, such as the determination of the diffuse layer capacitance by cyclic voltammetry or transient techniques. Thus, measuring the pzc on modified electrodes provides an experimentally easily accessible technique to follow ion adsorption processes.
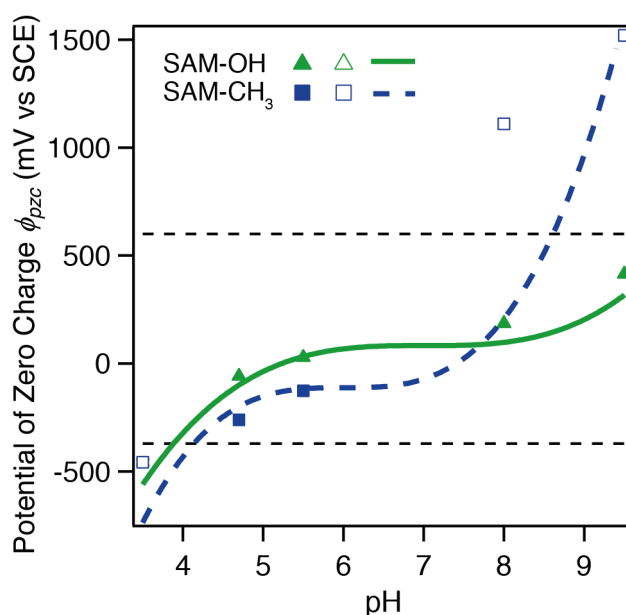
Figure 8: Potential of zero charge (pzc) as a function of pH for electrodes modified by OH- and CH3-terminated SAMs, respectively (I = 1.2 mM). The lines are calculated by the three-capacitor model

and the values from Table 2.. The horizontal dashed lines indicate the potential range in which the SAMs are stable.[37]

In order to compare our results with the comprehensive studies by streaming potential of Werner and coworkers[4,17,31], we determined additionally the diffuse layer potentials at open circuit conditions. These measurements were performed again by direct force measurements, however, the potentiostat has been disconnected from the electrochemical cell (data not shown). The resulting diffuse layer potentials as determined from the fits to the PB-equation with CR-boundary conditions are compiled in Table 3.

Table 3: Diffuse layer potentials determined by direct force measurements under open circuit potential conditions at $I = 1.2$ mM

pH	3.5	4.7	5.5	8.0	9.5
ψ_{OC}^{D} (mV), SAM-CH$_3$	30.3 ± 11.0	28.4 ± 4.3	20.9 ± 11.2	-34.2 ± 4.6	-48.6 ± 5.1
ψ_{OC}^{D} (mV), SAM-OH		22.7 ± 5.8	19.0 ± 5.3	-1.1 ± 4.7	-18.9 ± 2.9

The open circuit potentials as determined by direct force measurements confirm the trend found for both electrodes. Under acidic conditions positive charge is accumulated by hydronium adsorption to the SAMs, while under basic conditions a negatively charge ion layer results from the adsorption of hydroxyl-ions. The latter effect is more pronounced, in particular for the hydrophobic CH$_3$-terminated SAM. From Table 3 the isoelectric point (iep) can be estimated, which corresponds to the pH where the diffuse layer charge vanishes. We find, that the pH^{iep} lies between 5.5 and 8.0 for hydrophobic as well as for hydrophilic interfaces. This corresponds to the findings of Dicke et al. of pH^{iep} close to 6.0-7.0 by AFM for an hydrophobic SAM, which is consistent with our data.[30] The potentials in Table 3 are also in line with streaming potential measurements, which show the same but a somewhat lower isoelectric point at pH^{iep} 3.5-4.0, which might be attributed to the position of shear plane.[17]

Conclusions

By employing colloidal probe force microscopy in combination with electrochemical setup the diffuse layer properties of modified electrodes were determined at different applied potentials and solution composition. As a result the variations of diffuse layer

potential on hydrophobic and hydrophilic interfaces with electric potential and pH were deduced. Because the background electrolyte does not contribute to the charging of the surface, the found pH- and potential-controlled changes in the diffuse layer properties may be attributed to the specific interfacial adsorption of hydronium and hydroxide ions. The adsorption is more pronounced on hydrophobic interface than on hydrophilic. The simple three-capacitor model provides semi-quantitative description of the data. Therefore we used a novel approach to quantify the ion adsorption on non-conductive organic surfaces, that has possible implications in the development of selective electrodes, "smart" coatings and membranes with ion selective properties.

Acknowledgments:

References:

1.   Israelachvili, J. N. *Intermolecular and Surface Forces* (Academic Press, 2011).

2.   Costanza, M. S. & Brusseau, M. L. Contaminant Vapor Adsorption at the Gas−Water Interface in Soils. *Environmental Science & Technology* **34**, 1-11 (2000).

3.   Aveyard, R. et al. Measurement of Long-Range Repulsive Forces between Charged Particles at an Oil-Water Interface. *Phys. Rev. Lett.* **88**, 246102 (2002).

4.   Zimmermann, R., Freudenberg, U., Schweiß, R., Küttner, D. & Werner, C. Hydroxide and Hydronium Ion Adsorption — A survey. *Current Opinion in Colloid & Interface Science* **15**, 196-202 (2010).

5.   Beattie, J. K., Djerdjev, A. M., Franks, G. V. & Warr, G. G. Dipolar Anions Are Not Preferentially Attracted to the Oil/Water Interface. *The Journal of Physical Chemistry B* **109**, 15675-15676 (2005).

6.   Vácha, R. et al. The Orientation and Charge of Water at the Hydrophobic Oil Droplet−Water Interface. *J. Am. Chem. Soc.* **133**, 10204-10210 (2011).

7.   Mucha, M. et al. Unified Molecular Picture of the Surfaces of Aqueous Acid, Base, and Salt Solutions. *The Journal of Physical Chemistry B* **109**, 7617-7623 (2005).

8.   Gopalakrishnan, S., Liu, D., Allen, H. C., Kuo, M. & Shultz, M. J. Vibrational Spectroscopic Studies of Aqueous Interfaces: Salts, Acids, Bases, and Nanodrops. *Chemical Reviews* **106**, 1155-1175 (2006).

9.   Tarbuck, T. L., Ota, S. T. & Richmond, G. L. Spectroscopic Studies of Solvated Hydrogen and Hydroxide Ions at Aqueous Surfaces. *J. Am. Chem. Soc.* **128**, 14519-14527 (2006).

10.   Beattie, J. K. The Intrinsic Charge on Hydrophobic Microfluidic Substrates. *Lab on a Chip* **6**, 1409 (2006).

11.   Creux, P., Lachaise, J., Graciaa, A., Beattie, J. K. & Djerdjev, A. M. Strong Specific Hydroxide Ion Binding at the Pristine Oil/Water and Air/Water Interfaces. *The Journal of Physical Chemistry B* **113**, 14146-14150 (2009).

12.   Healy, T. W. & Fuerstenau, D. W. The Isoelectric Point/Point-of-Zero-Charge of Interfaces Formed by Aqueous Solutions and Nonpolar Solids, Liquids, and Gases. *J. Colloid Interface Sci.* **309**, 183-188 (2007).

13.   Leroy, P., Jougnot, D., Revil, A., Lassin, A. & Azaroual, M. A Double Layer Model of the Gas Bubble/Water Interface. *J. Colloid Interface Sci.* **388**, 243-256 (2012).

14.   Lützenkirchen, J., Preočanin, T. & Kallay, N. A Macroscopic Water Structure Based Model for Describing Charging Phenomena at Inert Hydrophobic Surfaces in Aqueous Electrolyte Solutions. *Physical Chemistry Chemical Physics* **10**, 4946 (2008).

15.   Manciu, M. & Ruckenstein, E. Ions Near the Air/Water Interface: I. Compatibility of Zeta Potential and Surface Tension Experiments. *Colloids and Surfaces A: Physicochemical and Engineering Aspects* **400**, 27-35 (2012).

16.   Preočanin, T. et al. Surface charge at Teflon/Aqueous Solution of Potassium Chloride Interfaces. *Colloids and Surfaces A: Physicochemical and Engineering Aspects* **412**, 120-128 (2012).

17.   Schweiss, R., Welzel, P. B., Werner, C. & Knoll, W. Dissociation of Surface Functional Groups and Preferential Adsorption of Ions on Self-Assembled Monolayers Assessed by Streaming Potential and Streaming Current Measurements. *Langmuir* **17**, 4304-4311 (2001).

18. Zimmermann, R., Rein, N. & Werner, C. Water Ion Adsorption Dominates Charging at Nonpolar Polymer Surfaces in Multivalent Electrolytes. *Physical Chemistry Chemical Physics* **11**, 4360 (2009).

19. Sendner, C., Horinek, D., Bocquet, L. & Netz, R. R. Interfacial Water at Hydrophobic and Hydrophilic Surfaces: Slip, Viscosity, and Diffusion. *Langmuir* **25**, 10768-10781 (2009).

20. Jungwirth, P. & Tobias, D. J. Specific Ion Effects at the Air/Water Interface. *Chemical Reviews* **106**, 1259-1281 (2006).

21. Kreuzer, H. J., Wang, R. L. C. & Grunze, M. Hydroxide Ion Adsorption on Self-Assembled Monolayers. *J. Am. Chem. Soc.* **125**, 8384-8389 (2003).

22. Barten, D., Kleijn, J. M., Duval, J. & Leeuwen, H. P. v. Double Layer of a Gold Electrode Probed by AFM Force Measurements. *Langmuir* **19**, 1133-1139 (2003).

23. Fréchette, J. & Vanderlick, T. K. Double layer forces over large potential ranges as measured in an electrochemical surface forces apparatus. *Langmuir* **17**, 7620-7627 (2001).

24. Hillier, A. C., Kim, S. & Bard, A. J. Measurement of Double-Layer Forces at the Electrode/Electrolyte Interface Using the Atomic Force Microscope: Potential and Anion Dependent Interactions. *The Journal of Physical Chemistry* **100**, 18808-18817 (1996).

25. Hu, K., Chai, Z., Whitesell, J. K. & Bard, A. J. In Situ Monitoring of Diffuse Double Layer Structure Changes of Electrochemically Addressable Self-Assembled Monolayers with an Atomic Force Microscope. *Langmuir* **15**, 3343-3347 (1999).

26. Kwon, H.-C. & Gewirth, A. A. AFM Force Measurements between SAM-Modified Tip and SAM-Modified Substrate in Alkaline Solution. *The Journal of Physical Chemistry B* **109**, 10213-10222 (2005).

27. Valtiner, M., Kristiansen, K., Greene, G. W. & Israelachvili, J. N. Effect of Surface Roughness and Electrostatic Surface Potentials on Forces Between Dissimilar Surfaces in Aqueous Solution. *Advanced Materials* **23**, 2294-2299 (2011).

28. Rentsch, S., Siegenthaler, H. & Papastavrou, G. Diffuse Layer Properties of Thiol-Modified Gold Electrodes Probed by Direct Force Measurements. *Langmuir* **23**, 9083-9091 (2007).

29. Kuznetsov, V. & Papastavrou, G. Adhesion of Colloidal Particles on Modified Electrodes. *Langmuir* **28**, 16567-16579 (2012).

30. Dicke, C. & Hähner, G. pH-Dependent Force Spectroscopy of Tri(ethylene Glycol)- and Methyl-Terminated Self-Assembled Monolayers Adsorbed on Gold. *J. Am. Chem. Soc.* **124**, 12619-12625 (2002).

31. Zimmermann, R., Dukhin, S. & Werner, C. Electrokinetic Measurements Reveal Interfacial Charge at Polymer Films Caused by Simple Electrolyte Ions. *The Journal of Physical Chemistry B* **105**, 8544-8549 (2001).

32. Wagner, P., Hegner, M., Guentherodt, H. J. & Semenza, G. Formation and in itu Modification of Monolayers Chemisorbed on Ultraflat Template-Stripped Gold Surfaces. *Langmuir* **11**, 3867-3875 (1995).

33. Stamou, D. et al. Uniformly Flat Gold Surfaces: Imaging the Domain Structure of Organic Monolayers Using Scanning Force Microscopy. *Langmuir* **13**, 2425-2428 (1997).

34. Hutter, J. L. & Bechhoefer, J. Calibration of Atomic-Force Microscope Tips. *Rev. Sci. Instrum.* **64**, 1868 (1993).

35. Rentsch, S. *Direct Force Measurements Between Surfaces Under Potentiostatic Control.* PhD Thesis (University of Geneva, Geneva, 2008).

36. Ammann, E. et al. Local pH-Controlled Reactivity Investigations by Thin-Layer Scanning Tunnelling Microscopy. *Electrochim. Acta* **47**, 327-334 (2001).

37. Boubour, E. & Lennox, R. B. Stability of ω-Functionalized Self-Assembled Monolayers as a Function of Applied potential. *Langmuir* **16** (19), 7464-7470 (2000).

38. Butt, H.-J., Cappella, B. & Kappl, M. Force Measurements with the Atomic Force Microscope: Technique, Interpretation and Applications. *Surface Science Reports* **59**, 1-152 (2005).

39. Pericet-Camara, R., Papastavrou, G., Behrens, S. H. & Borkovec, M. Interaction between Charged Surfaces on the Poisson−Boltzmann Level: The Constant Regulation Approximation. *The Journal of Physical Chemistry B* **108**, 19467-19475 (2004).

40. Considine, R. F. & Drummond, C. J. Surface Roughness and Surface Force Measurement: A Comparison of Electrostatic Potentials Derived from Atomic

Force Microscopy and Electrophoretic Mobility Measurements. *Langmuir* **17**, 7777-7783 (2001).

41. Rentsch, S., Pericet-Camara, R., Papastavrou, G. & Borkovec, M. Probing the Validity of the Derjaguin Approximation for Heterogeneous Colloidal Particles. *Physical Chemistry Chemical Physics* **8**, 2531 (2006).

42. Duval, J., Lyklema, J., Kleijn, J. M. & van Leeuwen, H. P. Amphifunctionally Electrified Interfaces: Coupling of Electronic and Ionic Surface-Charging Processes. *Langmuir* **17**, 7573-7581 (2001).

43. Butt, H. J. Measuring Electrostatic, Van der Waals, and Hydration Forces in Electrolyte Solutions with an Atomic Force Microscope. *Biophys Journal* **60**, 1438-1444 (1991).

44. Behrens, S. H. & Grier, D. G. The Charge of Glass and Silica Surfaces. *The Journal of Chemical Physics* **115**, 6716 (2001).

45. Hartley, P. G., Larson, I. & Scales, P. J. Electrokinetic and Direct Force Measurements between Silica and Mica Surfaces in Dilute Electrolyte Solutions. *Langmuir* **13**, 2207-2214 (1997).

46. Hu, K. & Bard, A. J. Use of Atomic Force Microscopy for the Study of Surface Acid-Base Properties of Carboxylic Acid-Terminated Self-Assembled Monolayers. *Langmuir* **13**, 5114-5119 (1997).

47. Toikka, G. & Hayes, R. A. Direct Measurement of Colloidal Forces between Mica and Silica in Aqueous Electrolyte. *J. Colloid Interface Sci.* **191**, 102-109 (1997).

48. Lützenkirchen, J., Richter, C. & Brandenstein, F. Some Data and Simple Models for the Silanated Glass-Electrolyte Interface. *Adsorption* **16**, 249-258 (2010).

49. Bard, A. J. & Faulkner, L. R. *Electrochemical Methods* (Wiley, 2000).

50. Duval, J., Kleijn, J. M., Lyklema, J. & van Leeuwen, H. P. Double Layers at Amphifunctionally Electrified Interfaces in the Presence of Electrolytes Containing Specifically Adsorbing Ions. *Journal of Electroanalytical Chemistry* **532**, 337-352 (2002).

51. Chaki, N. K., Aslam, M., Sharma, J. & Vijayamohanan, K. Applications of Self-Assembled Monolayers in Materials Chemistry. *Proceedings of the Indian Academy of Sciences-Chemical Sciences* **113**, 659-670 (2001).

52. Janek, R. P., Fawcett, W. R. & Ulman, A. Impedance Spectroscopy of Self-Assembled Monolayers on Au (111): Evidence for Complex Double-Layer Structure in Aqueous NaClO4 at the Potential of Zero Charge. *The Journal of Physical Chemistry B* **101**, 8550-8558 (1997).

53. Kim, Y. T., McCarley, R. L. & Bard, A. J. Scanning Tunneling Microscopy Studies of Gold(111) Derivatized with Organothiols. *The Journal of Physical Chemistry* **96**, 7416-7421 (1992).

54. Strong, L. & Whitesides, G. M. Structures of Self-Assembled Monolayer Films of Organosulfur Compounds Adsorbed on Gold Single Crystals: Electron Diffraction Studies. *Langmuir* **4**, 546-558 (1988).

55. Finklea, H. O., Bard, A. J. & Rubinstein, I. *Electroanalytical chemistry: a series of advances*. (Marcel Dekker, Inc, New York, 1996).

56. Gray-Weale, A. & Beattie, J. K. An Explanation for the Charge on Water's Surface. *Physical Chemistry Chemical Physics* **11**, 10994 (2009).

57. Asthagiri, D., Pratt, L. R., Kress, J. D. & Gomez, M. A. Hydration and Mobility of HO$^-$(aq). *Proceedings of the National Academy of Sciences* **101**, 7229-7233 (2004).

58. Choi, P., Jalani, N. H. & Datta, R. Thermodynamics and Proton Transport in Nafion. *J. Electrochem. Soc.* **152**, E123 (2005).

59. Chourasia, M., Sastry, G. M. & Sastry, G. N. Proton Binding Sites and Conformational Analysis of H$^+$K$^+$-ATPase. *Biochem. Biophys. Res. Commun.* **336**, 961-966 (2005).

60. Hautman, J. & Klein, M. L. Microscopic Wetting Phenomena. *Phys. Rev. Lett.* **67**, 1763-1766 (1991).

61. Scatena, L. F., Brown, M. G. & Richmond, G. L. Water at Hydrophobic Surfaces: Weak Hydrogen Bonding and Strong Orientation Effects. *Science (New York, N.Y.)* **292**, 908-912 (2001).

62. Shibukawa, M., Kondo, Y., Ogiyama, Y., Osuga, K. & Saito, S. Interfacial Water on Hydrophobic Surfaces Recognized by Ions and Molecules. *Physical Chemistry Chemical Physics* **13**, 15925 (2011)

7. Tuning of the elastic modulus of polyelectrolyte multilayer films built up from polyanions mixture

Katja Trenkenschuh[a], Johann Erath[a], Volodymyr Kuznetsov[a], Julia Gensel[a], Fouzia Boulmedais[b], Peter Schaaf[b], Georg Papastavrou[a], and Anreas Fery[a,*]

[a] Department of Physical Chemistry II, University of Bayreuth, Universitätstraße 30, 95440 Bayreuth, Germany

[b] Institut Charles Sadron, Université de Strasbourg, Centre National de la Recherche Scientifique, UPR 22, rue du Loess 23, 67034 Strasbourg Cedex, France.

*E-mail corresponding author: Andreas.Fery@uni-bayreuth.de
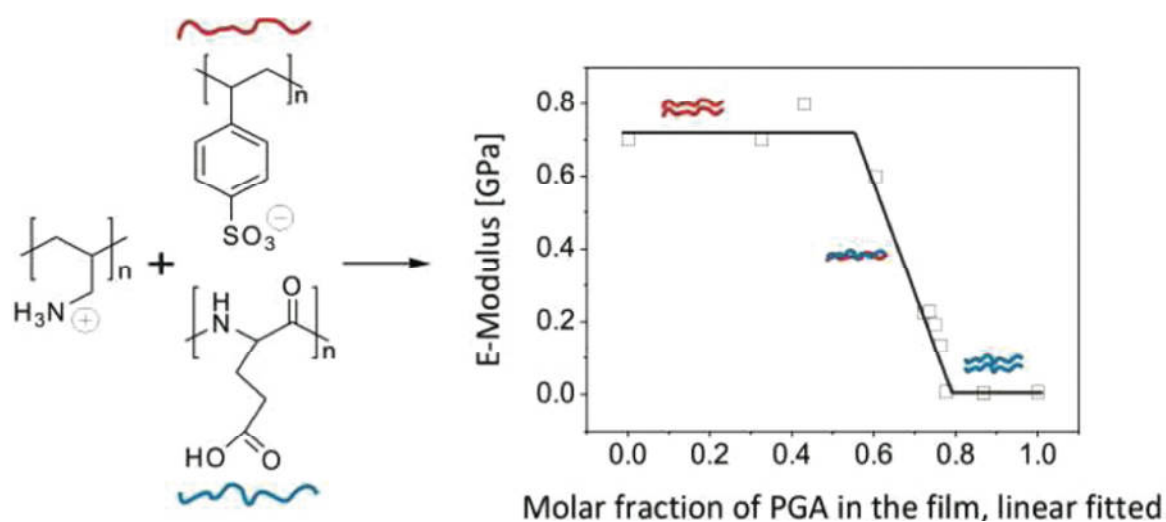
Abstract

In this paper we report on the mechanical characterization of polyelectrolytes multilayer (PEM) films prepared from poly(glutamic acid)-poly(styrene sulfonate) (PGA-PSS) blends, deposited in alternated spray deposition with poly(allylamine hydrochloride) (PAH). The polyanion composition of the blended film was first investigated using Fourier transformed infrared spectroscopy in the attenuated total reflection mode. The monomer molar fraction of PGA in the film increases almost linearly as a function of x, i.e. the monomer molar fraction of PGA in the sprayed polyanion solution. The mechanical properties of the blended $(PAH/PGA_x\text{-}PSS_{1-x})_n$ film were measured using two methods: wrinkling metrology method and the colloidal probe atomic force microscopy technique. We demonstrate that the Young´s modulus of the $PAH/PGA_x\text{-}PSS_{1-x}$ multilayer films can be systematically controlled by the chemical composition of these films, depending on x. Measurements indicate that increasing the monomer molar fraction of PGA in the blended film results in a decrease in film modulus up to three orders of magnitude as compared to the PAH/PSS system. At a monomer molar fraction of PGA in the film around 0.7 (corresponding to $x = 0.7$), this system shows such a transition. We also show that for a given x the elastic properties of these films can be significantly affected by the humidity conditions. For $(PAH/PGA_{0.88}\text{-}PSS_{0.22})$ film, the Young's modulus of the film varies from several hundred of MPa to some kPa only by altering the relative humidity from 12.5% to 80%.

Introduction

Polyelectrolyte multilayer (PEM) films prepared by the layer-by-layer (LbL) technique became very popular since the concept was introduced by Decher *et al*. in the early 1990s.[1] The method relies on the sequential adsorption of oppositely charged polyelectrolytes to construct thin multilayered films. The adsorption results in charge overcompensation after each polyelectrolyte deposition. This allows the alternated assembly of oppositely charged polyelectrolytes. Numerous polymeric materials with different functional groups are available for the multilayer construction which resulted in numerous applications such as controlling wetting properties or interactions with biological systems,[2] anticorrosion coatings,[3-5] free-standing membranes,[6-10] osmotic pressure sensors,[11] and to build up micro- and nanocapsules.[12, 13] Adjusting mechanical properties of PEMs is desirable for most applications mentioned above. This can be

achieved within a limited range by variation of solution conditions during adsorption (pH,[14, 15] ionic strength[16]), by changing the molecular weight of used polyelectrolytes,[17] by cross-linking of the film[18, 19] or by adding a linear growing capping multilayer films on an exponential growing one[20]. In order to tune mechanical properties over many orders of magnitude using the same chemical building blocks, synthetic approaches relying on the use of random copolymers of controlled ratio of charged and uncharged monomers have been used.[21-23] It has been also shown that the elastic modulus of PEM films can be significantly affected by changing the ambient relative humidity (RH).[24]

Using blends of either polyanions[25-31] or polycations[32, 33] provide a potentially interesting alternative to tune several properties of PEMs without synthesis of novel molecular compounds. To control the mechanical property of PEMs, our approach relies on using blends of components, which are known to result in very different mechanical properties where pure components are used. We study LbL films prepared with weakly charged poly(allylamine hydrochloride) (PAH) and two polyanions, poly(styrenesulfonate, sodium salt) (PSS) and a polypeptide poly(L-glutamic acid, sodium salt) (PGA). Our motivation is to investigate the effect of polyanion mixing ratio and the humidity on the mechanical properties since in the literature a huge difference in elastic modulus of $(PAH/PSS)_n$ and $(PAH/PGA)_n$ films is reported. In previous work, the Young's modulus of PAH/PSS capsules was estimated to be between 1.3 and 1.9 GPa.[34] Nolte *et al.* reported for the PAH/PSS multilayer system a modulus of 2.7 ± 0.3 GPa[24] and Gao *et al.,* who measured hollow polyelectrolyte capsules, found that the Young's modulus for the PAH/PSS system ranges between 500 and 700 MPa.[35] Boudou *et al.* reported for the PAH/PGA system the elastic constant value of 118 ± 34 kPa as measured by AFM nanoindentation in liquid.[19]

In this study, we show that the different chemical nature of these two polyanions, PGA and PSS, strongly affects the elasticity of the blended PAH/PGA_x-PSS_{1-x} PEM films, with x representing the molar fraction of the monomer repeat unit of PGA in the polyanion solution. The polyanion composition of the blended film was first investigated using Fourier transformed infrared spectroscopy in the attenuated total reflection mode. The monomer molar fraction of PGA in the film increases almost linearly as a function of x. The film modulus decreases up to three orders of magnitude by transition from the PSS behaviour to the PGA behaviour. Interestingly this transition occurs around $x = 0.7$. This behavior is remarkable, because for many systems preferential adsorption of one

compound shifts transitions in physical properties of multilayers to extreme compositions.[26-28, 30-32, 36] Therefore examples, where transition occur at moderate ratios are rare.[27] We also demonstrate that we can tune the mechanical properties by altering the relative humidity. We show that by changing the humidity from 12% to 80% for $x = 0.88$, the Young's modulus of the $PAH/PGA_x\text{-}PSS_{1-x}$ film varies from hundreds of MPa to some kPa.

Materials and Methods

Materials. To buildup of the $(PAH/PGA_x\text{-}PSS_{1-x})_n$ multilayer architecture the following commercially available polyelectrolytes were used: Poly(allylamine hydrochloride) (PAH, $M_W = 56\ 000$ g mol^{-1}, CAS: 71550-12-4; cat.no.: 28,322-3), poly(styrenesulfonate, sodium salt) (PSS, $M_W = 70\ 000$ g mol^{-1}, CAS: 25704-18-1; cat.no.: 24,305-1), poly(L-glutamic acid, sodium salt) (PGA, $M_W = 15\ 000$ g mol^{-1}, CAS: 26247-79-0; cat.no.: P-4761) and branched poly(ethylene imine) (PEI, $M_W = 750\ 000$ g mol^{-1}, 50 wt. % in H$_2$O, CAS: 9002-98-6; cat.no.: 18,197-8). All polyelectrolytes were purchased from Sigma-Aldrich and were used without further purification. The used polyelectrolytes are listed in Figure 1.
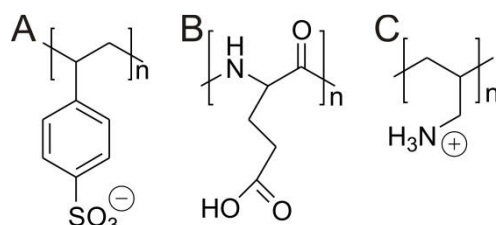

Figure 1. Chemical structures of the polyelectrolytes used in this study: the two polyanions (A) PSS, (B) PGA and the polycation (C) PAH.

Solutions of Polyelectrolytes. The polyelectrolyte solutions were prepared by dissolving the appropriate amounts of polyelectrolytes in filtered (0.20 μm Carl Roth) 0.15 M aqueous sodium chloride (NaCl, Riedel-de Haën) solutions. Millipore water (resistivity = 18.2 MΩ cm) was used in all experiments. The pH of all the solutions was adjusted to pH 7.4 by addition of appropriate volumes of either HCl solution (Grüssing GmbH Analytika, Germany) or NaOH solution (Grüssing GmbH Analytika, Germany) immediately before measurement. The $(PAH/PGA_x\text{-}PSS_{1-x})_n$ films were constructed by using a 1 mg mL^{-1} PAH solution as polycation and a polyanion solution obtained by mixing x mL of a 0.733 mg mL^{-1} PGA solution and $(1 - x)$ mL of a 1 mg mL^{-1} solution of PSS (x represents the molar percentage of the monomer repeat unit of PGA). The mixed

PGA_x-PSS_{1-x} solution thus has a total monomer repeat unit concentration of 4.85 ± 10^{-3} mol L^{-1}.

Substrate Preparation. To determine the mechnanical properties of PEM films, colloidal probe atomic force microscopy (CP-AFM) and wrinkling metrology (WM) method were used. For the CP method, substrates of silicon wafers (CrysTec) were cleaned as follows. First the substrates were immersed for at least 1 h in the 0.15M NaCl aqueous solution at pH 7.4. Then the surfaces were immersed in 1 mg mL^{-1} PEI solution for 10 min. The substrates were then rinsed 10 min with 0.15 M NaCl aqueous solution. For the WM method, poly(dimethylsiloxane) (PDMS) sheets (a typical elastomer) with thicknesses of ~ 2 mm were prepared by mixing the curing agent and base monomer (Sylgard 184, Dow Corning, USA) with 1:10 weight ratio. The mixture was stirred and filled in a carefully cleaned, plain glass dish.[37] After 24 h degassing at room temperature and curing at 60 °C for 3 h in an oven, the cross linked PDMS was cut into 40×10 mm stripes. In order to facilitate the multilayer assembly the surfaces of PDMS sheets were first hydrophilized (PDMS sheets were exposed for 2 min to air plasma at 0.1 mbar using a plasma etcher operating at 1 W (Flecto10, Plasma Technology, Germany)) and then immersed in 1 mg mL^{-1} PEI solution for 30 min.

PEM Film Preparation by Spraycoating. The PEM films were assembled on silicon wafers and on plasma treated (see above) PDMS sheets by the spraycoating method.[38, 39] The PEI-coated substrates were placed vertically in a homemade spray unit to allow liquid drainage along their surfaces. The appropriate polyelectrolyte solutions were filled into spray bottles (30 mL, NeoLab Migge GmbH, Germany) which were manually pressurized twice for each deposition step. After each step, the polymer was sprayed for 10 s followed by a rinsing step with water for 3 s (200 mL spray bottles "air boy", Carl Roth GmbH, Germany) to rinse the surface. The films were dried in a stream of nitrogen before characterization.[21]

Characterization Methods. *Ellipsometry*. Layer thicknesses of the multilayers grown on silicon wafers and on PDMS substrates were determined with a Sentech SE 850 spectroscopic ellipsometer at a fixed incidence angle of 70° (on silicon wafers) and of 40° (on PDMS substrates). The wavelength was set to 632.8 nm. Layer thicknesses on transparent PDMS substrates were determined using a Cauchy dispersion relationship.[40, 41] To calculate the film thicknesses, we used a three-layer model with layer 1, hydrophilized PDMS substrate ($n = 1.41$), layer 2, PEM film ($n = 1.52$) and layer 3, air (n

= 1.00). For each sample, at least three spots were measured and averaged and the results were cross-checked with AFM.

Optical Microscopy. Optical microscopy images of the wrinkled surfaces were recorded using an inverted Zeiss Axiovert 200 (Zeiss, Jena) microscope with a Zeiss Achroplan 20 × /0.45 objective. The microscope was connected to a digital camera (AxioCam HRm, Zeiss) for quantitative data acquisition.

Colloidal Probe Atomic Force Microscopy. The mechanical properties of the samples with PGA_x-PSS_{1-x} polyanion mixtures, where x ranges from 0.71 to 1 were investigated by force-distance measurements using the colloidal probe technique.[42, 43] All force curves were recorded with a Nanowizard AFM (JPK instrument, Berlin). We used a tipples cantilever with Si-colloidal probe prepared using Optical adhesive Norland 63 (for cured glue E = 1.65 GPa) with a radius of R = 3.4 μm (NSC12, Micromash, USA) and a spring constant of 0.257 N/m. The spring constant k was determined by the thermal noise method, introduced by Hutter and Bechhoefer.[44]

To investigate the influence of humidity on the mechanical properties of PEM, an Asylum MFP 3D AFM was used with Asylum Humidity control cell. The humidity is maintained by injecting saturated salt solutions, which determine the water vapor pressure in the chamber (relative humidities are 84 – 85% (KCl_{sat}), 33% ($MgCl_{2,sat}$) and 8 – 9% (KOH_{sat}) in the temperature range of 20 – 25°C[45, 46]). The sample was fixed with double-sided adhesive over the area of ca. 1.1 cm^2 that has a negligible effect on the indentation of a film with E = (8 – 900) MPa. Colloidal probes with R = 3.4 μm and R = 2.3 μm were prepared by gluing Silica-particles (Bang laboratories) with Optical adhesive Norland 63 (for cured glue E = 1.65 GPa) to tipless silicon cantilevers (NSC12, Mikromasch, USA, k = 0.25 and 0.77 N/m). Cantilevers were calibrated by Hutter and Bechhoefer method.[44]

Fourier Transform Infrared Spectroscopy in the Attenuated Total Reflection Mode (ATR-FTIR). The Fourier Transform Infrared (FTIR) experiments were performed on a Vertex 70 spectrometer (Bruker, Germany) using DTGS detector. The spectra relative to the multilayers were determined in the Attenuated Total Reflection (ATR) mode using a 45° trapezoidal ZnSe (internal reflection element) crystal (6 reflections, dimensions 72 × 10 × 6 mm^3) in ATR cell (GRASEBY-SPECAC, England). Reference (bare ZnSe crystal) and sample spectra were taken by collecting 128 interferograms between 800 and 4000 cm^{-1} at 2 cm^{-1} resolution, using Blackman-Harris three-term apodization and the standard Bruker OPUS/IR software (version 5.0). The PEM films were assembled on ZnSe crystal

by the spray coating method described above. All the sample spectra, as for the reference, were recorded with the ZnSe crystal in contact with air.

To estimate the molar percentage of monomer of PGA and PSS in the $(PAH/PGA_x\text{-}PSS_{1-x})_n$ films, we performed calibration curves aimed at correlating the absorbance with concentration of pure polyelectrolyte. The PGA and PSS were dissolved in deuterated solution of 150 mM NaCl at pH 7.4. D_2O was used as solvent instead of water because the amide I band of PGA is affected by the strong absorption of water around 1643 cm^{-1} (O-H bending), whereas the corresponding vibration in D_2O is found at around 1209 cm^{-1}. IR spectra of PGA and PSS solutions were acquired using Bruker Vector 70 FTIR spectrometer with Platinum ATR accessory that contained a diamond crystal (Bruker Optics, USA).

Results and Discussion

Buildup and film composition of $(PAH/PGA_x\text{-}PSS_{1-x})_n$ films. We focused on the system $(PAH/PGA_x\text{-}PSS_{1-x})_n$ because it is known, that the elastic modulus of multilayer films constructed from pure PSS solution and PAH resides in GPa region[24, 34] whereas films built up from pure PGA solution and PAH exhibit an elastic modulus in the kPa range.[19] The buildup of $(PAH/PGA_x\text{-}PSS_{1-x})_n$ films was studied previously.[25] It was shown that the growth regime of this film is changing from exponential to linear by adjusting monomer molar fraction of PGA in solution. Indeed, pure PAH/PSS and pure PAH/PGA are respectively a linear and an exponential growing films. To examine the mechanical properties of $(PAH/PGA_x\text{-}PSS_{1-x})_n$ multilayer films, the spraycoating technique was used by systematically tuning x, monomer molar fraction of PGA in the polyanion sprayed solution.

To investigate the relative composition of PGA and PSS inside the $(PAH/PGA_x\text{-}PSS_{1-x})_n$ film as a function of x, we performed FTIR measurements. We first performed calibration curves aimed at correlating the absorbance with concentration of pure PGA and PSS polyelectrolytes. At a wavenumber of 1567 cm^{-1} corresponding to the carboxylic band,[47-49] we obtained an apparent extinction coefficient of 7.9×10^{-2} M^{-1} in monomer of PGA. In the case of PSS, we obtained apparent extinction coefficients of 7.2×10^{-2} and 7.8×10^{-2} M^{-1} in monomer of PSS respectively at the wavelengths of 1009 and 1037 cm^{-1}, characteristic bands of PSS.[50-52] We then performed FTIR-ATR spectroscopy on $(PAH/PGA_x\text{-}PSS_{1-x})_n$ films for x varying from 0 to 1. It has to be noted that, for all the

experiments performed, the films were built to reach a thickness of 80 ± 10 nm in the dry state, which is significantly smaller than the penetration depth of the evanescent wave ($\sim$ 600 nm at 1000 cm^{-1}). By measuring after baseline subtraction the absorbance of PGA and PSS in the films, we calculated the molar concentrations of PGA and PSS monomers using the extinction coefficients from the calibration curves.
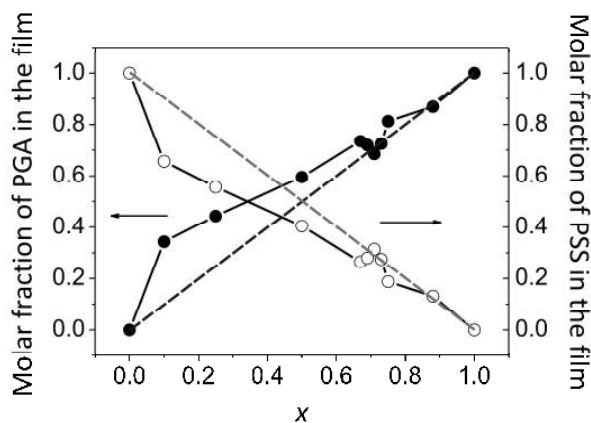
Figure 1. Evolution of the monomer molar fractions of PGA (closed circle) and of PSS (open circle) in the (PAH/PGA$_x$-PSS$_{1-x}$)$_n$ blended film as a function of x, the monomer molar fraction of PGA in solution used for the buildup by alternated contact with a polyanion PGA and PSS mixture and a PAH solutions. The dashed line corresponds to the ideal partitioning of PGA (black) and PSS (grey) between the solution and the film. These data where obtained from films with a thickness of 80 ± 10 nm.

Figure 1 shows the monomer molar fraction of PGA and PSS in the film as a function of monomer molar fraction of PGA in the polyanion solution. A strong adsorption preference of PGA is found especially for $x \leq 0.5$. Such a preferential adsorption was also found in the case of PSS/DNA-PAH,[28] poly(aspartic acid)/PGA-poly(L-Lysine)[26] and poly(4 vinyl pyridine)/PAH mixtures.[32] Beyond $x = 0.5$, the film composition is close to the solution composition and follow then a linear behavior.

Based on the choice of the components and the tunable composition of (PAH/PGA$_x$-PSS$_{1-x}$)$_n$ film, we expect a broad range of elastic constants (ranging from lower MPa region for pure PAH/PGA up to GPa region for pure PAH/PSS). At the same time film thicknesses are in the range of 100 nm. These requirements are extremely challenging in terms of characterization techniques. To the best of our knowledge there is no single technique covering the whole range of elastic properties for this thin film regime. Therefore, we used two complementary techniques, wrinkling method (WM) and indentation technique (CP-AFM) in terms of range of elastic constants measured. Wrinkling experiments allow

us to analyse more rigid materials with moduli in the order of GPa until some hundreds of MPa region. In contrast, the CP - AFM technique is suitable for weak films with moduli of MPa until kPa range. For each technique, a minimum film thickness is required for reliable measurements. The number of PAH/PGA$_x$-PSS$_{1-x}$ bilayers was then tuned to obtain a sufficient thickness (Table 1).

Table 1. Monomer molar fraction of PGA in the polyanion solution, number of bilayers, corresponding film thickness and resulting Young's modulus of (PAH/PGA$_x$-PSS$_{1-x}$)$_n$ multilayer films prepared with 0.15 M NaCl at pH 7.4.

PGA molar fraction in solution (x)	number of bilayers (n)	thickness (nm)[a]
0	32	95.3 ± 7.0
0.10	30	107.8 ± 3.6
0.25	21	111.2 ± 8.7
0.50	12	115.5 ± 3.1
0.67	11	112.4 ± 6.3
0.69	11	102.5 ± 7.8
0.71	11	94.5 ± 4.1
0.73	11	94.4 ± 6.0
0.75	25	521.4 ± 2.9
0.88	25	544.5 ± 7.9
1.00	23	505.4 ± 4.8

[a]Determined by ellipsometry.

High Modulus Regime: Wrinkling Metrology. The mechanical properties of (PAH/PGA$_x$-PSS$_{1-x}$)$_n$ multilayer films, where x ranges from 0 to 0.73 were investigated with the sensitive technique named strain-induced elastic buckling instability for mechanical measurements (SIEBIMM) introduced by Stafford et al..[53] The basic idea of the buckling-based metrology is that a thin, stiff film coated onto an elastomeric substrate will buckle when subjected to planar compressive forces in order to relieve the strain energy in the system.

The wrinkling experiments were performed on a plasma-treated PDMS sheets with a hydrophilic surface. In order to minimize the influence of the silica surface layer on the buckling wavelength, plasma intensity and durations were kept at minimum. The film thicknesses of all samples were ca. 100 nm as recommended by Nolte et al. in order to minimize film thickness measuring errors.[41] Multilayer coated PDMS slides were

stretched uniaxially in a customer-designed strain stage with the strains of only a few percent. The buckling wavelength, λ, was obtained after the subsequent relaxation of the specimens using optical microscopy. To determine the mechanical properties, the wavelength was evaluated via Fourier analysis of images using ImageJ. The average wavelength was determined by collecting data from at least five locations on each sample. Knowing the wrinkling wavelength, λ, film thickness, d, and the modulus values of the PDMS substrates, E_s, (1.1 MPa ± 0.1 MPa, determined using Universal Tester, Model 5565), the Young´s modulus of the film, E_f, can be determined using eq. 1:[53]

$$E_f = \frac{3E_s\left(1-v_f^2\right)}{1-v_s^2}\left(\frac{\lambda}{2\pi d_f}\right)^3 \tag{1}$$

The Poisson´s ratio of 0.33 was required for multilayers (v_f), and a value of 0.5 was required for the elastomeric PDMS substrate (v_s).[54]

The wrinkling experiments were carried out at the ambient RH of (55 ± 1)%. Figure 2 illustrates the optical microscopy images of (PAH/PGA$_x$-PSS$_{1-x}$)$_n$ multilayer films with x ranges from 0 to 0.73.
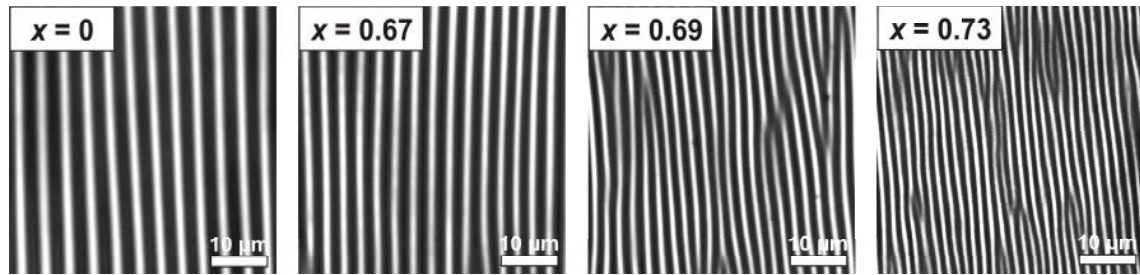
Figure 2. Optical microscopy images of wrinkled (PAH/PGA$_x$-PSS$_{1-x}$)$_n$ multilayer films taken in the transmission mode; x ranges from 0 to 0.73. Samples prepared by stretching multilayer films coated PDMS slides by ε = 2% and releasing the strain.

At the same film thickness, the wrinkling wavelength decreases from (3.6 ± 0.2) µm for x = 0 to (1.8 ± 0.1) µm for x = 0.73. According to the wavelength, the elastic modulus also decreases from (0.7 ± 0.2) GPa to (0.14 ± 0.09) GPa, respectively. The value of (0.7 ± 0.2) GPa for x = 0, i.e. pure PAH/PSS film, is comparable to those given in literature.[34, 35]

**Low Modulus Regime: AFM Technique.** Young's modulus of (PAH/PGA$_x$-PSS$_{1-x}$)$_n$ films where x ranges from 0.75 to 1, which are too soft to be analyzed via the wrinkling method, was then determined via indentation experiments with the colloidal probe technique. The indentation experiments were performed on thick films (> 500 nm). Therefore, the indentation depths did not exceed 10% of the film thickness which allows

negligible effects.[55] To record elastic modulus, the samples were measured on different spots using the force-mapping mode. Measurements were performed on 20 different positions on a digital 100 μm^2 grid on the surface. The force-distance curves were analyzed using the JPK Image Processing software. To determine the Young's modulus, the approach curve was fitted by the Hertz sphere model[56] According to this model, the relation between the Young's modulus (E), the force (F), and the deformation (δ) is

$$F = \frac{4}{3(1-v^2)} \cdot ER^{1/2} \cdot \delta^{3/2} \tag{2}$$

where R is the radius of the sphere tip (3.4 μm) and v is the Poisson ratio (0.33 for multilayers).

Figure 3 displays force-deformation curves measured in approach of the (PAH/PGA$_x$-PSS$_{1-x}$)$_n$ films and the corresponding log-log profiles of these curves for $x = 0.75$, $x = 0.88$ and $x = 1$.
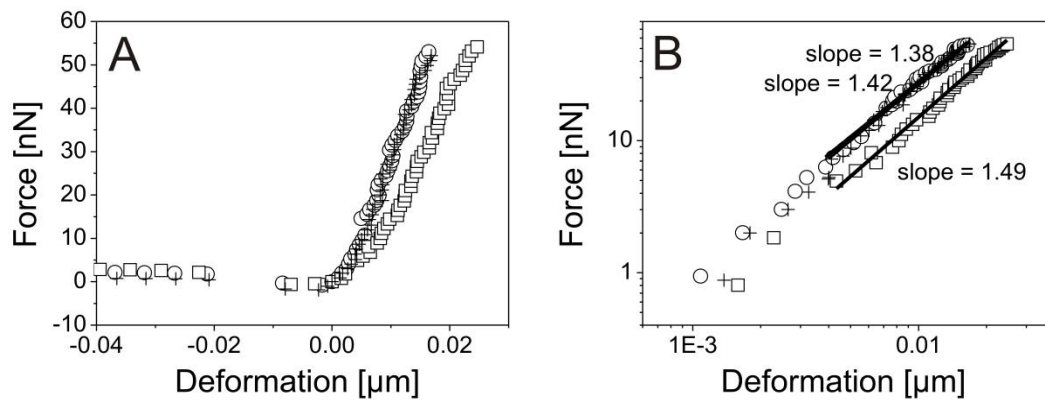

Figure 3. (A) Force vs deformation curves measured by AFM in approach for (PAH/PGA$_x$-PSS$_{1-x}$)$_n$ multilayer films in a dry state, where $x = 0.75$ ($\circ$), $x = 0.88$ ($\square$) and $x = 1$ (+). (B) Force vs deformation log-log profiles. The black lines represent a linear fit for deformations from 4 to 17 nm ($x = 0.75$ and $x = 1$) and from 4 to 25 nm ($x = 0.88$). The slopes of the fits in these ranges are 1.38 and 1.42 ($x = 0.75$ and $x = 1$) and 1.49 ($x = 0.88$), close to 3/2 as predicted by the Herzian power law.

In the log-log plot the experimental data are correctly fitted by linear curves with slopes of about 1.5 which is in good agreement with the scaling law predicted by Hertz model. The average Young´s moduli determined according to the Hertz model (eq 2) are (7.4 ± 1.7) MPa, (4.7 ± 1.6) MPa, and (6.7 ± 2.1) MPa for (PAH/PGA$_x$-PSS$_{1-x}$)$_n$ films prepared respectively with for $x = 0.75$, $x = 0.88$ and $x = 1$. The indentation experiments were carried out at the ambient RH of 54%. The value of the Young´s modulus determined previously by Boudou *et al.* for PAH/PGA multilayers in the wet state was (118 ± 34)

kPa.[19] To our knowledge, the dry state stiffness of PAH/PGA films was not published before.

Figure 4 and table 2 summarize the results obtained from wrinkling metrology method and the colloidal probe atomic force microscopy technique and from FTIR – ATR experiments. By increasing x, (PAH/PGA$_x$-PSS$_{1-x}$)$_n$ films become softer with an elastic modulus three orders of magnitude smaller for $x \geq 0.75$ compared to $x \leq 0.5$. Thus, the elastic properties of (PAH/PGA$_x$-PSS$_{1-x}$)$_n$ multilayer films can be tailored over a wide range only by changing the monomer molar fraction of PGA in the polyanion solution from 0.5 to 0.75 (Figure 4).
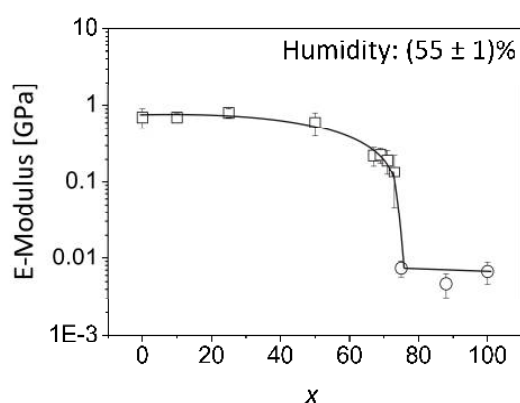
Figure 4. Elastic modulus E as a function of x, monomer molar fraction of PGA in the polyanion buildup solution. For x ranges from 0 to 0.73, E was deduced from wrinkling metrology measurements (□). For x ranges from 0.75 to 1, E was calculated from force vs deformation curves measured by colloidal probe AFM (o). The line is drawn to guide the eyes.

Table 2. Monomer molar fraction of PGA in the polyanion solution, the corresponding monomer molar fraction of PGA in the film and the resulting Young's modulus of (PAH/PGA$_x$-PSS$_{1-x}$)$_n$ multilayer films prepared with 0.15 M NaCl at pH 7.4.

PGA molar fraction in solution (x)	PGA molar fraction in the film[a]	Young's Modulus (GPa)[b]
0	0	0.7 ± 0.2
0.10	0.34	0.7 ± 0.1
0.25	0.44	0.8 ± 0.1
0.50	0.60	0.6 ± 0.2
0.67	0.73	$(2.3 \pm 0.6) \times 10^{-1}$
0.69	0.72	$(2.3 \pm 0.5) \times 10^{-1}$
0.71	0.69	$(1.9 \pm 0.7) \times 10^{-1}$

0.73	0.72	$(1.4 \pm 0.9) \times 10^{-1}$
0.75	0.81	$(7.4 \pm 1.7) \times 10^{-3}$
0.88	0.87	$(4.7 \pm 1.6) \times 10^{-3}$
1.00	1	$(6.7 \pm 2.1) \times 10^{-3}$

[a]Determined by FTIR spectroscopy. [b]Determined by wrinkling metrology ($x = 0 - 0.73$) and by colloidal probe AFM ($x = 0.75 - 1$) at (55 ± 1)% of humidity.

Data from Table 2 allows plotting the evolution of the Young's Modulus of the blended PAH/PGA-PSS film as a function of the monomer molar fraction of PGA in the film (Figure 5). In the region where the PGA fraction in the film is lower or equal to 0.5, the E-Modulus remains nearly constant and resides around 0.7 GPa (Figure 5). Despite the preferential incorporation of PGA over PSS in this region (Figure 1), the major fraction of polyanion present in the film is PSS leading to its significant contribution to the elastic properties of the film. When the molar fraction of PGA in the film increases from 0.5 to 1, the elastic modulus of the film decreases linearly until a plateau at around 6×10-3 GPa from x = 0.8. Thus, the elastic properties of (PAH/PGAx-PSS1-x)n multilayer films evolves linearly with the molar fraction of PGA in the film between 0.5 and 0.8.
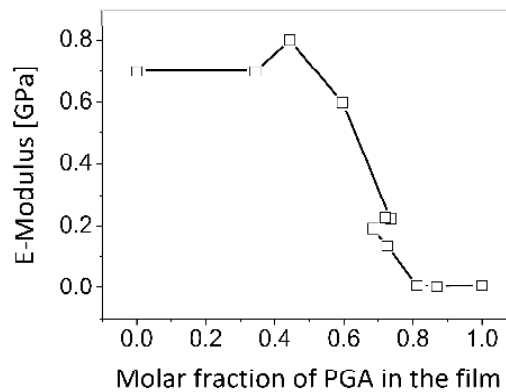
Figure 5. Young´s Modulus of (PAH/PGAx-PSS1-x)n blended film as a function of the monomer molar fraction of PGA in the film.

Overlap regime: comparison of AFM and Wrinkling Method results. There is a regime in a range around x = 0.7 where both techniques can be applied to measure the elastic modulus. Therefore, we present a direct comparison of elastic constants in Table 3. These results demonstrate a good agreement between both methods. As expected, since AFM is on the limit of its applicability, errors of the AFM measurements are large. But

the order of magnitude agrees with the wrinkling results, indicating that the results are method independent.

Table 3. Young modulus of $(PAH/PGA_x\text{-}PSS_{1-x})_n$ multilayer films for $x = 0.71$ and 0.73 as measured by wrinkling metrology and colloidal probe AFM.

	Young's Modulus ($\times 10^{-1}$ GPa)		
	$x = 0.71$	$x = 0.73$	RH (%)
WM	1.9 ± 0.7	1.4 ± 0.9	56
CP - AFM		2.2 ± 0.4	60
	5.1 ± 1.6	4.4 ± 1.4	50

In order to determine how strong our system responds to the humidity changes, we performed experiments with the colloidal probe technique in a humidity cell under controlled humidity conditions. The measurements were performed on samples with x = 0.88. Data analysis was carried out by Asylum MFP 3D build-in software (v. 10102010) for nanoindentation.
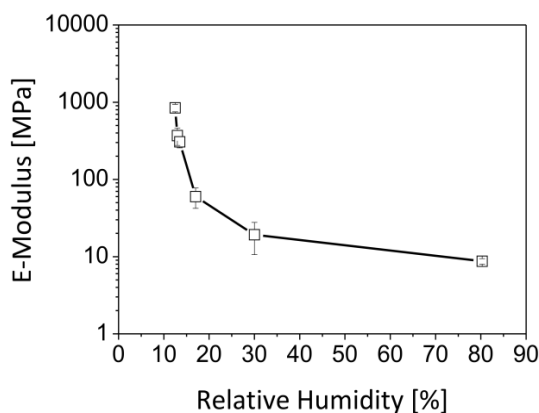
Figure 6. Evaluation of the elastic modulus E of the (PAH/PGA0.88-PSS0.22)n multilayer films as a function of relative humidities as measured by CP - AFM in the humidity cell.

Figure 6 shows that at higher humidities the elastic modulus increases slowly with the decreasing humidity. The Young modulus changes from (8.7 ± 0.7) MPa to (19.2 ± 8.6) MPa when the RH decreases from 80 to 30%. Thus, the modulus value of (4.7 ± 1.6) MPa measured at 54% ambient humidity is in a good agreement with the modulus values obtained at controlled humidity (by comparing the modulus values between 80% and 30% RH). At lower humidities, the modulus increases rapidly with the negligible changes in the humidity values. By reduction of the humidity from 17% to 13.5% to 12.5%, the

modulus increases from (60.0 ± 17.8) MPa to (307.6 ± 51.2) MPa and to (843.7 ± 94.8) MPa.

Summary and Conclusions

In this study, we have investigated the mechanical properties of (PAH/PGAx-PSS1-x)n multilayer films made from blended solutions of PGA and PSS. Using ATR-FTIR experiments, we first determined the relative composition in PGA and PSS inside the film as a function of x, the monomer molar fraction of PGA in the polyanion solution. We showed that with increasing the PGA molar fraction in the mixed PGA/PSS solution, the PGA molar fraction in the film increases almost linearly. To determine the elastic constants of (PAH/PGAx-PSS1-x), we used two techniques the wrinkling method and the colloidal probe AFM technique. We found that with increasing the PGA molar fraction in the mixed solution, the blended film become softer and the elastic modulus becomes three orders of magnitude smaller for x ≥ 0.75 compared to x ≤ 0.5. This system shows a transition at a mixing ratio of around x = 0.7. The elastic properties of (PAH/PGAx-PSS1-x)n multilayer films can be tailored over a wide range from 0.7 GPa to 6 MPa only by changing monomer molar fraction of PGA in solution from 0.5 to 0.75. We also showed that for a given x the Young´s modulus of the blended film strongly depends on the humidity changes as demonstrated by means of the colloidal probe AFM in a humidity cell under controlled humidity conditions. For (PAH/PGA0.88-PSS0.22) film, the Young's modulus increases from hundreds of MPa region at 12.5% RH to some kPa region at the 80% RH.

Acknowledgments

References:

1.   Decher, G.; Hong, J. D.; Schmitt, J. *Thin Solid Films* **1992,** 210, (1-2), 831-835.

2.   Jaber, J. A.; Schlenoff, J. B. *Current Opinion in Colloid & Interface Science* **2006,** 11, (6), 324-329.

3.   Mamedov, A. A.; Kotov, N. A. *Langmuir* **2000,** 16, (13), 5530-5533.

4.   Farhat, T. R.; Schlenoff, J. B. *Electrochemical and Solid State Letters* **2002,** 5, (4), B13-B15.

5.   Andreeva, D. V.; Fix, D.; Mohwald, H.; Shchukin, D. G. *Advanced Materials* **2008,** 20, (14), 2789-+.

6.   Jiang, C. Y.; Markutsya, S.; Tsukruk, V. V. *Advanced Materials* **2004,** 16, (2), 157-+.

7.   Mallwitz, F.; Laschewsky, A. *Advanced Materials* **2005,** 17, (10), 1296-+.

8.   Lavalle, P.; Boulmedais, F.; Ball, V.; Mutterer, J.; Schaaf, P.; Voegel, J. C. *Journal of Membrane Science* **2005,** 253, (1-2), 49-56.

9.   Nolte, M.; Fery, A. *Iee Proceedings-Nanobiotechnology* **2006,** 153, (4), 112-120.

10.   Ott, P.; Trenkenschuh, K.; Gensel, J.; Fery, A.; Laschewsky, A. *Langmuir* **2010,** 26, (23), 18182-18188.

11.   Nolte, M.; Donch, I.; Fery, A. *Chemphyschem* **2006,** 7, (9), 1985-1989.

12.   Sukhorukov, G.; Fery, A.; Mohwald, H. *Progress in Polymer Science* **2005,** 30, (8-9), 885-897.

13.   Johnston, A. P. R.; Cortez, C.; Angelatos, A. S.; Caruso, F. *Current Opinion in Colloid & Interface Science* **2006,** 11, (4), 203-209.

14.   Shiratori, S. S.; Rubner, M. F. *Macromolecules* **2000,** 33, (11), 4213-4219.

15.   Burke, S. E.; Barrett, C. J. *Biomacromolecules* **2003,** 4, (6), 1773-1783.

16.   Ladam, G.; Schaad, P.; Voegel, J. C.; Schaaf, P.; Decher, G.; Cuisinier, F. *Langmuir* **2000,** 16, (3), 1249-1255.

17.   Sui, Z. J.; Salloum, D.; Schlenoff, J. B. *Langmuir* **2003,** 19, (6), 2491-2495.

18.   Richert, L.; Boulmedais, F.; Lavalle, P.; Mutterer, J.; Ferreux, E.; Decher, G.; Schaaf, P.; Voegel, J. C.; Picart, C. *Biomacromolecules* **2004,** 5, (2), 284-294.

19.   Boudou, T.; Crouzier, T.; Auzely-Velty, R.; Glinel, K.; Picart, C. *Langmuir* **2009,** 25, (24), 13809-13819.

20.   Senger, B.; Francius, G.; Hemmerle, J.; Ball, V.; Lavalle, P.; Picart, C.; Voegel, J. C.; Schaaf, P. *Journal of Physical Chemistry C* **2007,** 111, (23), 8299-8306.

21.   Ott, P.; Gensel, J.; Roesler, S.; Trenkenschuh, K.; Andreeva, D.; Laschewsky, A.; Fery, A. *Chemistry of Materials* **2010,** 22, (11), 3323-3331.

22.   Steitz, R.; Jaeger, W.; von Klitzing, R. *Langmuir* **2001,** 17, (15), 4471-4474.

23.   Qu, D.; Pedersen, J. S.; Garnier, S.; Laschewsky, A.; Mohwald, H.; von Klitzing, R. *Macromolecules* **2006,** 39, (21), 7364-7371.

24.   Nolte, A. J.; Cohen, R. E.; Rubner, M. F. *Macromolecules* **2006,** 39, (14), 4841-4847.

25.   Hubsch, E.; Ball, V.; Senger, B.; Decher, G.; Voegel, J. C.; Schaaf, P. *Langmuir* **2004,** 20, (5), 1980-1985.

26.   Debreczeny, M.; Ball, V.; Boulmedais, F.; Szalontai, B.; Voegel, J. C.; Schaaf, P. *Journal of Physical Chemistry B* **2003,** 107, (46), 12734-12739.

27.   Cho, J. H.; Quinn, J. F.; Caruso, F. *Journal of the American Chemical Society* **2004,** 126, (8), 2270-2271.

28.   Quinn, J. F.; Yeo, J. C. C.; Caruso, F. *Macromolecules* **2004,** 37, (17), 6537-6543.

29.   Sun, J.; Wang, L. Y.; Gao, J.; Wang, Z. Q. *Journal of Colloid and Interface Science* **2005,** 287, (1), 207-212.

30.   Francius, G.; Hemmerle, J.; Voegel, J. C.; Schaaf, P.; Senger, B.; Ball, V. *Langmuir* **2007,** 23, (5), 2602-2607.

31.   Quinn, A.; Tjipto, E.; Yu, A. M.; Gengenbach, T. R.; Caruso, F. *Langmuir* **2007,** 23, (9), 4944-4949.

32.   Li, Q.; Quinn, J. F.; Caruso, F. *Advanced Materials* **2005,** 17, (17), 2058-+.

33.   Benkirane-Jessel, N.; Lavalle, P.; Hubsch, E.; Holl, V.; Senger, B.; Haikel, Y.; Voegel, J. C.; Ogier, J.; Schaaf, P. *Advanced Functional Materials* **2005,** 15, (4), 648-654.

34.   Dubreuil, F.; Elsner, N.; Fery, A. *European Physical Journal E* **2003,** 12, (2), 215-221.

35.   Gao, C.; Donath, E.; Moya, S.; Dudnik, V.; Mohwald, H. *European Physical Journal E* **2001,** 5, (1), 21-27.

36.   Ballt, V.; Bernsmann, F.; Betscha, C.; Maechling, C.; Kauffmann, S.; Sengert, B.; Voegelt, J. C.; Schaaf, P.; Benkirane-Jesselt, N. *Langmuir* **2009,** 25, (6), 3593-3600.

37.   Nolte, M.; Schoeler, B.; Peyratout, C. S.; Kurth, D. G.; Fery, A. *Advanced Materials* **2005,** 17, (13), 1665-+.

38.   Schlenoff, J. B.; Dubas, S. T.; Farhat, T. *Langmuir* **2000,** 16, (26), 9968-9969.

39.   Izquierdo, A.; Ono, S. S.; Voegel, J. C.; Schaaf, P.; Decher, G. *Langmuir* **2005,** 21, (16), 7558-7567.

40.   Born, M.; Wolf, E., *Principles of Optics*. 5th ed.; Pergamon New York: 1975.

41.   Nolte, A. J.; Rubner, M. F.; Cohen, R. E. *Macromolecules* **2005,** 38, (13), 5367-5370.

42.   Butt, H. J. *Biophysical Journal* **1991,** 60, (4), 777-785.

43.   Ducker, W. A.; Senden, T. J.; Pashley, R. M. *Nature* **1991,** 353, (6341), 239-241.

44.   Hutter, J. L.; Bechhoefer, J. *Review of Scientific Instruments* **1993,** 64, (7), 1868-1873.

45.   Greenspan, L. *Journal of Research of the National Bureau of Standards-A. Physics and Chemistry* **1976,** 81A, (1), 89-96.

46.   Young, J. F. *Journal of Applied Chemistry of the Ussr* **1967,** 17, (9), 241-&.

47.   Lenormant, H.; Baudras, A.; Blout, E. R. *Journal of the American Chemical Society* **1958,** 80, (23), 6192-6195.

48.   Koenig, J. L.; Frushour, B. *Biopolymers* **1972,** 11, (9), 1871-&.

49.   Jackson, M.; Haris, P. I.; Chapman, D. *Journal of Molecular Structure* **1989,** 214, 329-355.

50.   Yang, J. C.; Jablonsky, M. J.; Mays, J. W. *Polymer* **2002,** 43, (19), 5125-5132.

51.   Zundel, G., *Hydration and intermolecular interaction*. Academic Press: New-York, 1969.

52.   Orler, E. B.; Yontz, D. J.; Moore, R. B. *Macromolecules* **1993,** 26, (19), 5157-5160.

53.   Stafford, C. M.; Harrison, C.; Beers, K. L.; Karim, A.; Amis, E. J.; Vanlandingham, M. R.; Kim, H. C.; Volksen, W.; Miller, R. D.; Simonyi, E. E. *Nature Materials* **2004,** 3, (8), 545-550.

54.   Hendricks, T. R.; Lee, I. *Nano Letters* **2007,** 7, (2), 372-379.

55.   Van Landingham, M. R. *Microsc. Today* **1997,** 97, 12.

56.   Hertz, H. J. *J. reine angew. Math.* **1881,** 92, 156-171.

List of Publications

1. Kuznetsov, V.; Papastavrou, G. **Mechanically and Chemically Stable Colloidal Probes from Silica Particles for Atomic Force Microscopy**. *Rev. of Scientific Instruments* **83**, 116103 (2012)

2. Kuznetsov, V.; Papastavrou, G. **Adhesion of Colloidal Particles on Modified Electrodes**. *Langmuir* **28**(48), 16567-79 (2012)

3. Kuznetsov, V.; Papastavrou, G. **Study of Ion Adsorption on Modified Electrodes by Direct Force Measurements** (tentative). To be submitted to *Physical Chemistry Chemical Physics* in 2013

4. Trenkenschuh, K.; Erath, J.; Kuznetsov, V.; Gensel, J.; Boulmedais, F.; Schaaf, P.; Papastavrou, G.; Fery, A. **Tuning of the elastic modulus of polyelectrolyte multilayer films built up from polyanions mixture.** *Macromolecules*, **44**(22), 8954-8961 (2011)

In preparation:

5. Kuznetsov, V.; Papastavrou, G. **Novel Principle for Micro- and Nanomanipulation by AFM and Electrochemistry** (tentative). Intended for submission to *Proceedings of the National Academy of Sciences*

6. Kuznetsov, V.; Kunz, D.; Helfricht, N.; Kalo, H.; Breu J.; Papastavrou, G. **Quantification of Diffuse Layer Properties of Artificial Clays** (tentative). Intended for submission to *Langmuir*

7. Kuznetsov, V.; Behr, M.; Lehman, M.; Bernet, A.; Schmidt, H.-W.; Papastavrou, G. **In-situ Characterization of Electrogelated Trisamide Films** (tentative). Intended for submission to *Soft Matter*

Acknowledgements

I would like to thank to all the people, who made this work possible and contributed to its success.

At first I would like to acknowledge my gratitude to my Doktorvater Prof. Dr. Georg Papastavrou for the interesting topics and strict supervision as well as for introducing me to the world of AFM and many fruitful discussions. Moreover, even more I thank him for his constant support and motivation. I have learned much during our collaboration.

Additionally I am grateful to Prof. Michal Borkovec for his supervision, fruitful discussions, and his kind advices during my work at the University of Geneva.

I say many thanks to all colleagues at the Department of Inorganic, Analytical, and Applied Chemistry (University of Geneva), and at the Department of Physical Chemistry II (University of Bayreuth) for their helpfulness and the best working atmosphere. Special thanks to Anne-Marie Loup and Sybille Zimmermann for their hospitality and help with all my administrative questions, as well as for lovely atmosphere at work.

To Prof. Dr. Andreas Fery, Prof. Dr. Axel Müller, Prof. Dr. Josef Breu, Prof. Dr. Peter Schaaf, Dr. Andreas Bernet, Dr. Hussein Kalo, Dr. Fouzia Boulmedais, Dr. Katja Trenkenschuch, Johan Erath, Julia Gensel, Marina Behr, Daniel Kunz, Maren Lehmann and Nicolas Helfricht I would like to thank for fruitful cooperation and successful projects.

Help in construction, testing and improving the potentiostat by Stephane Jeanneret is acknowledged.

I am thankful to Jana Dulle for her constant support and inspiration.

I also thank especially to Carmen Kunert for her kind help with SEM images and FIB instrumentation and to Evgeny Maximov for his help in preparation of graphical illustrations.

Finally, I am deeply indebted to my wife and my relatives for their support and encouragement throughout the years.

Erklärung

Hiermit erkläre ich, dass ich die Arbeit selbständig verfasst und keine anderen als die von mir angegebenen Quellen und Hilfsmittel benutzt habe.

Ferner erkläre ich, dass ich anderweitig mit oder ohne Erfolg nicht versucht habe, diese Dissertation einzureichen. Ich habe keine gleichartige Doktorprüfung an einer anderen Hochschule endgültig nicht bestanden.

Bayreuth, 5 März 2013

Volodymyr Kuznetsov